8-2016

Development of a Patient Machine Time Model to Evaluate Dose Perturbation by Respiratory Tumor Motion in Pencil Beam Scanning Proton Radiation Therapy

Mark Artz
University of Tennessee, Knoxville, martz@vols.utk.edu

To the Graduate Council:

I am submitting herewith a dissertation written by Mark Artz entitled "Development of a Patient Machine Time Model to Evaluate Dose Perturbation by Respiratory Tumor Motion in Pencil Beam Scanning Proton Radiation Therapy." I have examined the final electronic copy of this dissertation for form and content and recommend that it be accepted in partial fulfillment of the requirements for the degree of Doctor of Philosophy, with a major in Nuclear Engineering.

Lawrence Heilbronn, Major Professor

We have read this dissertation and recommend its acceptance:

Wes Hines, Ralph Lydic, Rebecca Prosser

Accepted for the Council:

Carolyn R. Hodges

Vice Provost and Dean of the Graduate School

(Original signatures are on file with official student records.)

Development of a Patient Machine Time Model to Evaluate Dose Perturbation by Respiratory Tumor Motion in Pencil Beam Scanning Proton Radiation Therapy

A Dissertation Presented for the
Doctor of Philosophy
Degree
The University of Tennessee, Knoxville

Mark Artz
August 2016

ACKNOWLEDGEMENTS

To Dr. Heilbronn and Dr. Hines, from the UT Nuclear Engineering department, thank you for support with this collaboration across institutions.

Thank you to all of my colleagues at the Provision Center for Proton Therapy for allowing me gather data at your facility.

To Niek Schreuder at PCPT, thank you for you for providing a sounding board for my ideas and instilling confidence in the value of this work.

ABSTRACT

The pencil beam scanning (PBS) modality for delivering intensity modulated proton radiation therapy is being adopted quickly. Drawing from the dosimetric advantages provided by the Bragg Peak, PBS proton therapy has been shown to produce dose distributions with improved healthy tissue sparing.

Although PBS proton therapy is very promising, lung cancer treatment is not without its challenges. Rapid tissue density changes and respiratory tumor motion present a particularly difficult treatment geometry. The tumor moves continuously within the lung as the patient breathes.

In this project, the dose perturbation of a PBS proton therapy lung plan is evaluated and time based models of respiratory cycle and radiation delivery of a pencil beam scanning treatment are created. The combined model of the patient and machine is referred to as the patient machine time model (PMTM). The PMTM is used to calculate the respiration rate at which the treatment machine dose delivery and patient respiration rate produce frequency matching (FM).

Frequency matching between the respiratory cycle and radiation delivery is demonstrated to reduce intra-fraction dose perturbation. The use of the PMTM to produce FM provides an advanced tool to mitigate respiratory dose perturbation with minimal impact on the patient or the treatment delivery time.

TABLE OF CONTENTS

LIST OF TABLES

LIST OF FIGURES

ABBREVIATIONS

PMTM	Patient Machine Time Model
FM	Frequency Matching
CT	Computed Tomography
4D CT	Four Dimensional Computed Tomography
IMPT	Intensity Modulated Proton Therapy
PLD	Pencil beam scanning Layer Definition
FWHM	Full Width Half Max
ESS	Energy Selection System
US	Uniform Scanning
DS	Double Scattering
SOBP	Spread Out Bragg Peak
VMAT	Volumetric Arc Therapy
RF	Radio Frequency
ITV	Internal Target Volume
PTV	Planning Target Volume
GTV	Gross Tumor Volume
ICTV	Internal Clinical Target Volume
IGTV	Internal Gross Tumor Volume
PCPT	Provision Center for Proton Therapy
IBA	Ion Beam Applications

CHAPTER ONE
CONTRIBUTIONS AND BACKGROUND INFORMATION

Problem Statement

During the past two years, the treatment of thoracic tumors with proton therapy has shown promise due to increased availability of pencil beam scanning proton therapy treatment machines. Pencil beam scanning (PBS) proton therapy treatment plans have demonstrated reduced dose to healthy tissue in treatment of lung cancer with radiation therapy. Although the dose distribution of proton therapy treatment plans is promising, the radiation dose is susceptible to perturbation from respiratory motion.

This dissertation attempts to develop a model of the dose perturbation resulting from respiratory motion based on the dose delivery of the treatment machine and the respiration cycle of the patient. The model is termed the patient machine time model (PMTM). Once the dose perturbation has been evaluated, a dose perturbation mitigation method is developed to provide minimal impact to the patient. The developed dose perturbation mitigation method is termed frequency matching (FM).

Contributions of this Dissertation

This dissertation makes contributions in the field of radiation therapy specific to respiratory motion and pencil beam scanning proton therapy. A patient machine time model (PMTM) has never been applied to the treatment planning process in proton radiation therapy. A new method to mitigate radiation dose perturbation from respiratory motion, frequency matching (FM), is also presented. These contributions, and others, are listed below with a detailed explanation located in Chapter 3.

1) Development of a model using machine specific parameters to establish the dose delivery time for pencil beam scanning proton treatment fields delivered by an isochronous cyclotron based radiation therapy machine.
2) Development of methods to calculate the delivery time of a pencil beam scanning layer definition (PLD) file included in the treatment plan of a proton therapy treatment.
3) Development of methods to establish the corresponding respiratory amplitude during the delivery of each energy layer of a proton treatment field.
4) Application of the PMTM to reduce dose perturbation by establishing FM between the dose delivery and respiration cycle.

Organization of the Dissertation

This dissertation is organized into five chapters. Chapter 1 outlines the contributions to the field of study as well background information relevant to the topic of proton therapy and respiratory motion. Chapter 2 provides a literature review of the investigation of respiratory motion and proton therapy dose delivery. Chapter 3 includes the description of the data used to build the patient machine time model. Chapter 4 provides the results and discussion of the application of the patient machine time model (PMTM). Chapter 5 concludes the dissertation and discusses the future work related to this research.

Project Description

This project was undertaken to produce a patient machine time model in order to evaluate dose perturbation from respiratory target motion in radiation therapy. The possibility of frequency matching (FM) between the patient's respiratory motion and the dose delivery of pencil beam scanning proton therapy is also discussed. This work is significant because it demonstrates the impact of the time scale of the dose delivery of the treatment machine on the dose distribution of the delivered radiation therapy treatment. The coupling of the machine delivery and patient respiratory motion has the potential to reduce uncertainty in radiation therapy. With

adequate machine characterization, these concepts could be applied to numerous radiation therapy machines.

In radiation therapy, the unit most commonly used to describe the prescribed amount of treatment to a target volume is the Gray. Gray is a measure of absorbed energy per unit mass or Joules per Kilogram. This unit is convenient for much of radiation therapy because a significant fraction of the human body is of very similar density to water, allowing easy scaling and conversion between volume and mass. Photon based radiation therapy has been established as the most prevalent form of external beam treatment in cancer therapy. Proton therapy has been expanding rapidly over the past few years due to the promise provided by the Bragg peak produced by the depth dose curve of a proton beam. Figure 1.1 displays the depth dose curves of both an 8 Megavoltage (MV) photon beam and a 200 Megaelectron Volt (MeV) proton beam [1]. Both the Pristine Bragg peak and Spread Out Bragg peak (SOBP) formed from the addition of multiple smaller Bragg peaks are shown. Notice that the photon beam produces significantly more entrance dose along its path to the tumor depth, while the proton beam produces a peak in the dose at the tumor depth. Another feature of the proton beam depth dose curve is that there is no significant dose beyond the distal edge of the Bragg peak. In comparison, even though the photon beam experiences exponential attenuation, the photon depth dose curve still demonstrates significant exit dose. An example of photon and proton based radiation therapy plans with multiple fields is discussed below.

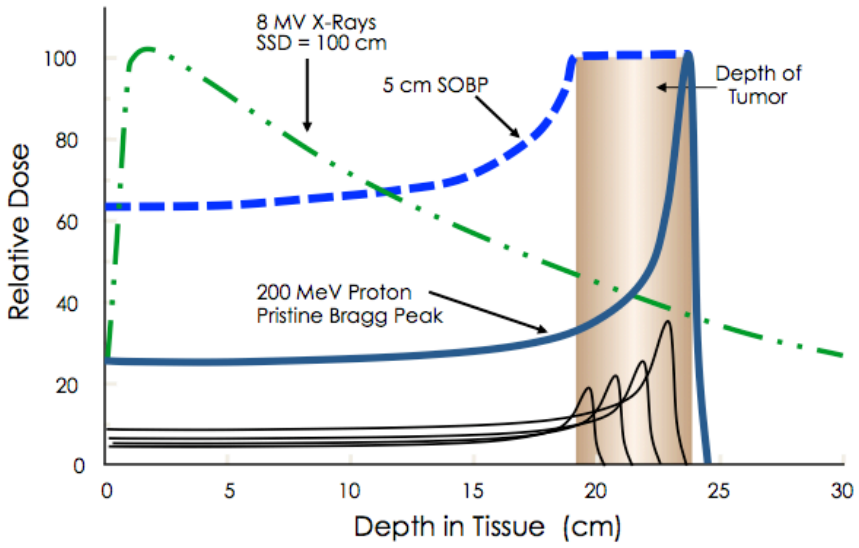

Figure 1.1. Depth dose of proton and photon beams [1]

Lung Cancer Treatment with Proton Therapy

Lung cancer is one of the most common cancers in both men and women. According to the American Cancer Society, about 14% of all cancer cases will be lung cancer cases, resulting in almost 225,000 new lung cancer cases in 2016 [2]. Both photon and proton radiation therapy are often used to treat lung cancer. There is growing interest in proton therapy use in lung cancer treatments due to its improved dose distribution. The improved dose distribution treats less healthy tissue, such and the heart and the opposite lung. Figure 1.2 displays the dose distributions of a proton therapy lung treatment plan on the left and a photon based treatment plan on the right [3]. The proton plan utilizes three treatments fields

while the photon plan is based on an intensity modulated arc referred to as volumetric arc therapy (VMAT). The distributions of these two treatment plans provide an interesting comparison between the modalities because they subtend a similar fraction of the 360° available treatment arc.

In Figure 1.2, the heart is located in the center of the axial CT slice. The dose distribution displayed in the figure shows a range of dose from 63 Gray shown in Red, 30 Gray in green, and everything below 20 Gray displayed in blue. It is important to take note of the increased dose to the heart and lungs shown by the photon plan in the right side of the figure.

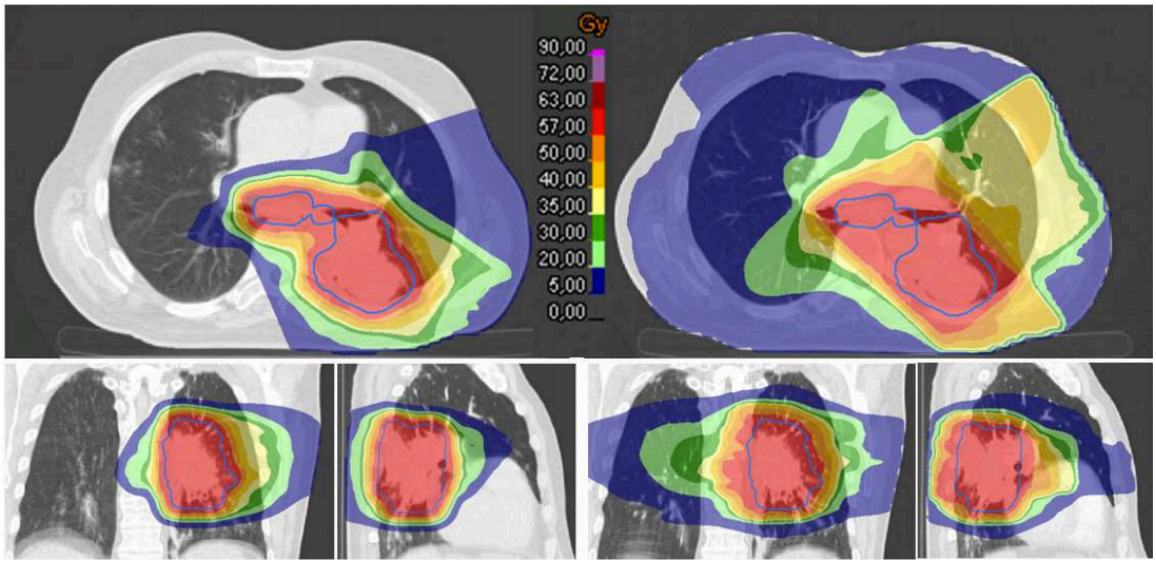

Figure 1.2. Dose distribution of three field pencil beam scanning proton and volumetric arc therapy photon lung treatments [3]

Figure 1.3 demonstrates the dose to the internal clinical target volume (ICTV) along with several other organs at risk (OARs), such as the heart and remainder of the lung [3]. The internal gross tumor volume (IGTV) designates the location of

the tumor expanded to include the entire respiration cycle motion.

Notice the significant reduction in dose to healthy organs shown by the proton dose. More than 20% of the heart received 20 Gray with the photon plan but the proton plan spared almost all of the heart from reaching this dose level. The dose to the heart is shown by the red dotted line and the dose to the lung by the black dotted line.

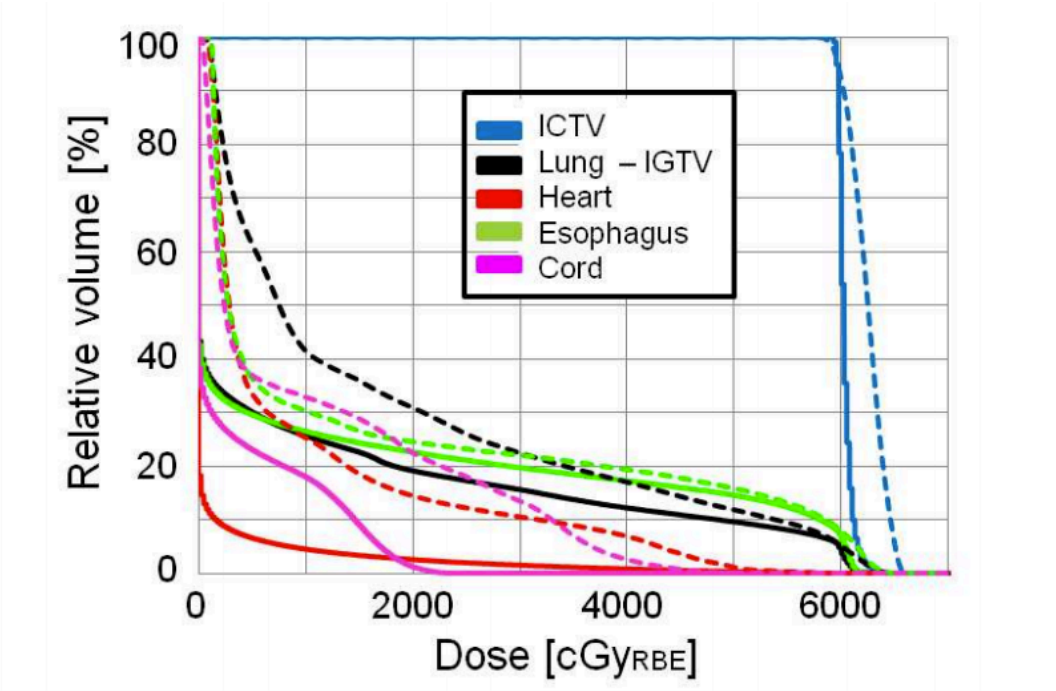

Figure 1.3. Dose volume histogram (DVH) of proton and photon treatments [3]

Proton Therapy Delivery

Uniform Scanning and Double Scattering

There are three types of proton dose deliveries: double scattering (DS), uniform scanning (US), and pencil beam scanning (PBS). Both DS and US create a uniform dose cube which is then modified with an aperture and compensator to match the tumor shape. The dose distribution produced by DS and US delivery techniques is shown in Figure 1.4 [1]. Notice that the high dose profile maintains the same square width in depth even though the tumor does not have this full width at the lateral edges of the field. These dose tails are the remnants of the original distribution of dose being in the shape of a cube.

In order to conform the dose distribution to the distal edge of the tumor, the cube of dose is deformed by the aperture and compensator. The aperture cuts the field down to the cross sectional area of the target and the compensator contours the dose to the distal edge of the target. The piece labeled 1 in the compensator is the inverse of the depth of the distal edge of the tumor. The compensator is thinner where the distal edge of target area is deepest and thinner where the distal edge is shallower. The second piece of the compensator is used to compensate for the curvature of the patient, and it is thicker where the target depth is shallower and thinner where the target depth is deeper. The third piece represents additional compensator thickness to offset the reduced water equivalent thickness cause by the air pocket inhomogeneity.

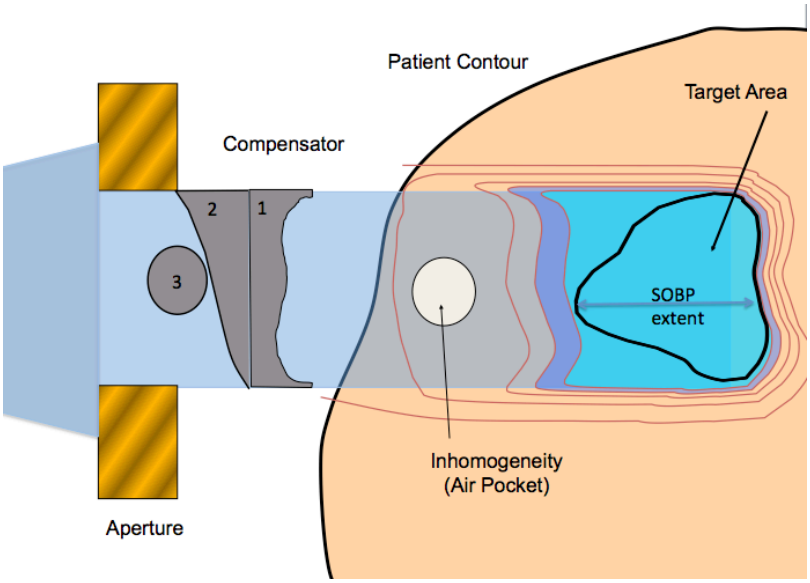

Figure 1.4. Double scattering & uniform scanning proton field dose distribution [1]

Pencil Beam Scanning

Pencil beam scanning (PBS) proton therapy is a type of treatment delivery that is comprised of individual beamlets. Each of these beamlets is deflected to transverse to the primary beams direction by scanning magnets in both the X and Y directions. In order to match the depth of the distal edge of the target volume the energy of the proton beam entering the patient is modulated by an energy degrader upstream of the scanning magnets. As the energy of the proton beam entering the patient is reduced, its range in the patient is also reduced. Figure 1.5 [1] displays the deflection of the proton beam by the scanning magnets to deliver dose to each spot on in the tumor, shown in red.

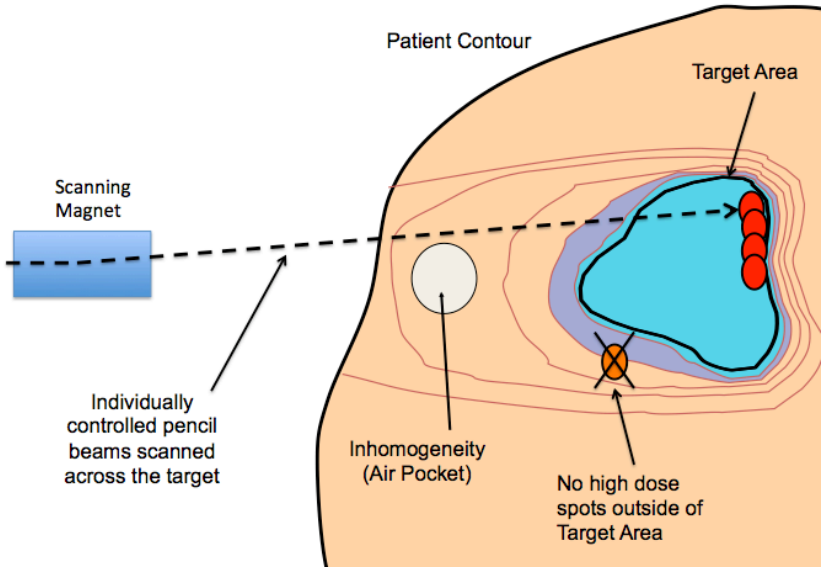

Figure 1.5. Pencil beam scanning proton field dose distribution [1]

Treatment Plan Optimization

PBS proton therapy plans are created with a process known as inverse planning. During inverse planning, the dosimetric goals for target coverage and organ sparing are given as an optimization problem. The solution to the inverse planning problem is solved through an iterative process of recalculating the dose of each beamlet in the treatment field until an optimal solution is found. An optimal solution occurs at the intersection of the multivariable surface representations of what is possible and what is preferable. The surface created by perfect substitution of solutions is called a Pareto surface. A Pareto surface is named after an Italian engineer and economist, Vilfredo Pareto, who first presented the concept in the field of economics as a country's production possibilities frontier.

Figure 1.6 illustrates a simplified visualization of a multi criteria optimization (MCO) problem often used to find solutions for PBS proton therapy treatment plans [4]. The optimal solution exists when what is possible intersects the surface of what is desirable. In this example the marginal rate of substitution (MRS) represents the surface of the limits of possibility, and the marginal rate of transformation (MRT) represents the tradeoffs between what is preferable. In this simplified problem, the MRS represents the Pareto surface on which dose to Organ 1 cannot be reduced without increasing the dose to Organ 2 and vice versa. The MRT curve represents the physician's preference for substitution between dose to Organ 1 and Organ 2. Curves 1 through 4 represent parallel shifts of the trade-off between dose to each organ showing increasing utility.

The preferences represented by this curve would be the clinical goals of the physician, ultimately representing an increasingly positive outcome for the patient. The intersection of what is possible from a given treatment modality such as PBS proton therapy would be represented by the MRS curve. The MRT curve represents what is clinically desirable. The intersection of what is possible and what is desirable is shown when MRS equals MRT and defines the optimally deliverable treatment plan for that modality. The same concepts would be applied in photon treatment planning but with a different shape to the MRS curve.

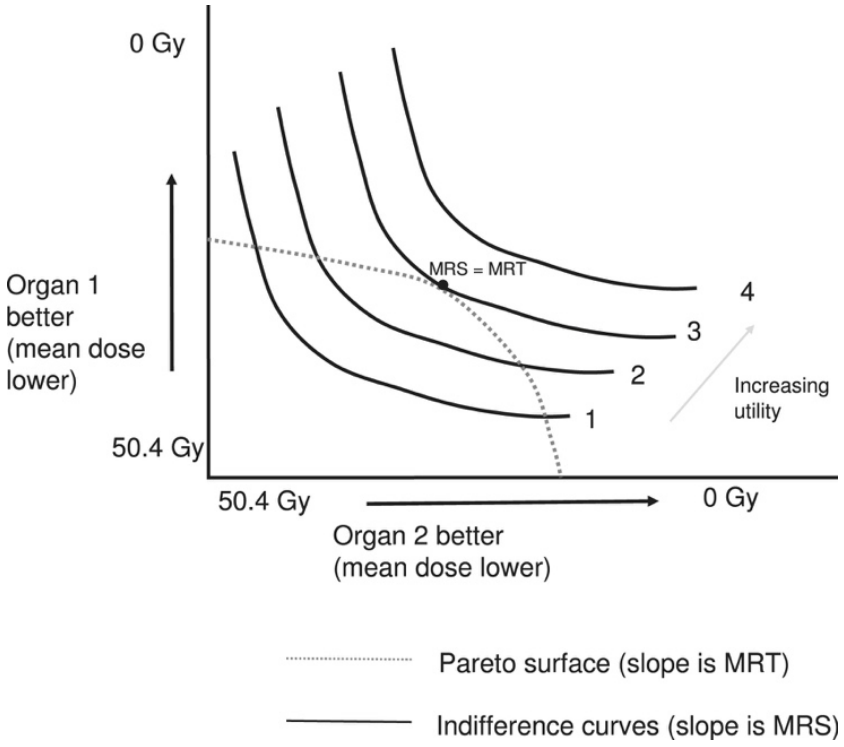

Figure 1.6. Simplified Pareto surface from treatment plan optimization [4]

Clinical Proton Therapy Cyclotrons

Many of the proton therapy system in the United States are cyclotron based systems. In order to reach the deepest treatment fields most clinical proton therapy cyclotrons produce a beam with a final beam energy of at least 230 MeV. There are two types of cyclotrons that are used to produce the proton beams in this energy range: isochronous cyclotrons and synchrocyclotrons. The primary difference between the two types of cyclotrons is the structure of the magnetic field they use to confine the proton beam.

1) Isochronous cyclotrons consist of a radially increasing magnetic field and a constant radio frequency (RF) accelerating voltage frequency. This radially increasing magnetic field creates a defocusing force which must be compensated by passing the proton beam through magnetic poles of alternating strength, call “hills” and “valleys”.

2) Synchrocyclotrons use a radially decreasing magnetic field and a variable RF accelerating voltage frequency. This radially decreasing magnetic field allows for a phenomena called weak focusing. The radially decreasing magnetic field reduces the need for the beam to pass through magnetic poles of alternating strength but creates the need for a variable frequency accelerating RF.

Isochronous Cyclotron

Figure 1.7 displays the magnetic field distribution of an isochronous cyclotron. The isochronous cyclotron displayed in Figure 1.7 is a four sector machine, producing four “hills” of high strength magnetic field and four “valleys” of reduced strength magnetic field [5]. This alternating magnetic field strength produces a restorative force, keeping the individual particles within the accelerating plane of the cyclotron.

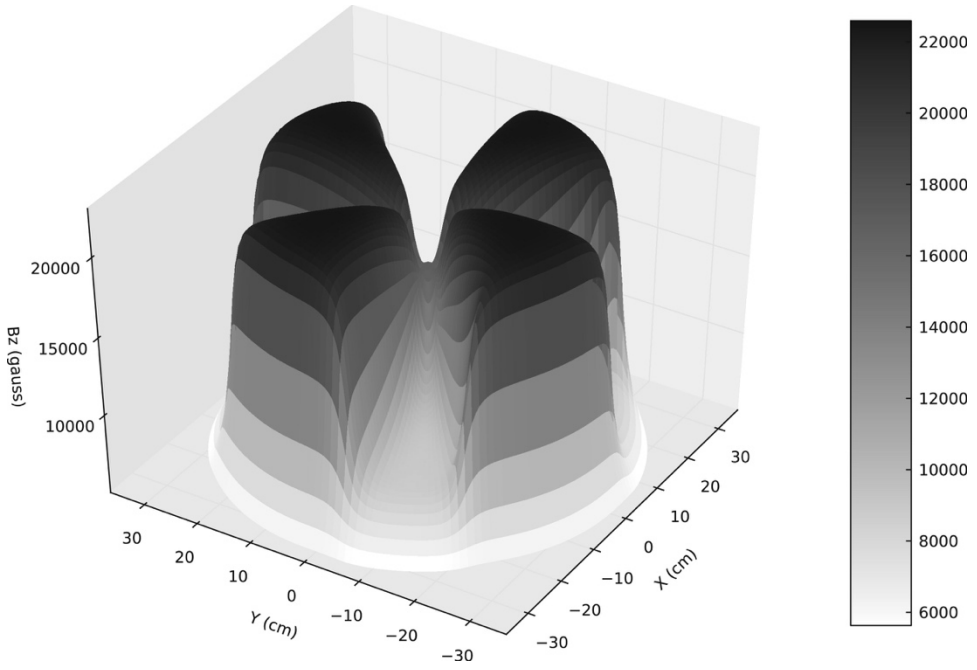

Figure 1.7. Magnetic field distribution of an isochronous cyclotron [5]

As a proton is accelerated to its final extraction energy of over 230 MeV, the particle begins to become relativistic and experiences a relativistic mass gain. This increase in mass results in a reduced charge-to-mass ratio of the accelerating proton. The radially increasing magnetic field of the isochronous cyclotron, shown in Figure 1.8, compensates for the relativistic mass gain and keeps the procession frequency of the accelerating proton in phase with the RF accelerating voltage from the inner orbitals of the cyclotron until the final extraction energy [5].

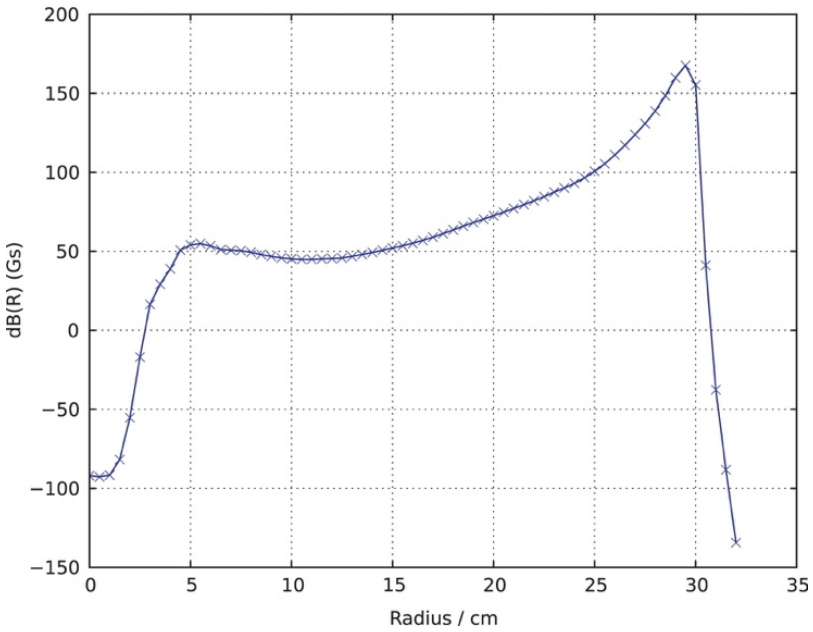

Figure 1.8. Radially increasing magnetic field isochronous cyclotron [5]

Synchrocyclotron

Synchrocyclotrons use a radially decreasing magnetic field and a variable RF accelerating voltage frequency. This radially decreasing magnetic field allows for a phenomena called weak focusing, removing the need for the beam to pass through magnetic poles of alternating strength. Figure 1.9 [6], displays a vertical cross-section of a synchrocyclotron along its rotational axis of symmetry taken from a magnetic field simulation in Opera [7]. Opera is a physics simulation software that is commonly used to design the magnetic field of particles accelerator components such as cyclotrons, dipoles and quadrupoles.

Cyclotrons are symmetric rotationally along the vertical axis as well as along the mid-plane. This symmetry allows the magnetic field simulation to be simplified to a single quadrant. The magnetic field components are used to confine and steer charged particles using the Lorenz force, $F = q (v \times B)$. Where F is the force, q is the particle charge, v is the velocity vector, and B is the magnetic field vector.

The blue volume, shown in Figure 1.9, represents the magnetized steel of the cyclotron and the multicolored component represents a cross-section of the solenoid coil used to magnetize it [6]. The color gradient in the figure shows the magnetic field, B [Tesla], ranging in strength from nearly zero, in blue, to up to over 5.7 Tesla, in red. The gradual reduction in the amount of steel during the first 400mm of distance from the center of the cyclotron is most pronounced between the radii of 300 mm and 400 mm. This reduction in steel produced a reduction in magnetized material and results in the characteristic radially decreasing magnetic field shown in Figure 1.10 [6].

Although the magnetic field within a synchrocyclotron is simplified when compared to an isochronous machine, the accelerating RF voltage frequency must still be matched to the procession frequency of the accelerating protons orbiting in the cyclotron. In order to produce an accelerating voltage that is in phase with the accelerating proton the RF frequency must be ramped down as the proton reaches higher energies and becomes more relativistic. Figure 1.11 demonstrates the ramp down of RF accelerating frequency, shown by the blue line between the beam capture and beam extraction windows shown in green dotted lines [6].

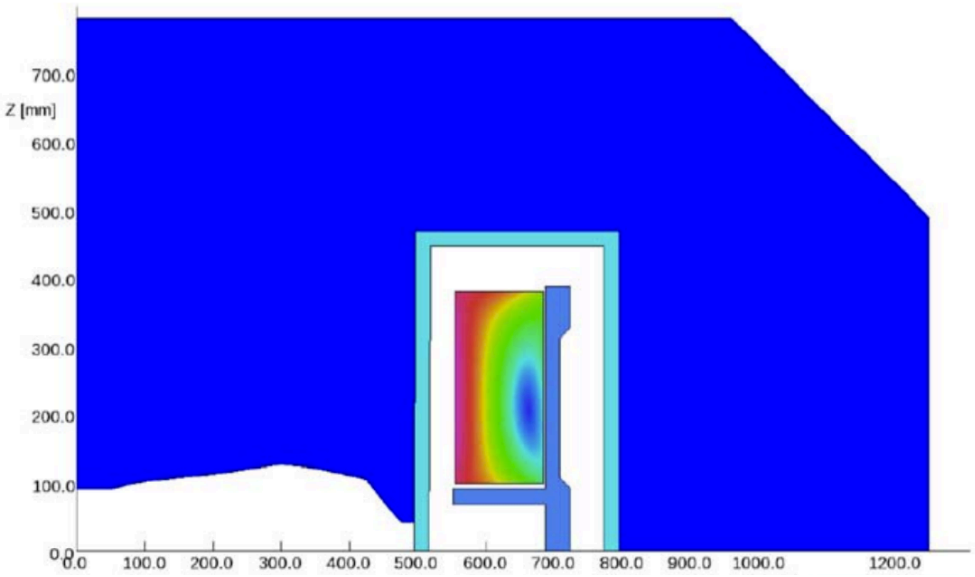

Figure 1.9. Synchrocyclotron cross section with radially decreasing iron [6]

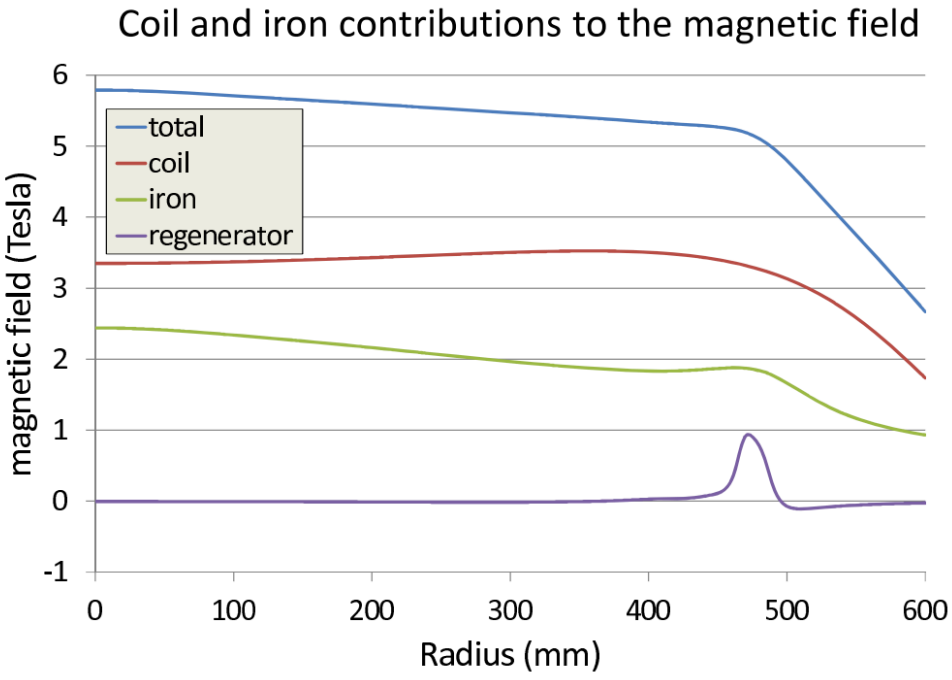

Figure 1.10. Radially decreasing synchrocyclotron magnetic field [6]

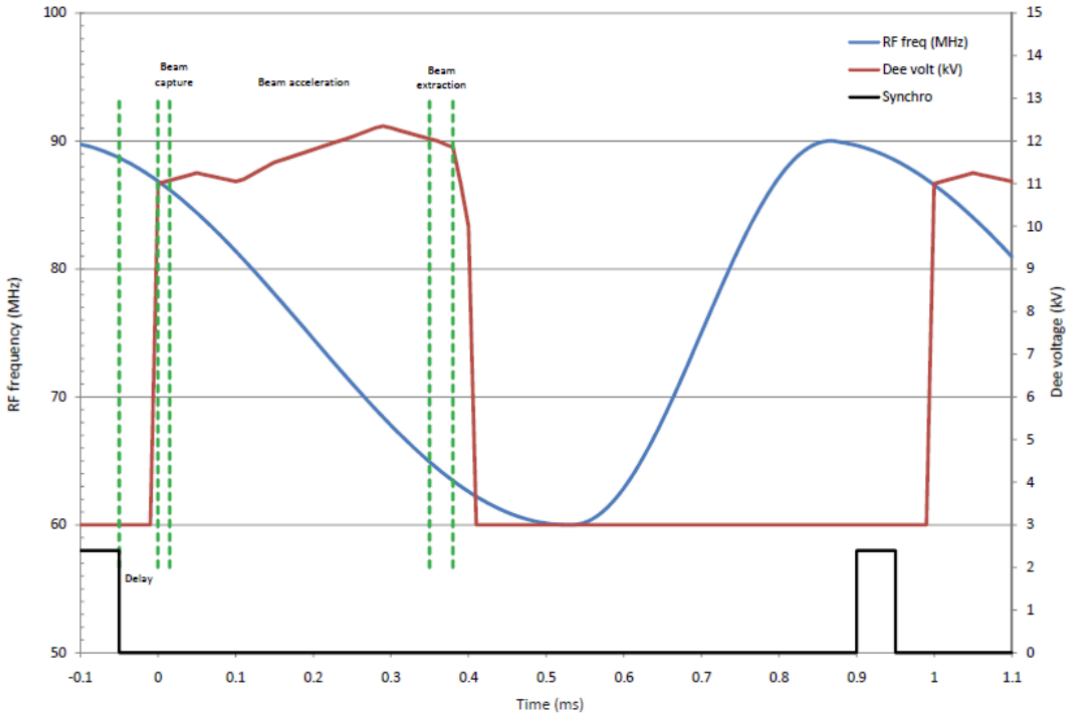

Figure 1.11. Synchrocyclotron radio frequency and beam cycling [6]

The example synchrocyclotron shown in Figure 1.9 would produce a proton beam extraction once every millisecond, resulting in a proton pulse frequency of 1 kHz. The pulse structure of a synchrocyclotron is much different than an isochronous cyclotron which produces proton beam pulses at the same frequency as the primary accelerating RF frequency of 50-100 MHz. The isochronous cyclotron beam can be treated as a continuous beam because the pulse frequency is extremely high. This may not be the case for synchrocyclotrons.

CHAPTER TWO
LITERTURE REVIEW

This section will review the previous work pertaining to respiratory tumor target motion and radiation therapy, particularly in the area of lung cancer treatments performed with pencil beam scanning (PBS) proton radiation therapy. Several other techniques for respiratory target motion mitigation are also reviewed. It should be noted that lung cancer treatment with PBS proton therapy is available at very few facilities which is why it is of particular interest at this time.

Respiration Frequency and Amplitude

The rate at which the patient is breathing along with the distribution of the patients inhale and exhale phases are necessary in order to create an accurate model of a patient's respiration.

Respiration Frequency

Figure 2.1 displays various respiration rates. The most relevant is that of the lying respiration rate, "LIE", at nearly 15 breaths per minute [8]. This respiration rate is significant because all of the PBS proton radiation therapy treatments at the Provision Center for Proton Therapy (PCPT) are conducting in the lying position, with the majority completed with the patient lying on their back. In Figure 2.1, the solid line represents a respiratory inductive plethysmograph (RIP) in which the respiration rate is measured with a traditional belt potentiometer around the

patient's chest. The dotted line represents an ambulatory inductive plethysmograph (AIP) which tracts the respiration rate with a set of sensors on the patient's chest, allowing the patient to have greater mobility.

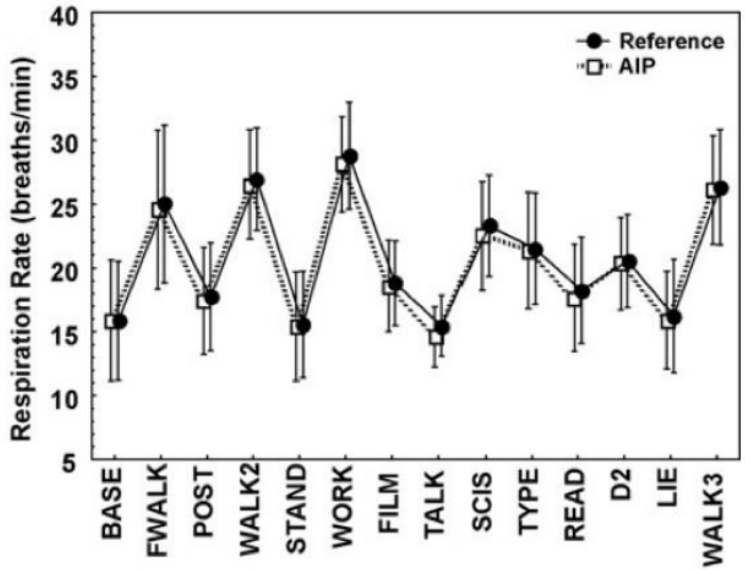

Figure 2.1. Respiration rate during various activities [8]

Amplitude

Figure 2.2 shows the relationship between the volumetric flow of air through the oral cavity and that of the expansion of the chest and movement of the diaphragm [9]. Figure 2.3 displays a typical time distribution of the inhale and exhale phases of the respiratory cycle [9]. This distribution was the basis of the distribution used to build the patient machine time model presented in Chapter 3. It is important to note that the inhalation of a volume of air precedes the rising of the chest.

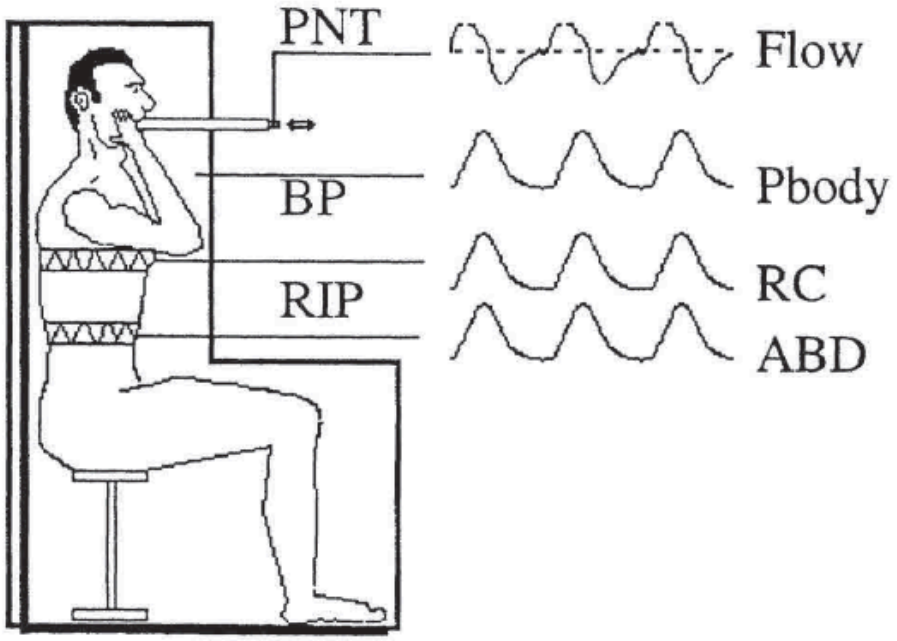

Figure 2.2. Respiratory amplitude at various locations on the body [9]

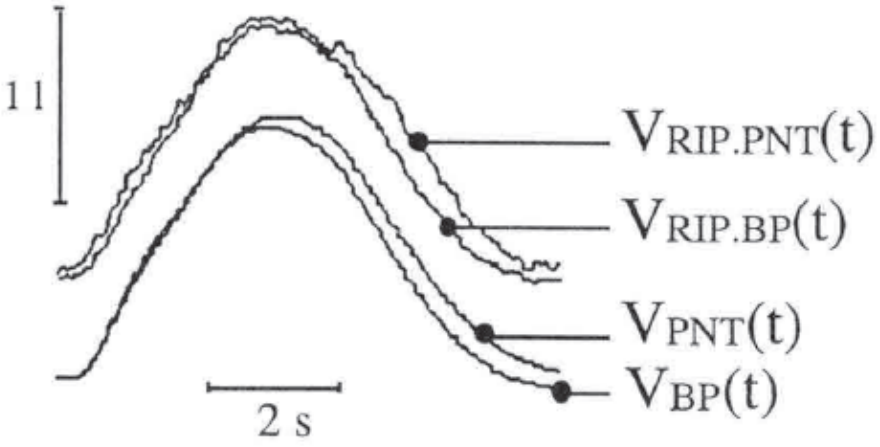

Figure 2.3. Single respiratory cycle [9]

PNT refers to pneumotachograph, which directly measures the airflow rate out of the patient's oral cavity. Body plethysmography (BP) is a measure of the respiration volume. Respiratory inductive plethysmography (RIP) is a measure of the physical displacement of the rib cage (RC) or the abdomen (ABD). Depending on the sensors used to determine the respiratory amplitude a phase lag may need to be determined in order to correspond to the respiratory amplitude of the internal patient anatomy.

4D Diagnostic CT Phase Binning

Four dimension computed tomography (4D CT) refers to a computed tomography diagnostic scan that is acquired while the respiratory amplitude is recorded. The 4D CT scan is acquired in all three spatial directions as well as over an extended period of time. The forth component, time, creates the four dimensions of a 4D CT. During a 4D CT, numerous CT slices of the patient are obtained at multiple respiratory amplitudes which are then sorted into full diagnostic quality CT scans at all of the respiratory amplitude phases. Figure 2.4 displays the concepts behind 4D CT binning [10]. The top part of the figure shows the ideal 4D CT acquisition. The CT scanner table is held is position long enough to acquire a CT slice at each phase of the reparatory cycle and tagged with its corresponding amplitude. The bottom of Figure 2.4 shows how the slices at the same respiratory amplitude are combined from multiple table positions. This process should provide 10 full CT scans of the patient, with one CT scan at each bin of the respiratory amplitude.

Respiratory Motion in Radiation Therapy

Many methods have been explored to reduce the respiratory motion-induced dose uncertainty in spot-scanning proton therapy. Unlike a photon beam, a proton beam has a specific depth at which the majority of its dose will be delivered. This feature of the proton depth dose allows the potential for greater respiratory motion dose perturbation than in a photon field delivery.

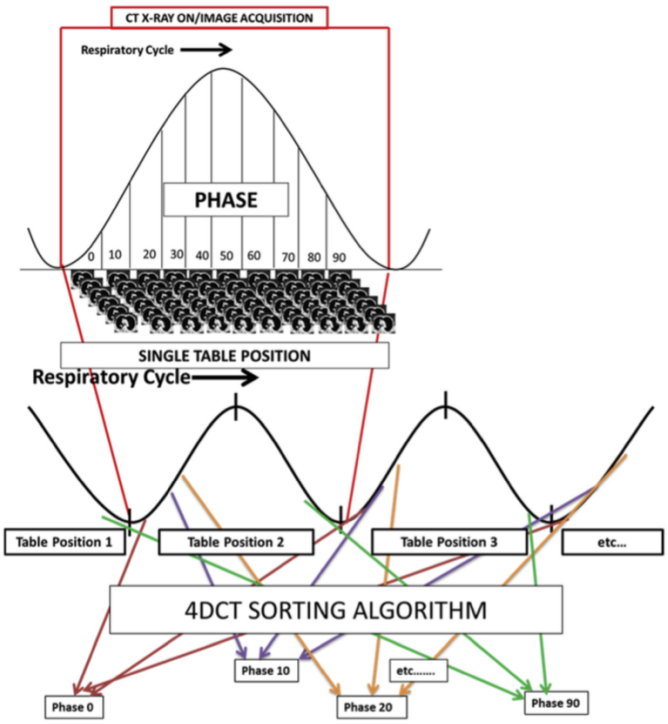

Figure 2.4. 4D CT phase binning [10]

Lung cancer tumors are often solid masses with a density much closer to water than the surrounding lung tissue, which is primarily air. Figure 2.5 displays the path

of the tumor, delineated as the clinical tumor volume (CTV), during a respiration cycle [11]. In photons the CTV tumor volume is typically expanded to a target volume that is large enough to include the full cycle of the tumor motion during respiration, marked internal target volume (ITV). The planning target volume (PTV), represents the expansion of the ITV for mechanical accuracy of the patient's position in the treatment room coordinate system and any possible movement of the patient's external anatomy.

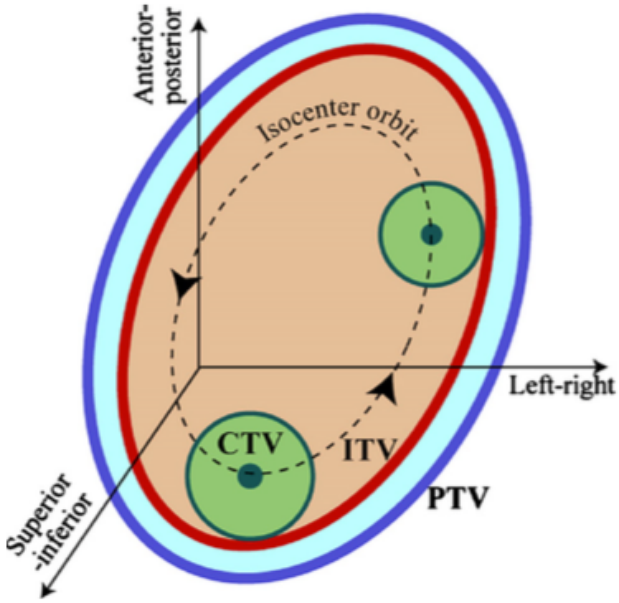

Figure 2.5. Cyclic motion of clinical tumor volume (CTV) [11]

Breath-Hold

A breath-hold technique can be used in an attempt to deliver the entire radiation field in the same respiratory amplitude that the patient is holding their breath.

Figure 2.6 shows the promising dosimetric results from a study on voluntary breath hold approach to lung treatment delivery [12]. Image (a) of Figure 2.6 shows the tight margin around the treatment volume outlined in red provided by the breath hold technique. Image (b) displays the larger dose perturbation resulting from a treatment field delivery with the patient is free-breathing.

The primary limitation of breath-hold approach is the short length a patient can hold their breath. Patients with lung cancer may already have impaired lung function that prevents them from holding their breath for an extended period of time. It would be very difficult to use a breath-hold approach for many pencil beam scanning lung treatment fields, as many have delivery times that extend well over one minute.

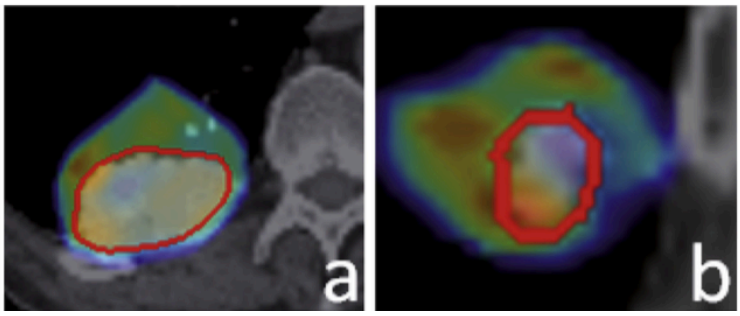

Figure 2.6. Breath-hold proton therapy delivery [12]

Gating

Gating offers an alternative to the breath-hold approach for motion management that would allow the patient to continue breathing with their natural respiration rate. Figure 2.7 displays a respiratory cycle with a gate at the lowest amplitude section of the respiration cycle [13]. The proton beam delivery to the treatment room is

controlled by the accelerating voltage within the cyclotron with the IBA ProteusPlus. Future proton therapy system may make use of high speed switching magnets that will control the beam's entry into the treatment room. The transition from RF manipulation to switching magnets may allow for improvements in beam delivery reliability.

Gating is the most similar to the patient machine time model (PMTM) model and frequency matching (FM) described in Chapter 3 and appears very promising. Gating is still limited by the quality of the respiration amplitude measurement during the treatment field delivery and often requires devices to be attached to the patient for each fraction.

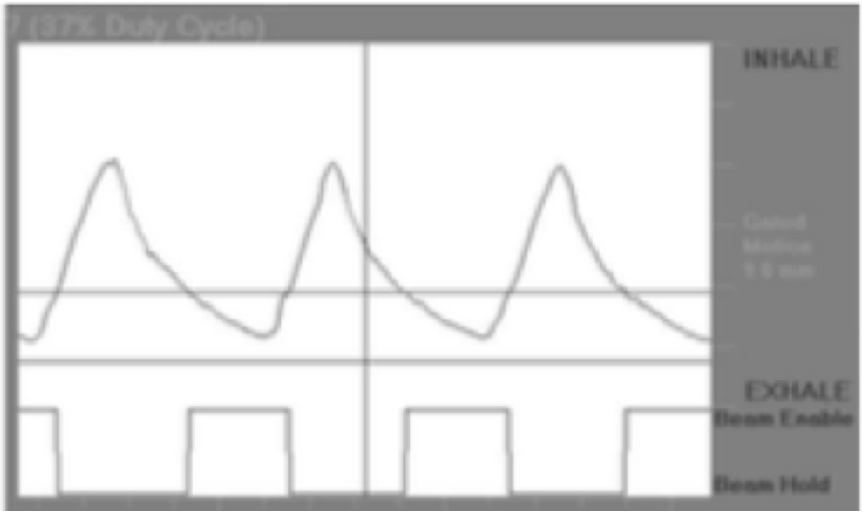

Figure 2.7. Respiratory gating signal with low amplitude gate window [13]

Scanning Modification

Several methods have been proposed to modify the scanning pattern of the proton pencil beam scanning fields to make them less susceptible to respiratory motion. Figure 2.8 displays typical dose scanning patterns in frames (a) and (b), moving from left to right [14]. Frame (c) displays the modified scanning pattern which delivers all of the proton beamlets in the field in a sparser pattern allowing dose to be delivered over the entire grid through the respiratory cycle. Another approach suggested increasing the spot size [15], but this would increase the penumbra of the field.

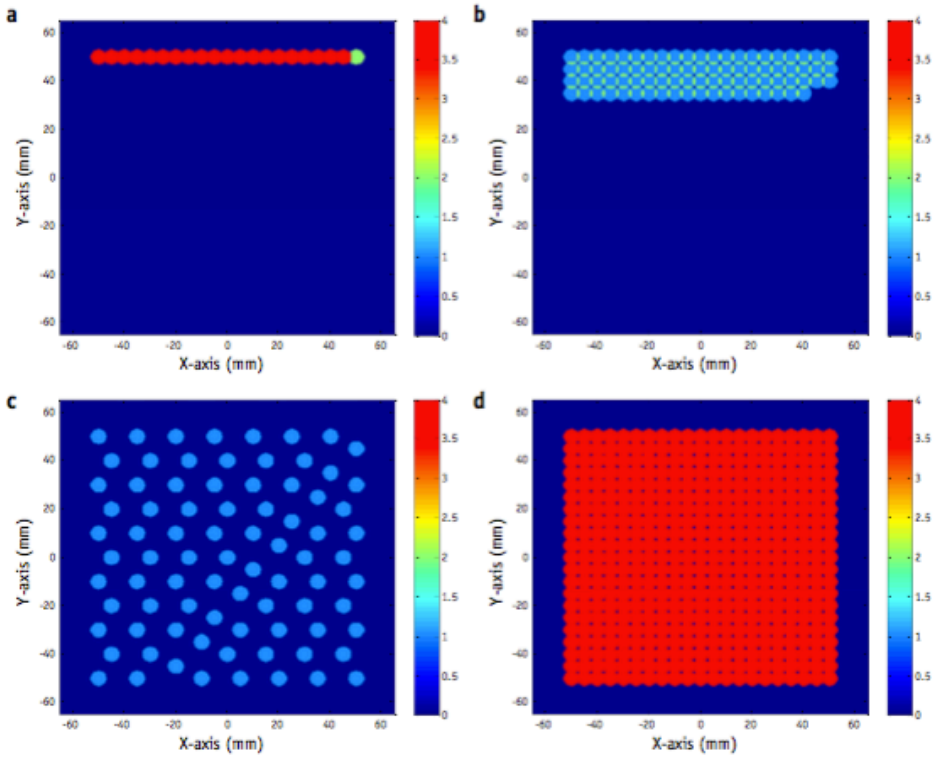

Figure 2.8. Modified pencil beam scanning pattern [14]

CHAPTER THREE
DEVELOPMENT OF THE PATIENT MACHINE TIME MODEL

This section will describe the parameters that were used to model the time scale of the dose delivery from the IBA Proteus Plus proton therapy system located at the Provision Center for Proton Therapy (PCPT) in Knoxville Tennessee. The time scale of the dose delivery is then overlaid with a typical patient's respiratory amplitude. The PCPT system described in this section makes use of an isochronous cyclotron and pencil beam scanning. The PCPT facility floor plan shown in Figure 3.1, displays the isochronous cyclotron in the right most bunker, represented by a large circular structure [1]. The primary function of analyzing the system was to identify the time scale of the dose delivery of proton radiation therapy treatment fields. The project was undertaken with the following goals.

1) Model the interval and length of time the proton beam dose is delivered within a pencil beam scanning treatment field.
2) Model the respiratory signal used to create 4D CT scans.
3) Couple the treatment machine dose delivery frequency and the respiratory cycle frequency to establish the patient machine time model (PMTM).
4) Provide information that can be used as input for treatment planning and machine delivery to produce frequency matching (FM) between the patient's respiration and treatment machine's dose delivery.

Similar concepts of dose delivery pulse structure could be used to describe other systems such as synchrotrons and synchrocyclotrons. Those systems would have different mechanisms contributing to the dose delivery time scale. The most significant difference between the isochronous cyclotrons and synchronous machines is that the pulse structure of the isochronous machine produces a beam that at the time scale of the treatment field appears as if it is direct current. For a proton therapy system based on an isochroous cyclotron, the only changes in the beam delivery are results of the energy degrader and the beam transport system.

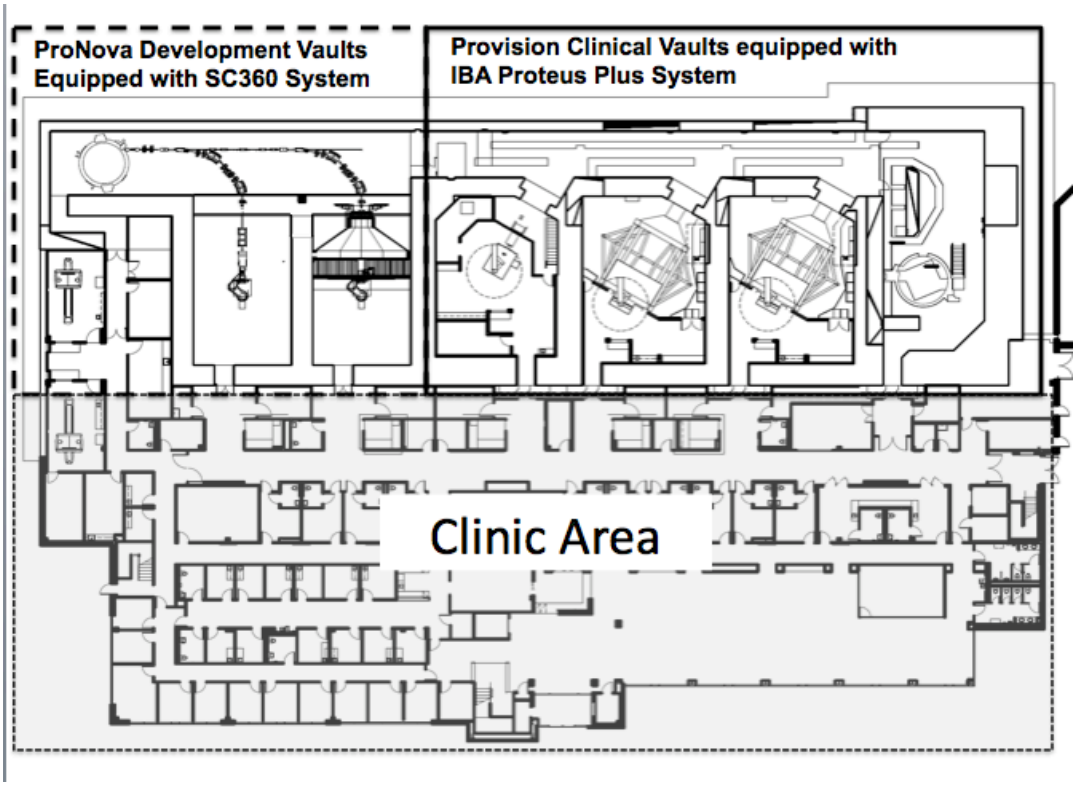

Figure 3.1. Provision Center for Proton Therapy layout with IBA Proteus Plus isochronous cyclotron [1]

Synchronous machines differ from isochronous machines in that these accelerators change the frequency of the accelerating voltage to match the kinetic energy and relativistic correction of the accelerating protons. After the proton beam reaches its final energy it is extracted and transported down the beamline. In order to deliver additional protons another bunch of protons must be injected into the accelerator and the accelerating voltage frequency reset to match the initial energy of the beam. The accelerating voltage is then ramped up again to match the beam energy and relativistic corrections. Creating a model of the time structure of dose delivery for synchronous accelerators would require additional parameters.

Proton PBS Treatment Field Specification

This section describes the parameters of the radiation fields that are sent to the IBA proton therapy treatment machine from the treatment planning system. These files are stored in an Oncology information system (OIS) and later transferred to the treatment machine for patient alignment and radiation delivery.

In order to deliver a pencil beam scanning proton treatment, several pieces of data are transferred to the treatment machines. The transferred data is comprised of a computed tomography x-ray based scan of the patient, computer generated structures to identify organs and target volumes, and the radiation treatment plan. The radiation treatment plan for PBS is generated by the treatment planning system and includes a spot map file with the energy, location, and amount of

monitor units (MU) to be delivered in each spot. This file is referred to as a pencil beam scanning layer definition file (PLD). MUs are a unit of measure that are proportional to the dose in the patient. MUs are measured by ionization chambers in the beam line upstream of the patient. The dose inside the patient in units of Gray can be accurately delivered as long as the energy of the proton beam is known along with the amount of monitor units delivered.

Figure 3.2 displays the treatment planning structures created by contouring the patient's autonomy on a diagnostic quality CT scan. The CT scan that is acquired is diagnostic quality and used to both identify the tumor target and the organs at risk (OARs). In the figure you can see the right lung represented in dark blue, the left lung in light blue and the heart in red. The target tumor volume is within the dark blue right lung structure.

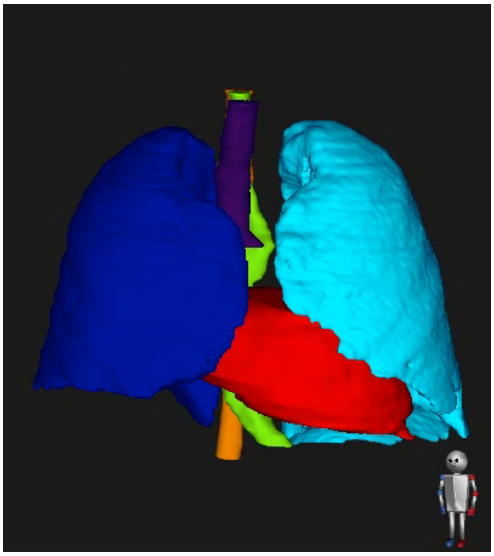

Figure 3.2. Structures representing organs at risk (OARs)

Figure 3.3 shows a visual representation of the individual proton beamlets within a layer of one field of the treatment plan. The location of the distal edge of the beamlets, where most of the dose is delivered, is often referred to as the proton beamlet's "spot". The individual beamlets within a treatment field layer are all delivered at the same energy, in this case 140.5 MeV, shown in the upper left corner of Figure 3.3.

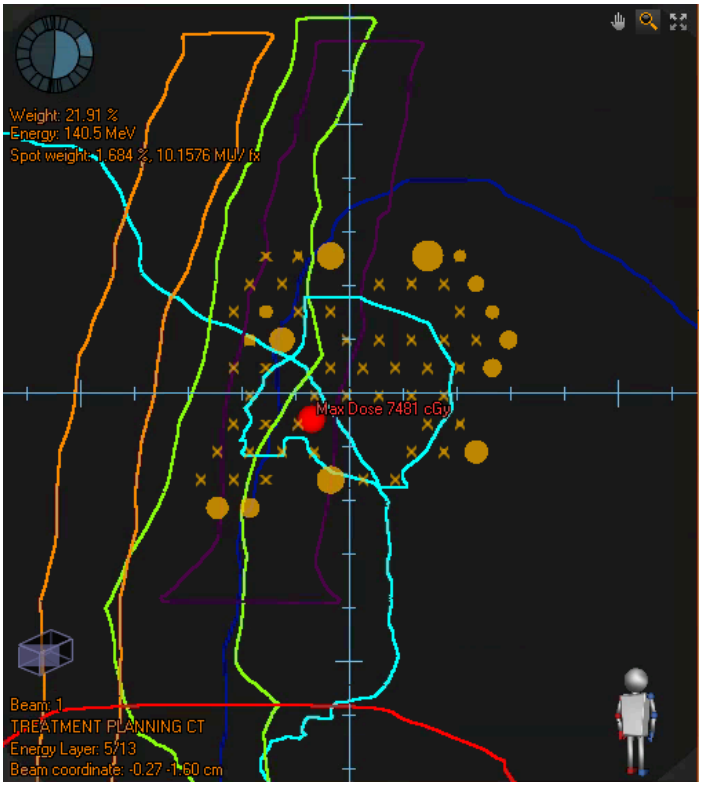

Figure 3.3. Beam's eye view of spots intensity and structures outlines

The dose from the spots within the layers is modulated to provide uniform composite coverage of the target volume. The dose is modulated by varying the amount of MUs that are delivered to each spot. The MUs from each spot are also

displayed in Figure 3.3, the highest MU beamlets are represented with the largest orange circles while the lower weighted spots shown by small orange circles. The lowest MU beamlets are shown by and orange “x”, this is done to indicate their location when the relative size of the MU would have been too small to visualize.

Pencil Beam Scanning Treatment Fields

Pencil beam scanning (PBS) treatment fields use a pair of electromagnets that deflect the beam perpendicular to its path. One of the magnets scans in the X direction and the other in the Y direction. The transverse X and Y location of each spot is specified in the treatment field calculated by the treatment planning system. These scanning magnets allow the proton beamlets to reach their specified location. The treatment planning system also specifies the amount of MUs and the beam energy to deliver each individual spot in the treatment plan. Each individual spot’s parameters are specified in the treatment plan within a PLD file.

Treatment Field – Pencil Beam Scanning Layer Definition

The treatment plan used to determine the IBA proton therapy machine parameters and create a beam model is shown in Figure 3.3. The treatment plan was created for a tumor target volume in the right lung. The plan is comprised of two posterior fields. Figure 3.4 shows the energy layers and spot parameters from one of the treatment fields in the plan. The first energy layer in each field’s PLD is at the highest energy and all the subsequent energy layers are at sequentially lower energies.

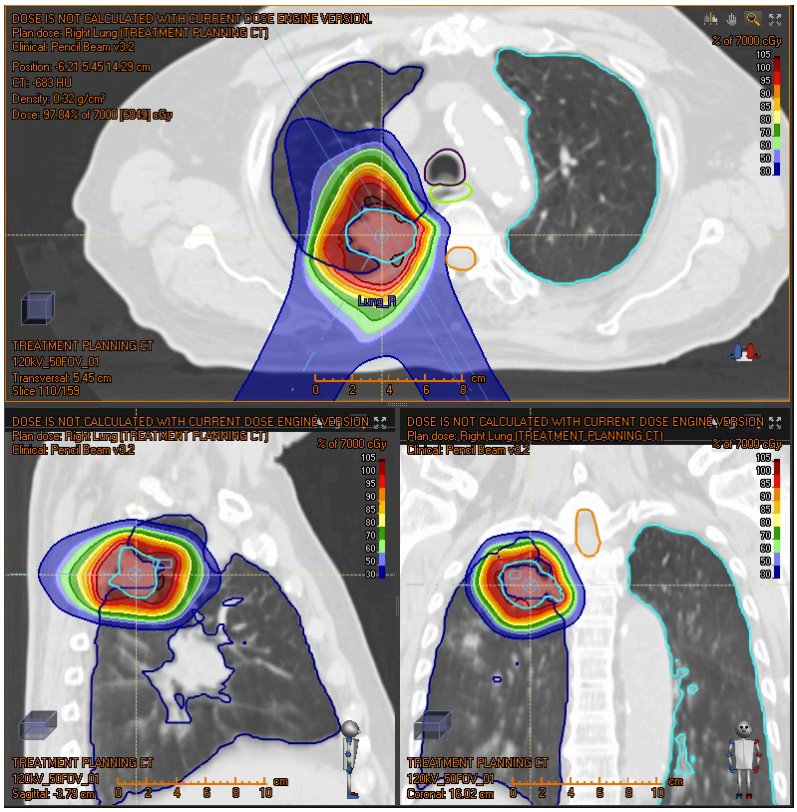

Figure 3.4. Two field pencil beam scanning proton therapy lung plan

Number	Energy [MeV]	Number of spots	Relative weight [%]	Spot weight [MU/fx] Min	Max
1	153.01	6	1.51	0.1059	3.4083
2	149.84	19	9.31	0.1051	7.7887
3	146.70	24	9.61	0.1051	11.3994
4	143.59	32	12.67	0.1051	11.0239
5	140.50	30	9.85	0.1051	11.3996
6	137.50	36	10.60	0.1050	11.3969
7	134.65	44	11.89	0.1051	7.7709
8	131.83	41	9.63	0.1051	11.3060
9	128.99	54	13.64	0.1051	8.2848
10	126.12	40	3.12	0.1052	4.3469
11	123.30	35	4.59	0.1066	5.8396
12	120.54	39	2.85	0.1066	3.2877
13	117.86	24	0.60	0.1070	0.4251
14	115.27	7	0.14	0.1074	0.1156

Figure 3.5. Field energy layers and spot parameters

Table 3.1 shows the parameters extracted from a portion of the first two layers in the PLD file. Each energy layer begins with a line that includes the spot tune ID, proton beam energy in MeV, total monitor units (MUs), location (X and Y) and the number of spots. The proton beam energy at the start of each layer in column two is set by the energy degrader.

The spot tune ID refers to the beam optics being used to transport the beam to the treatment isocenter. The spot tune ID of “4” listed in this PLD file is currently the only commissioned beam transport tune. Other tunes could be commissioned for treatment planning with the IBA system but the current tune of “4” represents the minimum spot size.

At the beginning of the layer and at each individual spot, the total number of MUs in each energy layer is listed in the third column of the PLD file. The rows in the PLD with zero monitor units represent tuning pulses, used to accurately position the beam before the full MUs of the spot are delivered.

The number of spots in an energy layer is listed at the beginning of each layer. The PLD file used by the IBA system indicates double the amount of spots as in the treatment planning system because it includes the tuning pulses. Since the amount of monitor units delivered in the tuning pulses is negligible they are ignored. For the purpose of this model only the nonzero spots were used.

As shown in Table 3.1, the X and Y locations of the spots in each energy layer are listed in the first two columns associated with each individual spot. These locations are given in mm and used by the scanning magnets to position the beam for each spot.

Table 3.1. Pencil beam scanning layer definition file parameters

Spot Tune ID	MeV	MU	# of Spots
4	153.0148692	8.347985446	12
x [mm]	y [mm]		
-2.4011037	1.9813852	0	0
-2.4011037	1.9813852	2.6692247	0
4.0348783	1.9813852	0	0
4.0348783	1.9813852	0.10815182	0
-5.619095	-3.5923386	0	0
-5.619095	-3.5923386	0.107137136	0
0.8168872	-3.5923386	0	0
0.8168872	-3.5923386	1.9492636	0
-2.4011037	-9.166062	0	0
-2.4011037	-9.166062	3.4083252	0
4.0348783	-9.166062	0	0
4.0348783	-9.166062	0.10588299	0
4	149.8405041	51.50052154	38
-15.652689	13.457595	0	0
-15.652689	13.457595	5.1544304	0
-12.46921	7.943646	0	0
-12.46921	7.943646	7.7887125	0
-6.1022496	7.943646	0	0
-6.1022496	7.943646	0.10519581	0
0.26471013	7.943646	0	0
0.26471013	7.943646	0.106116466	0

Measurement of Proton PBS Treatment Field Delivery Time

This section will describe the data used to model the time scale of the dose delivery from the IBA ProteusPlus machine at the Provision Center for Proton Therapy (PCPT). Parameters were taken both from the treatment planning system commissioning data and time measurements from proton therapy field deliveries.

Figure 3.6 shows the dose rate monitoring device (DCEU) used to measure the delivery time of pencil beam scanning layer definition (PLD) files. The DCEU generates an audio beep when the dose rate exceeds a preset value. The DCEU was set to alert the user at dose rates above 0.5 Gray per minute. In the case of pencil beam scanning proton treatment fields, the dose rate exceeds the threshold to trigger a beep on the dose rate monitoring unit any time the beam is on.

Figures 3.7 and 3.8 show the audio recording of both fields from a lung treatment plan. The high audio signal corresponds to each energy layer delivery, including all of the beamlet spots within the layer.

Figure 3.6. Dose rate monitor

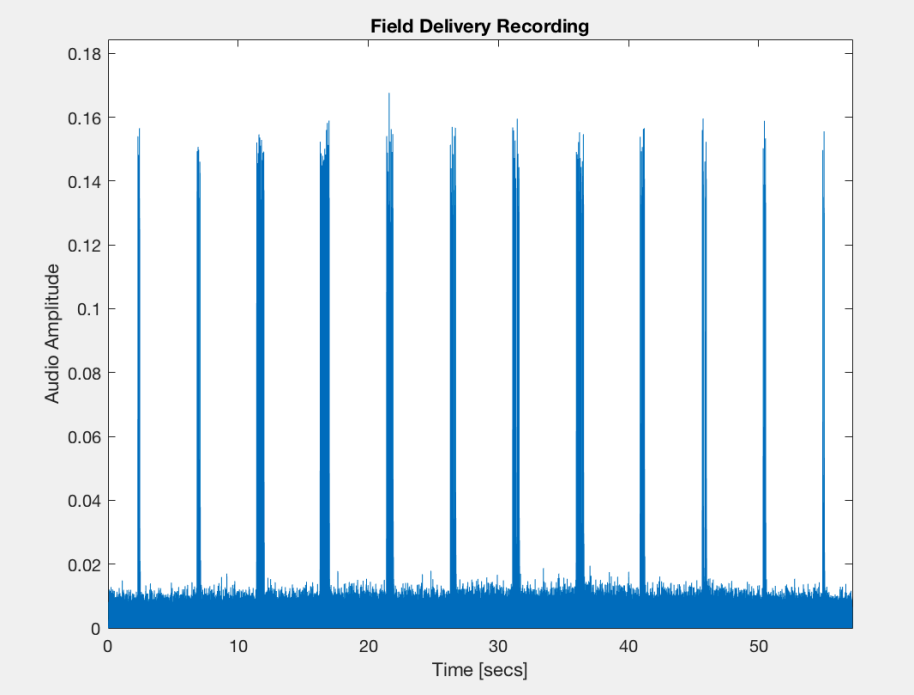

Figure 3.7. Field 1 - Measured dose delivery

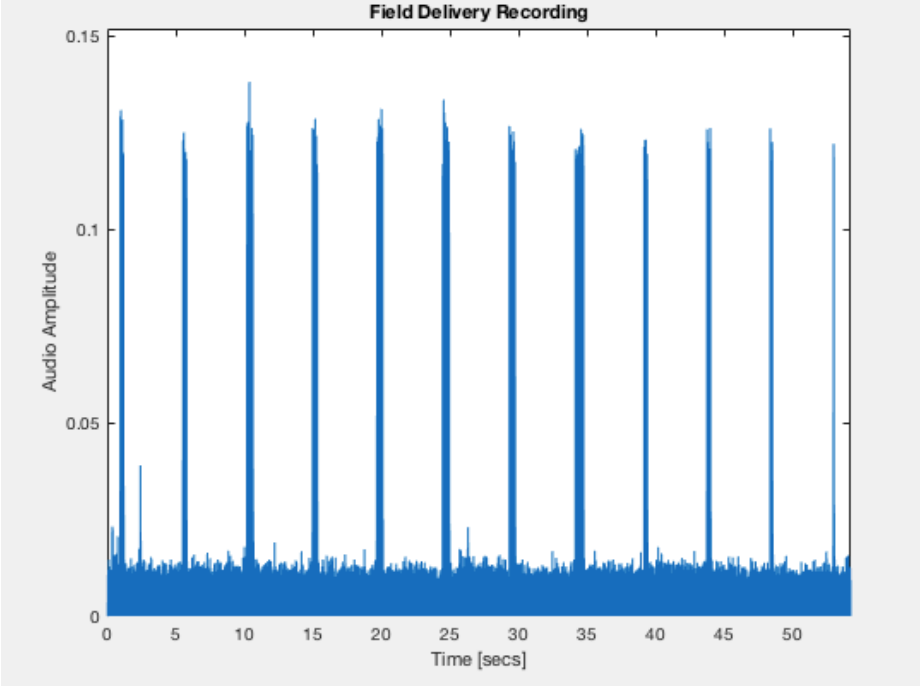

Figure 3.8. Field 2 - Measured dose delivery

Dose Rate Audio Analysis

The proton pencil beam scanning (PBS) treatment field delivery time scale is dominated by the amount of time the system requires to change between energy layers. Energy changes are much longer than changing between individual spots because the energy degrader must be further inserted into the proton beam, to reduce the range of the proton beam. After the energy has been reduced for the next energy layer, the entire beam line and gantry optics have to be returned to match the energy of the treatment layer. Based on the measured dose rate files, this process requires about 4.385 seconds.

Energy Switching Time

The most significant factor in modeling the time scale of the proton dose delivery of the IBA machine at PCPT is from energy switching time. Figure 3.7 and Figure 3.8 display audio recordings of the dose rate monitor signal from the secondary dose recording device (DCEU) shown in Figure 3.6.

Figure 3.9 displays the series of Bragg peaks that comprise a pencil beam scanning proton therapy field. Each energy layer shown is normalized to the peak dose making it easy to discern the range, i.e. water equivalent thickness, of each energy layer in the field. All of the fields used to model the proton PBS lung treatment fields are delivered with the same structure of higher energy layers followed by each subsequent lower energy layer.

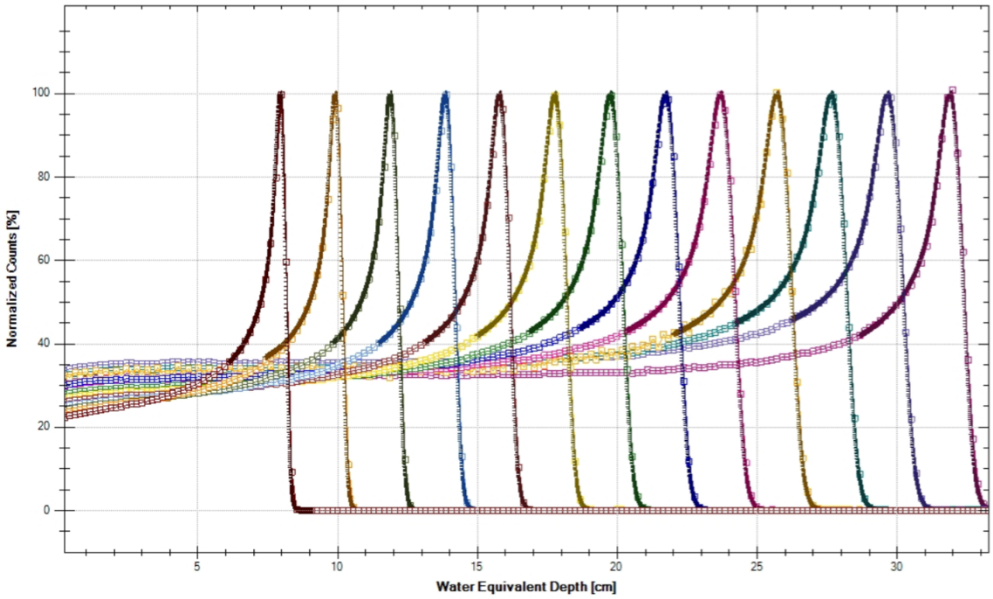

Figure 3.9. Pencil beam scanning energy layer Bragg peaks

The audio recordings from the dose rate monitoring beep were analyzed to calculate the amount of time for the IBA system to change between energy layers. The audio files were converted into amplitude vectors and analyzed in the forward and reverse direction.

When analyzing the audio files in the forward direction the start time was detected when the amplitude exceeded 45% of the maximum audio level. In order to find the next energy layer start time, the search was resumed three seconds after the start of the last detected layer. In order to calculate the energy layer end time, the audio files were analyzed in the reverse direction. The start and end times were compared for the field deliveries in the example lung treatment plan. Field 1 required an average of 4.383 seconds to transition between energy layers and field

2 required 4.384 seconds. A value of 4.385 seconds was used in the model of field delivery time based on this data.

Interspot Dead Time

Interspot dead time refers to the amount of time it takes for the scanning magnets to transition from on spot position in the PLD to another. This dead time was calculated in the model to ensure that the length of time for delivery of each layer in the measured audio matched the length of time in the audio recording. The model provided a close match to the measured dose delivery with an interspot dead time of 10 milliseconds.

Monitor Unit Rate Calculation

In order to calculate the time required for each individual spot, the monitor unit (MU) rate of the system had to be determined. Once the beam current in amperes (Coulomb/sec) was established for each energy in the clinical delivery range it could be converted using the stopping power to a dose rate (Gray/sec). After the dose rate was established for each energy, the system calibration between MUs and dose (cGy) for each energy was used to determine the MU rate at each energy (MU/sec).

Modeling of Proton PBS Treatment Field Delivery Time

This section describes features of the model used to determine the delivery time of a proton PBS treatment field. Individual parameters of a PBS treatment machine and pencil beam are evaluated to determine their contribution to the total delivery time. These parameters include energy selection system (ESS) efficiency, beam current requested, beam energy and range conversion, dose rate and monitor unit rate. All of the data was interpolated with a least-squares exponential fit. Fitting the data allowed the model to include the full range of values used in PLD field specification. The structure of the exponential fit function is shown in Equation 3.1. The coefficients A, B, C and D are used to fit the curve to the data.

$$f(x) = A \cdot e^{B \cdot x} + C \cdot e^{D \cdot x} \qquad 3.1$$

Energy Selection System Efficiency

The energy selection system (ESS) used in IBA proton therapy equipment is located just beyond the cyclotron shown in Figure 3.1. The energy degrader is located after the proton beam exits the extraction channel of the cyclotron. The proton beam is extracted at a specific radius and magnetic field. This final extraction radius results in a final energy of 230 MeV, two thirds the speed of light. Figure 3.10 shows the ESS efficiency of the IBA proton system at PCPT.

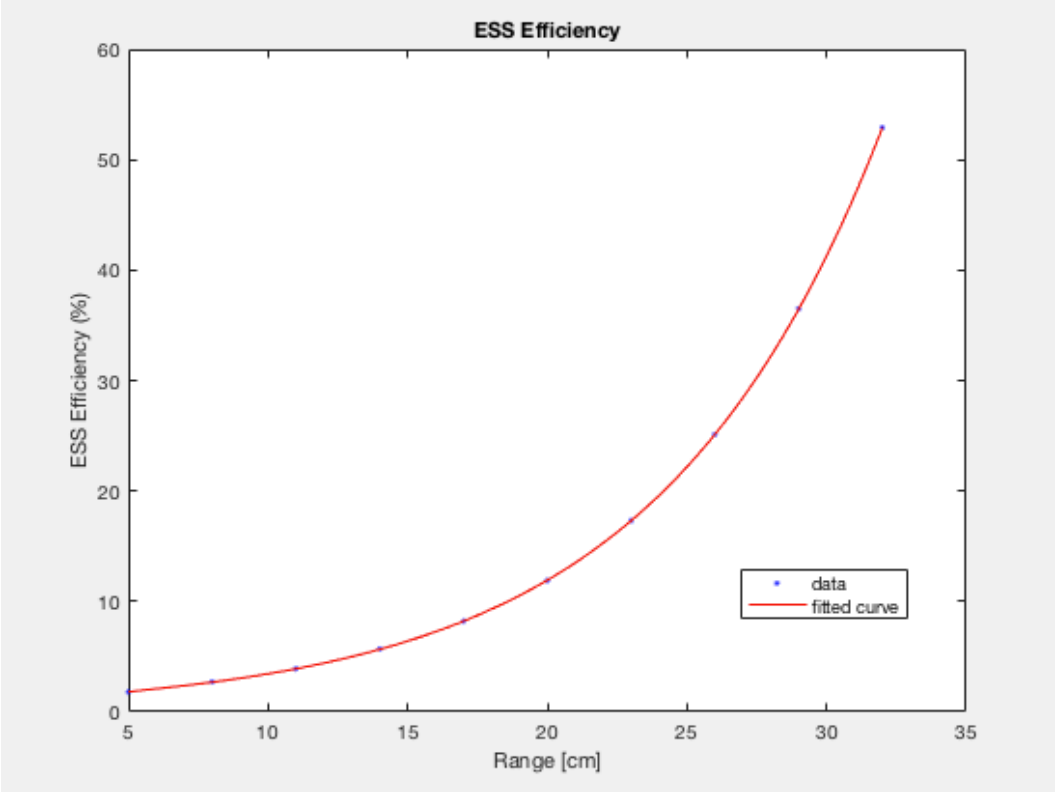

Figure 3.10. Energy selection system efficiency

After the proton beam is extracted from the cyclotron, an energy degrader is used to reduce the energy of the proton beam from the final cyclotron extraction energy down to the specific energy required for each layer within a treatment field. The ratio of beam current extracted from the cyclotron to that transmitted down the beam line after the energy degrader and energy selection system is referred to as the ESS efficiency.

At high energies, the ESS efficiency of the PCPT proton therapy installation are more comparable to those of the installation at Massachusetts General Hospital (MGH), 53% vs 40% at 32cm range, but efficiency differs significantly at lower

energies [16]. The lower energy ESS efficiency at PCPT is improved from the MGH data, 2.7% vs 1%. The improved ESS efficiency at PCPT is largely due to an updated degrader design. The PCPT degrader makes use of beryllium rather than graphite at lower energies, resulting in less scatter and higher ESS transmission efficiency.

Beam Current Request

The amount of beam current request from the cyclotron is energy dependent. In order to deliver lower energy proton beams to the treatment room, the energy degrader must be placed further into the path of the beam. As the protons pass through the energy degrader, their energy is reduced and thus their water equivalent depth in the patient is also reduced. In addition to reducing the energy of the beam the energy degrader also scatters the beam. Some of these scattered protons result in too large of an angle to be transported down the beam line.

To compensate for the loss of proton transmission efficiency, the IBA system increases the beam current requested from the cyclotron. This is accomplished by increasing the output from the ion source at the center of the ion source. This process is known at beam current feedback. Figure 3.11 displays the range of beam current requests for different deliveries.

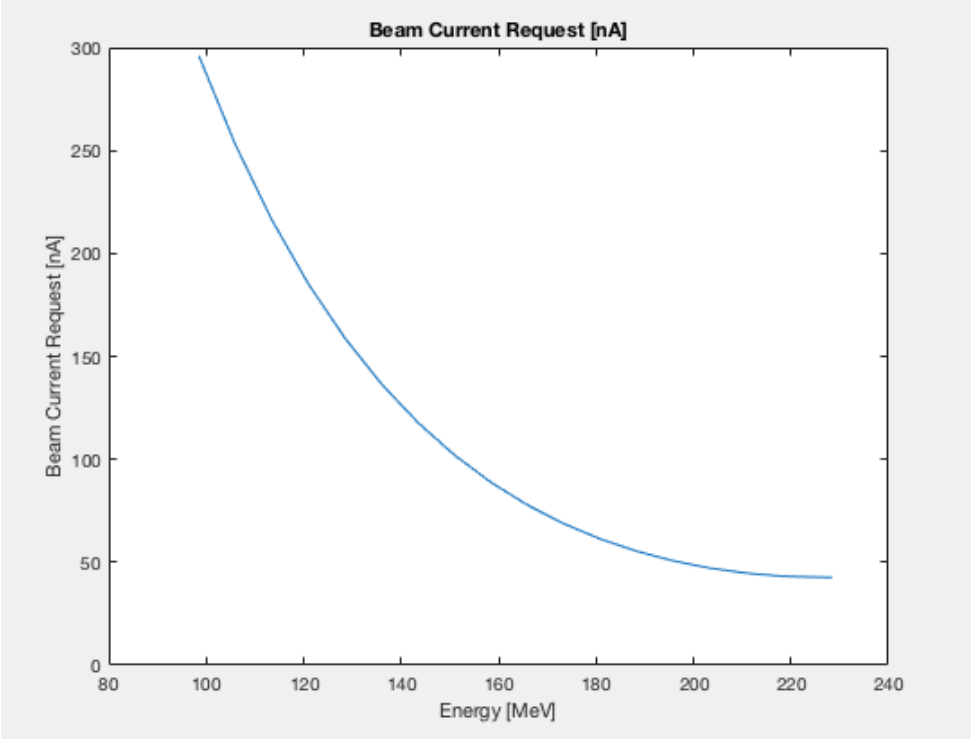

Figure 3.11. Beam current request [nA]

Shallow treatment fields, such as treatments close to the skin, may request in excess of 200 nA. Deeper treatment fields that require less energy degrader insertion, such as prostate treatments, may produce a beam current request of less than 50 nA. Figure 3.12 shows the inverse relationship between ESS efficiency and beam current requested. This relationship exists to keep the downstream beam current in a narrow range to provide stable dose rate monitoring. The beam current delivery at each energy in the treatment field is the product of the ESS efficiency multiplied by the beam current requested from the cyclotron.

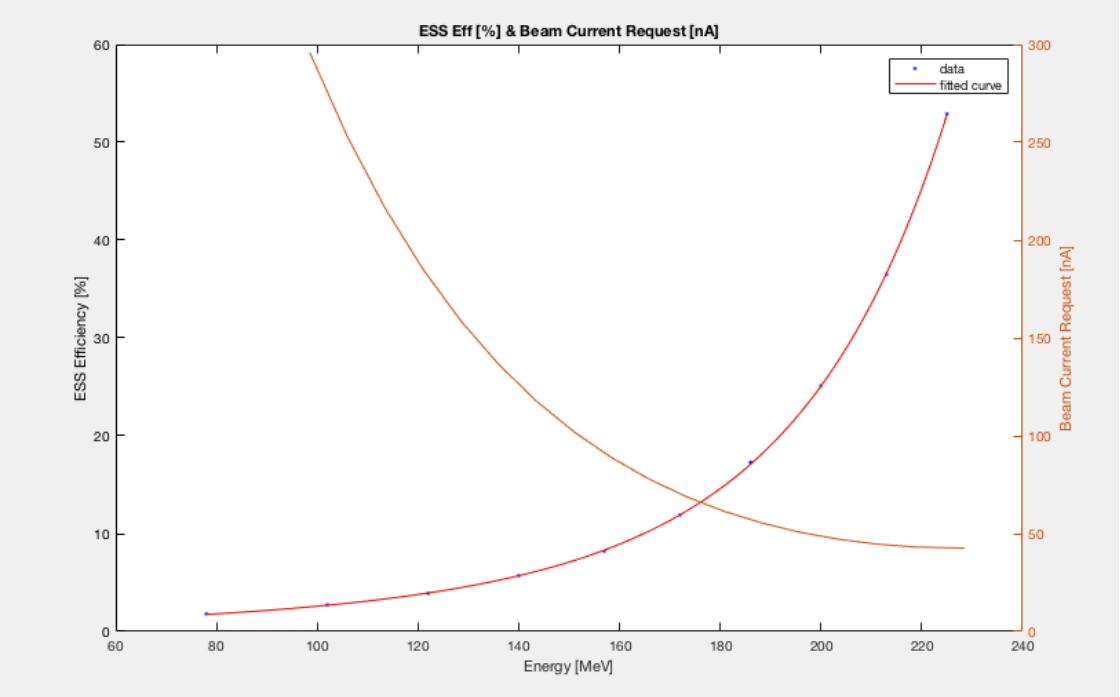

Figure 3.12. ESS Efficiency [%] vs Beam current request [nA]

Proton Fluence Rate

This section describes the calculation of fluence based on the field delivery parameters of the IBA system. Fluence is a measure of the number of protons per unit area. The proton fluence rate is calculated across the range of energies used in clinical proton radiation therapy. The ESS efficiency, full width half max (FWHM), and beam current request parameters were acquired during commissioning and during field delivery.

The beam current requested from the cyclotron is an energy dependent parameter specific to the IBA system. The requested beam current varies with energy to

ensure that after losses through the ESS and beam transport there is sufficient beam current for accurate beam measurement downstream of the energy degrader.

The FWHM is a statistical parameter with a width of 2.355 standard deviations taken from a Gaussian distribution of the data. The FWHM used to provide the surface area over which the calculated beam current was delivered. The FWHM was measured during the clinical commission of the IBA proton therapy equipment at the Provision Center for Proton Therapy (PCPT) [17]. Figure 3.13 displays the FWHM of the proton beam at the entrance as a function of energy. The lower energies have a larger spot size due to lower energies scattering more in air and additional scatter from passing through a thicker part of the degrader.

Conversion Between MeV and Range

Figure 3.14 shows the relationship used to convert data from range in centimeters to proton beam energy in megaelectron volts. The conversion was done using water equivalent range [18].

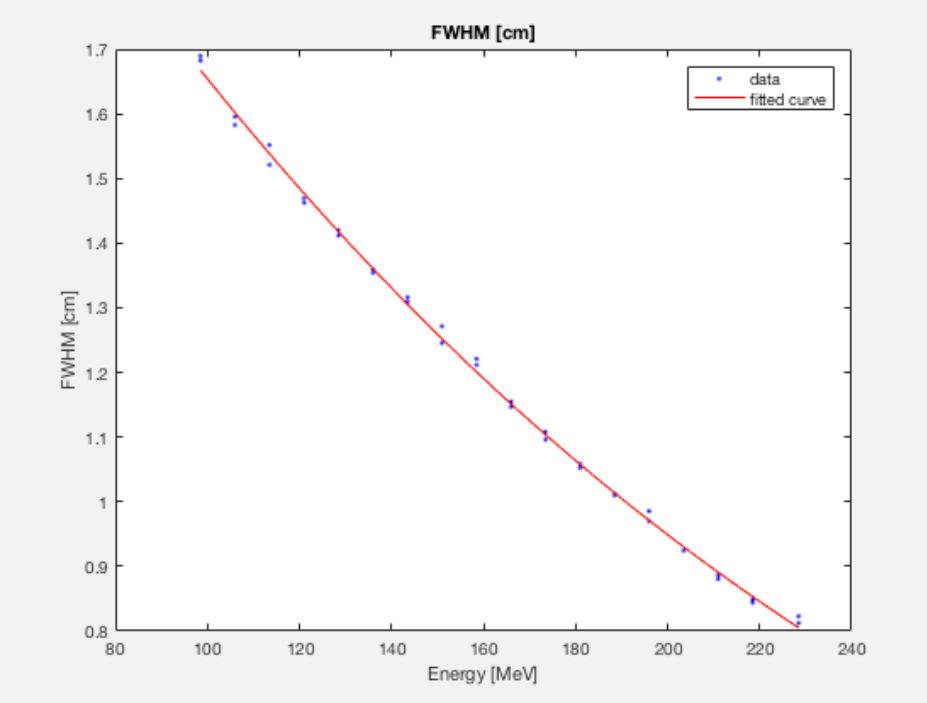

Figure 3.13. Full width half max (FWHM) of the proton beam spot vs. energy

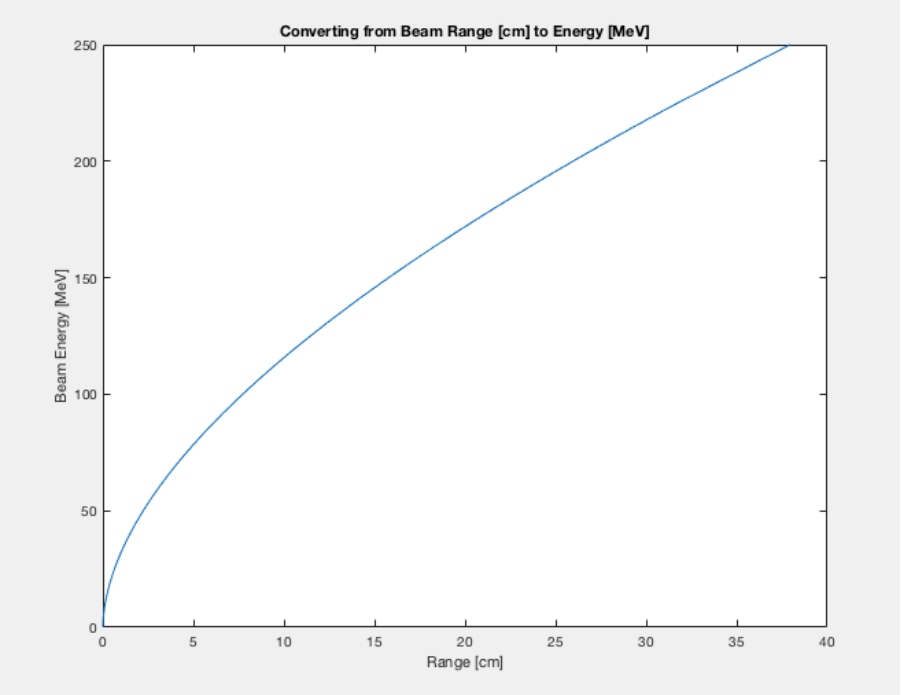

Figure 3.14. Proton range [cm] to energy [MeV] conversion

Dose Rate

This section describes the conversion from beam current to proton fluence rate. Proton fluence rate was calculated using the delivery spot size (FWHM), ESS efficiency and beam current request. Equation 3.2 refers to the dose rate calculation and Equation 3.3 refers to the proton fluence rate. Figure 3.15 shows the resulting dose rate in cGy per second resulting from the other parameters such as FWHM, beam current, and stopping power. Equation 3.4 shows, the beam current used in the dose rate calculation using the product of the beam current requested from the cyclotron multiplied by the ESS efficiency. Both ESS efficiency and the beam current request are energy dependent.

$$\frac{dD}{dt} = \frac{d\varphi}{dt}\left(\frac{dE}{dx}\right)\frac{1}{\rho} \qquad 3.2$$

$$\frac{dD}{dt} = Dose\ Rate\ \left[\frac{Gray}{sec}\right]$$

$$\frac{d\varphi}{dt} = \frac{I}{p \cdot A} \qquad 3.3$$

$$\frac{d\varphi}{dt} = Fluence\ Rate\ \left[\frac{protons}{cm^2 \cdot secs}\right]$$

$$I = Beam\ Current\ \left[\frac{C}{s}\right]$$

$$I = ESS\ Eff \cdot Beam\ Current\ Request \left[\frac{C}{s}\right] \quad 3.4$$

$$\frac{dE}{dx} = Mass\ Stopping\ Power \left[\frac{MeV \cdot cm^2}{g}\right]$$

$$\rho = density \left[\frac{g}{cm^3}\right]$$

$$A = Area = \pi\left(\frac{FWHM}{2}\right)^2 \ [cm^2]$$

$$p = proton\ charge \left[\frac{Coulomb}{proton}\right]$$

$$MeV \ = 1.602 \times 10^{-13}\ Joules$$

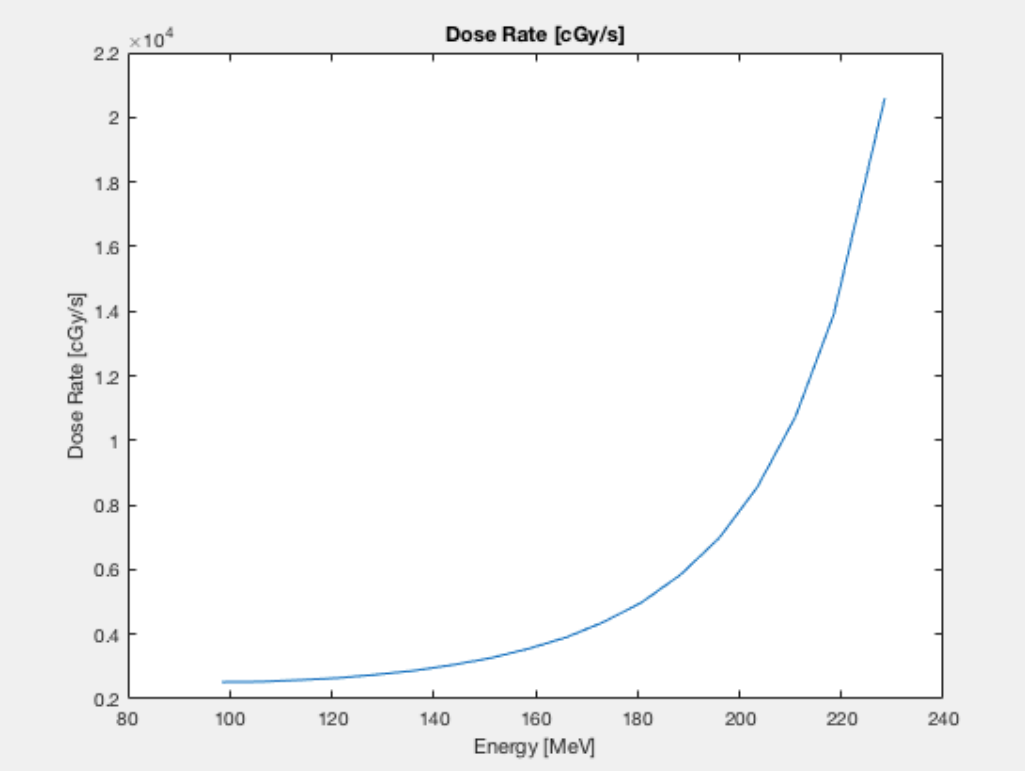

Figure 3.15. Dose rate [cGy/s] vs. energy [MeV]

Monitor Unit Rate

The Monitor Unit (MU) rate is the final piece to establish the dose delivery time scale from the pencil beam scanning layer definition (PLD) file associate with each treatment field. Figure 3.16 displays the relationship between MU and dose used by the treatment planning system to create clinically deliverable treatment fields. The relationship between entrance dose and range shown in Figure 3.16 was used to convert the dose rate for each spot in each energy layer into monitor units per second (MU/s), shown in Figure 3.17. MU/s was the final parameter used to calculate the time required for each spot at a given energy.

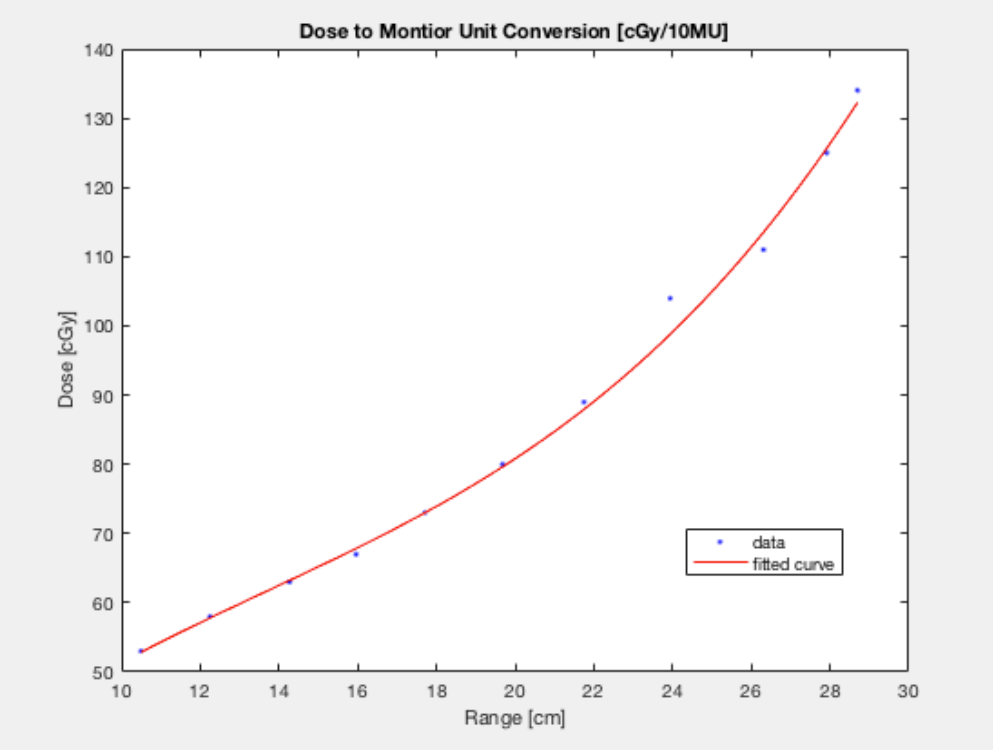

Figure 3.16. Dose [cGy/10MU] vs. range [cm]

Table 3.2 lists some of the first spots, interspot dead time, and the first energy change to deliver the second energy layer. The left column represents the time in seconds while the right hand column lists the does rate in MU/s. Table 3.2 also demonstrates the 4.385 seconds that is required for the machine to transition between energy layers. Notice that each spot's individual delivery time it is extremely short, often much shorter than the 10 millisecond interspot dead time. The significant amount of time dedicated to interspot dead time and energy layer transitions demonstrates the importance of modeling the machines delivery timescale in order to properly represent the resulting does perturbation that occurs as result of tumor target motion.

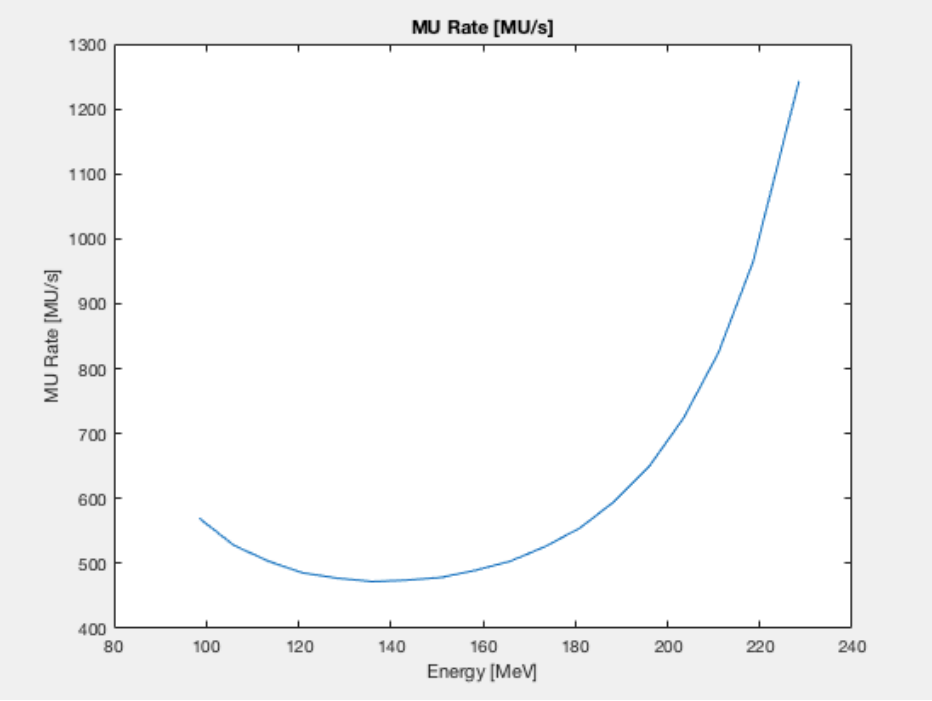

Figure 3.17. Monitor unit rate [MU/sec]

Table 3.2. Pencil beam scanning layer definition spot, interspot, and layer switching time

Time [secs]	Dose Rate [MU/sec]
0.000945517	480.8606824
0.01	0
0.000225585	480.8606824
0.01	0
0.000582868	480.8606824
0.01	0
4.385	0
0.006075084	477.1260972
0.01	0
0.017367621	477.1260972
0.01	0
0.001507805	477.1260972

Model of Respiratory Cycle

Respiratory Cycle Binning During 4D CT

A 4D CT refers to a computed tomography X-ray based diagnostic scan that is acquired over multiple breathing cycles. This allows CT slices to be captured at all of the respiratory amplitudes included in a patient's inhale and exhale. Ultimately the respiratory inhale and exhale cycle is broken up into 10 individual computed tomography CT scans. Each of these scans is comprised of all the CT slices acquired at a certain amplitude during the patient's inhale or exhale. This results

in five inhale CT scans and five exhale CT scans taken in 20% amplitude increments.

Respiratory Cycle Approximation

In order to calculate to which respiratory amplitudes the energy layer delivery corresponded, a model of the respiratory signal was created. Figure 3.18 displays one cycle of the respiratory amplitude produced from a breathing rate of 15 breaths per minute. The model that was developed allows for modification of this respiration rate, as it will vary from patient to patient. The shape of the respiratory cycle model is based on a sine wave shown by the blue part of the curve and an exponential decay shown in the orange part of the curve. The relative lengths of the inhale and exhale phase are about one third and two thirds, respectively. This ratio between the inhale and exhale phases of the respiratory cycle is designed to approximate thoracic respiratory motion. [9]

Figure 3.19 demonstrates the overlay of a 15 breaths per minute respiratory cycle with the modeled machine delivery time for treatment field 1 and respiratory amplitude during dose delivery. Figure 3.20 displays the corresponding respiratory amplitude associated with each energy layer delivery within the treatment field. The respiratory amplitude and inhalation or exhalation indication allows the dose from each energy layer to be computed on its corresponding phase of the 4D CT scan.

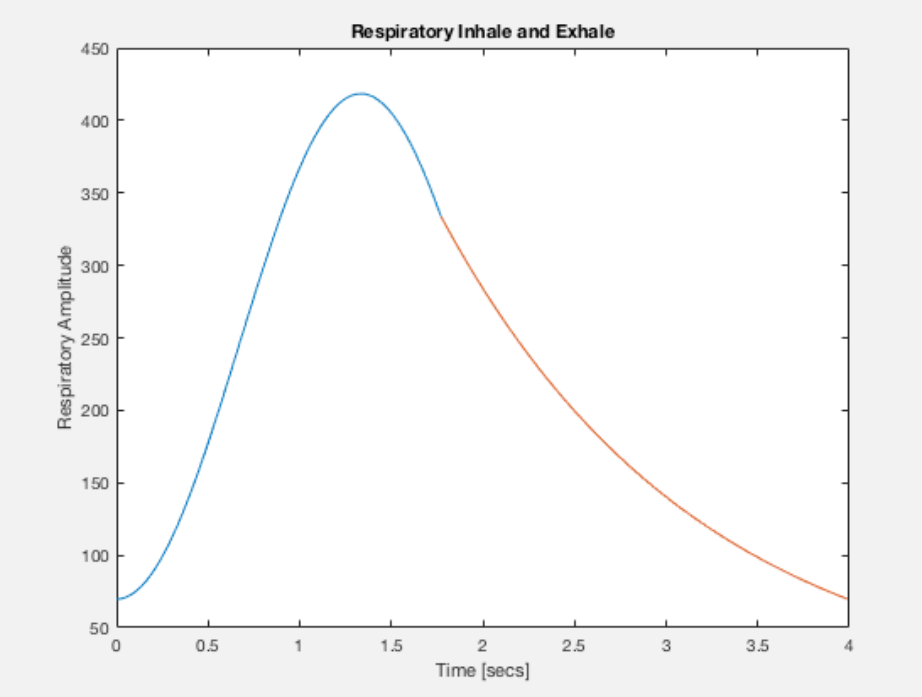

Figure 3.18. Respiration inhale and exhale

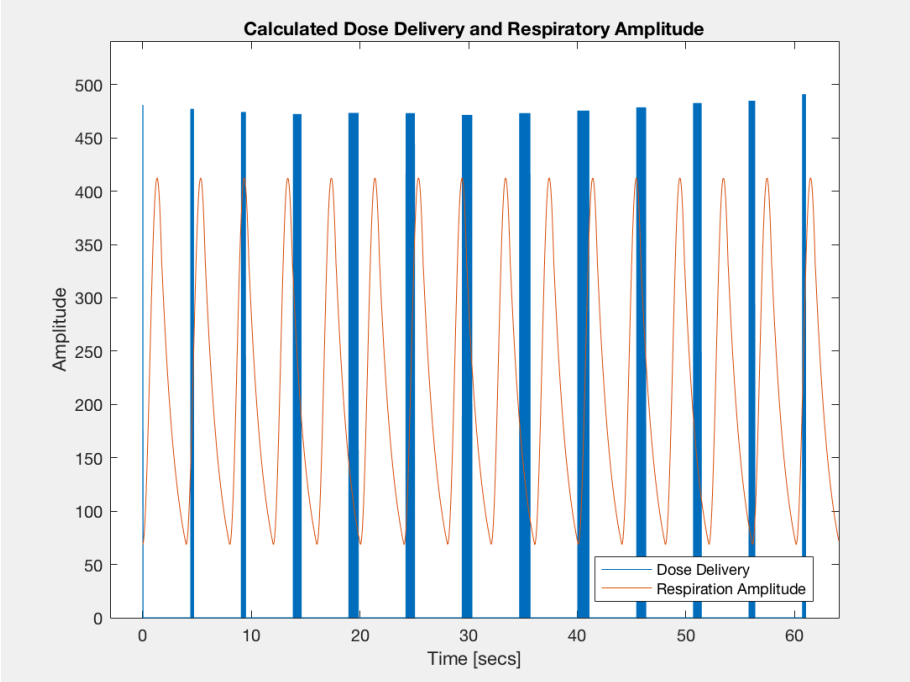

Figure 3.19. Field 1 – Modeled respiration and dose delivery

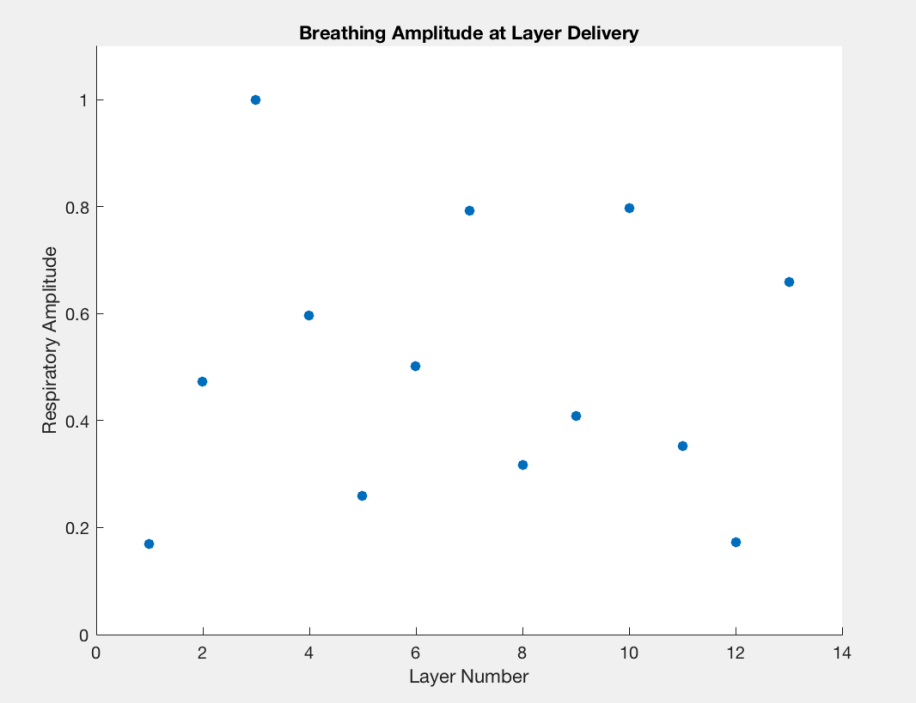

Figure 3.20. Field 1 - Layer and respiration intersection

Table 3.3 displays the respiratory amplitude during each energy layer delivery along with an indication as to the inhale or exhale component of the respiratory cycle. Once each energy layer of field 1 has been computed on its corresponding 4D CT phase, the dose from each 4D CT phase can be deformed onto a single phase of the 4D CT for evaluation.

Figure 3.21 demonstrates the overlay of a 15 breaths per minute respiratory cycle with the modeled machine delivery time for treatment field 2. Figure 3.22 displays the corresponding respiratory amplitude associated with each energy layer delivery within the treatment field.

Table 3.3. Field 1 - Layer and respiration intersection

Layer	Amplitude	In [1] or Ex [-1]
1	0.17	1
2	0.47	1
3	1.00	1
4	0.60	-1
5	0.26	-1
6	0.50	-1
7	0.79	1
8	0.32	-1
9	0.41	-1
10	0.80	-1
11	0.35	1
12	0.17	1
13	0.66	-1

Table 3.4 displays the respiratory amplitude during each energy layer delivery along with an indication as to the inhale or exhale component of the respiratory cycle for field 2. In the third column of the Table 3.4, a “1” indicates an inhale component of the respiratory cycle and a “-1” indicates an exhale component of the respiratory cycle. The respiratory amplitude and inhalation or exhalation indication allows the dose from each energy layer to be computed on its corresponding phase of the 4D CT scan. Once each energy layer from field 2 has been computed on its corresponding CT the composite this delivery can be deformed onto a single phase of the 4D CT for evaluation. The summation of the deformed dose from field 1 and field 2 gives the composite perturbed dose as modeled by the PMTM energy layer and respiratory amplitude intersections.

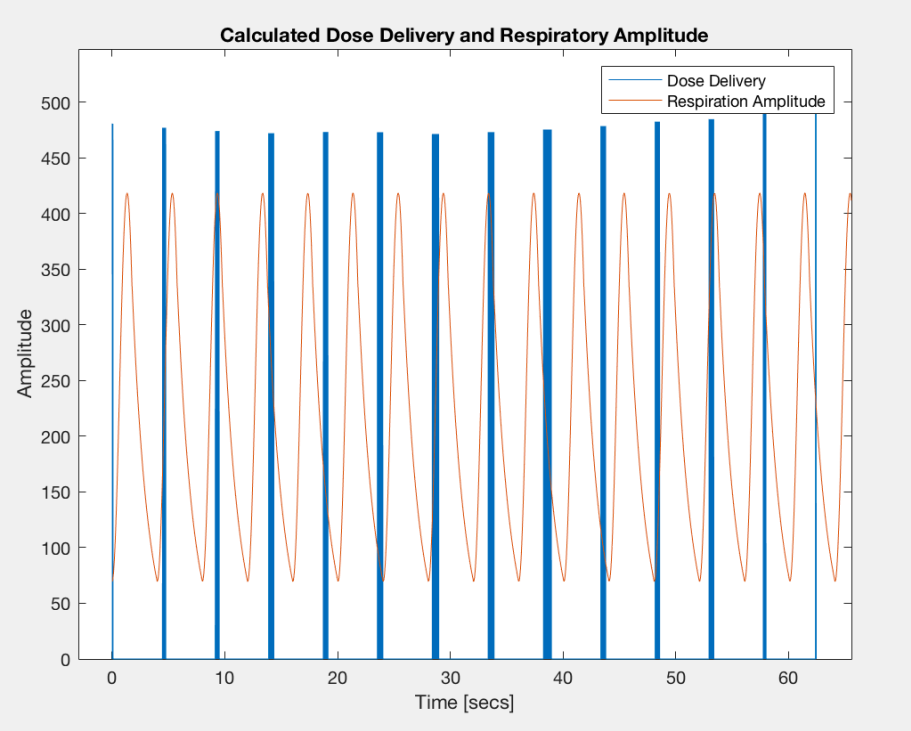

Figure 3.21. Field 2 – Modeled respiration and dose delivery overlay

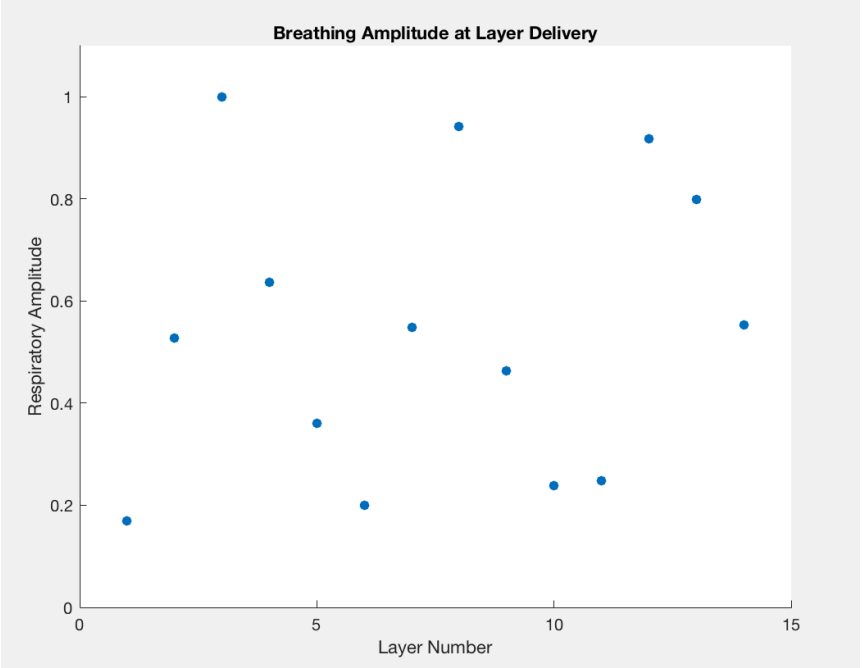

Figure 3.22. Field 2 - Layer and respiration intersection

Table 3.4. Field 2 - Layer and respiration intersection

Layer	Amplitude	In [1] or Ex [-1]
1	0.17	1
2	0.53	1
3	1.00	1
4	0.64	-1
5	0.36	-1
6	0.20	-1
7	0.55	1
8	0.94	-1
9	0.46	-1
10	0.24	-1
11	0.25	1
12	0.92	1
13	0.80	-1
14	0.55	-1

Once the corresponding respiratory amplitude and inhalation or exhalation has been determined for each energy layer delivery in both treatment fields each energy layer can be recalculated on its corresponding 4D phase.

Frequency Matching

This section demonstrates the potential for frequency matching (FM), which results when the respiratory frequency and machine frequency are close enough that all of the energy layers are delivered in the same phase of the 4D CT.

FM could have a significant impact on proton pencil beam scanning (PBS) treatment delivery by minimizing the necessity for more cumbersome motion

mitigation approaches such as breath hold techniques or machine gating. Based on the information from the 4D CT, the treatment plan could be optimized such that it is deliverable on any phase of the 4D CT. Once the treatment plan has been optimized across all CT phases, FM could be sufficient by itself. This would entail measuring the patient's respiratory rate in the treatment room and matching it to the machine delivery rate.

Figure 3.23 shows the results of field 1 delivered at a respiration rate of 11.8 breaths per minute. FM allows for all of the energy layers in field 1 to be delivered at the same respiratory amplitude.

Figure 3.24 displays the respiration amplitude at which each of the energy layers would be delivered with FM at 11.8 breaths per minute. The plot displays all of the energy layer deliveries intersecting the respiratory amplitude on a nearly horizontal line. Synchronizing the respiratory rate with the rate at which energy layers are delivered allows for FM and an unperturbed dose delivery.

Table 3.5 displays the respiratory amplitude at each intersection of the energy layers in field 1. FM allows for the layers to all be delivered on the same phase of the 4D CT. The intersection amplitude ranges from 0.17 to 0.3, normalized to the maximum respiratory amplitude.

Figure 3.23. Field 1 – Respiration and dose delivery

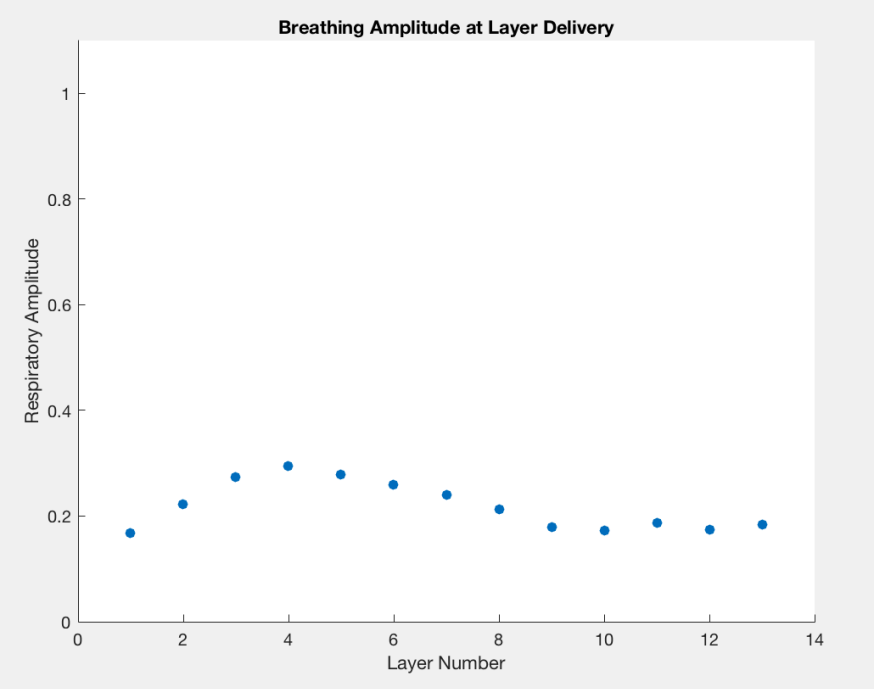

Figure 3.24. Field 1 - Layer and respiration intersection

Table 3.5. Field 1 - Layer and respiration intersection

Layer	Amplitude	In [1] or Ex [-1]
1	0.17	1
2	0.22	1
3	0.27	1
4	0.30	-1
5	0.28	-1
6	0.26	-1
7	0.24	1
8	0.21	-1
9	0.18	-1
10	0.17	-1
11	0.19	1
12	0.17	1
13	0.18	-1

Figure 3.25 shows field 2 delivered at a respiration frequency of 12.4 breaths per minute. Frequency matching (FM) allows for all of the energy layers in field 2 to be delivery at the same respiratory amplitude. Figure 3.26 displays the respiration amplitude at which each of the energy layers would be delivered with FM of field 2 at 12.4 breaths per minute. The increase in the respiration rate to achieve frequency matching when comparing field 1 to field 2 is most likely due to field 2 having one fewer energy layer, 13 vs 14 energy layers and the individual energy layers in field 1 being delivered more quickly. When comparing the individual energy layers within each treatment field, the longest energy layers in field 1, Figure 3.21, are delivered more quickly than in Figure 3.25, field 2, as shown by the narrower width of the field 1 energy layers.

The plot displays all of the energy layer deliveries intersecting the respiratory amplitude on a nearly horizontal line. Synchronizing the respiratory frequency with the energy layer delivery allows for FM and an unperturbed dose delivery. Table 3.6 displays the respiratory amplitude at each intersection of the energy layers in field 2. FM at 12.4 breaths per minute allows for the layers to all be delivered on the same phase of the 4D CT. The intersection amplitude ranges from 0.17 to 0.22.

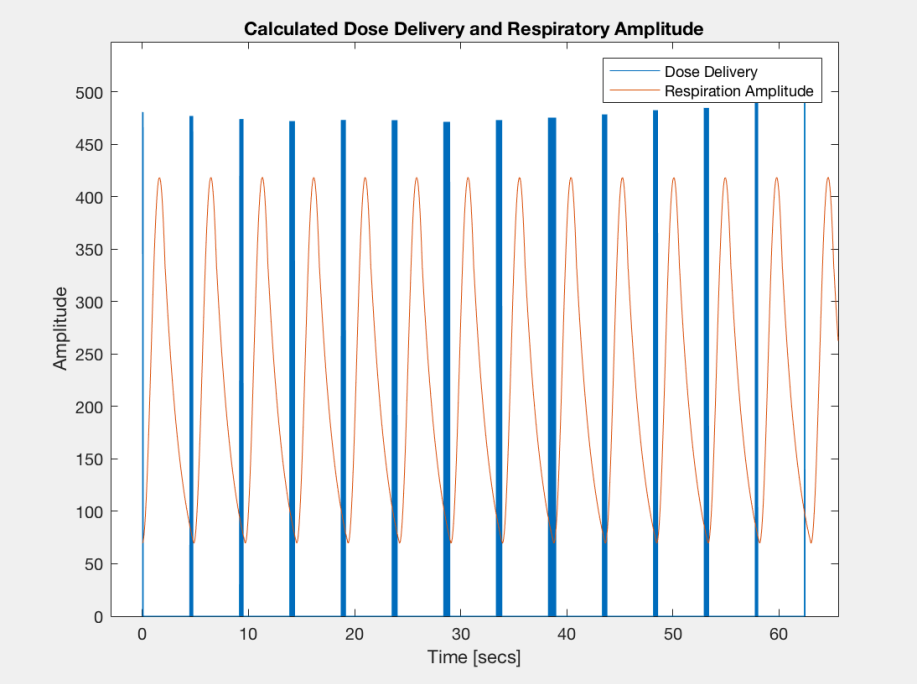

Figure 3.25. Field 2 - Respiration and dose delivery

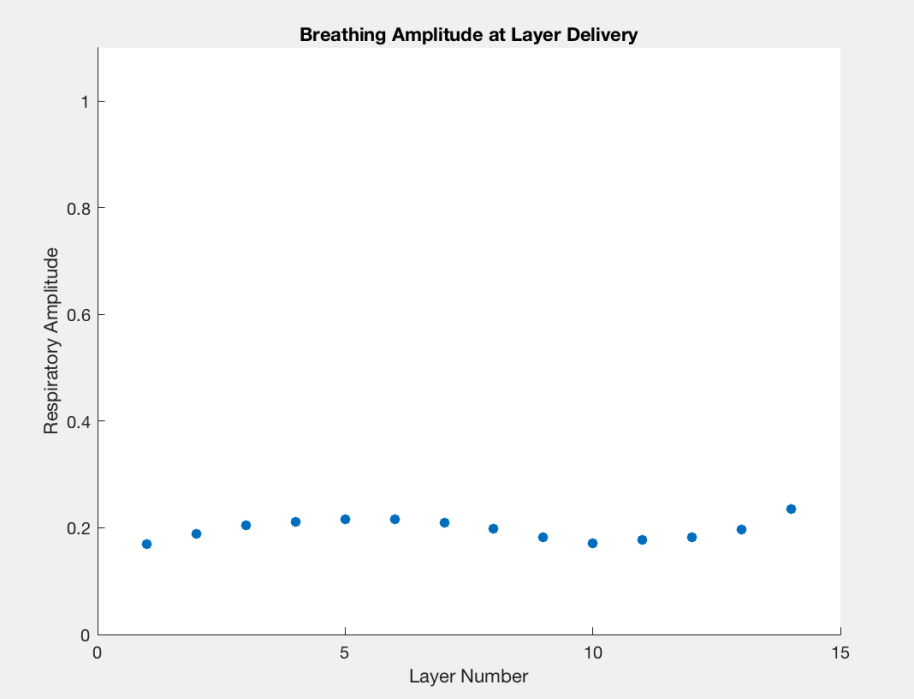

Figure 3.26. Field 2 - Layer and respiration intersection

Table 3.6. Field 2 - Layer and respiration intersection

Layer	Amplitude	In [1] or Ex [-1]
1	0.17	1
2	0.19	1
3	0.21	1
4	0.21	-1
5	0.22	-1
6	0.22	-1
7	0.21	1
8	0.20	-1
9	0.18	-1
10	0.17	-1
11	0.18	1
12	0.18	1
13	0.20	-1
14	0.23	-1

CHAPTER FOUR
APPLICATION OF THE PATIENT MACHINE TIME MODEL

This section will discuss the results of applying the patient machine time model (PMTM) to a two field lung treatment plan that was evaluated with a fifteen breathes per minute respiratory rate. The primary purpose of this section is to demonstrate the use of the PMTM to evaluate the dose perturbation from respiratory motion. Frequency matching (FM) is also shown by matching the radiation therapy dose delivery frequency to that of the respiratory frequency.

In this section the respiratory frequency is modified to synchronize with the treatment machines does delivery frequency. The treatment delivery frequency is dominated by energy layer switching time with the inter-spot dead time and monitor unit (MU) delivery rate serving as secondary effects. The treatment machine used to produce the PMTM currently has a fixed energy layer switching time that is too slow to match the respiratory rate of 15 breaths per minute. Another option to achieve FM would be to deliver the energy layers at half the respiration rate to avoid hitting the energy layer switching rate limit. This should allow for all of the energy layers to be delivered on the same phase of the 4D CT but would extend the treatment field delivery time significantly.

Future improvements in technology should allow the energy layer switching time to be reduced significantly. If the energy layer switching time were reduced from the 4.384 seconds available in the current system configuration to below 3 seconds, FM could be achieved at the patient's natural breathing rate.

Alternatively, the patient's respiration frequency could be slowed to match the treatment machine's energy layer delivery frequency. The patient could be coached with audio or visual feedback to slow their respiration rate and achieve FM.

Multi Field Optimization Dose Reconstruction

The section describes the application of the patient machine time model (PMTM) described in Chapter 3. The model was applied to the following two field treatment plan in order to calculate the phases of the 4D CT that each energy layer of dose would be delivered on. Figure 4.1 displays the proton pencil beam scanning treatment plan calculation on one of the 10 phases of the 4D CT. This is equivalent to the dose distribution achieved by frequency matching (FM).

Figures 4.2 and Figure 4.3 display the individual dose contributions from each treatment field. Each individual beam does not provide uniform tumor cover but rather delivers dose in the area where the combine contributions from each treatment field produce an optimal dose distribution. The high dose region of field 1, shown in red, is delivered on the left side of the target volume while the high does from field 2 is delivered on the right side of the target volume. This division of target coverage between the two fields can leave the plan more susceptible to target volume motion form respiration.

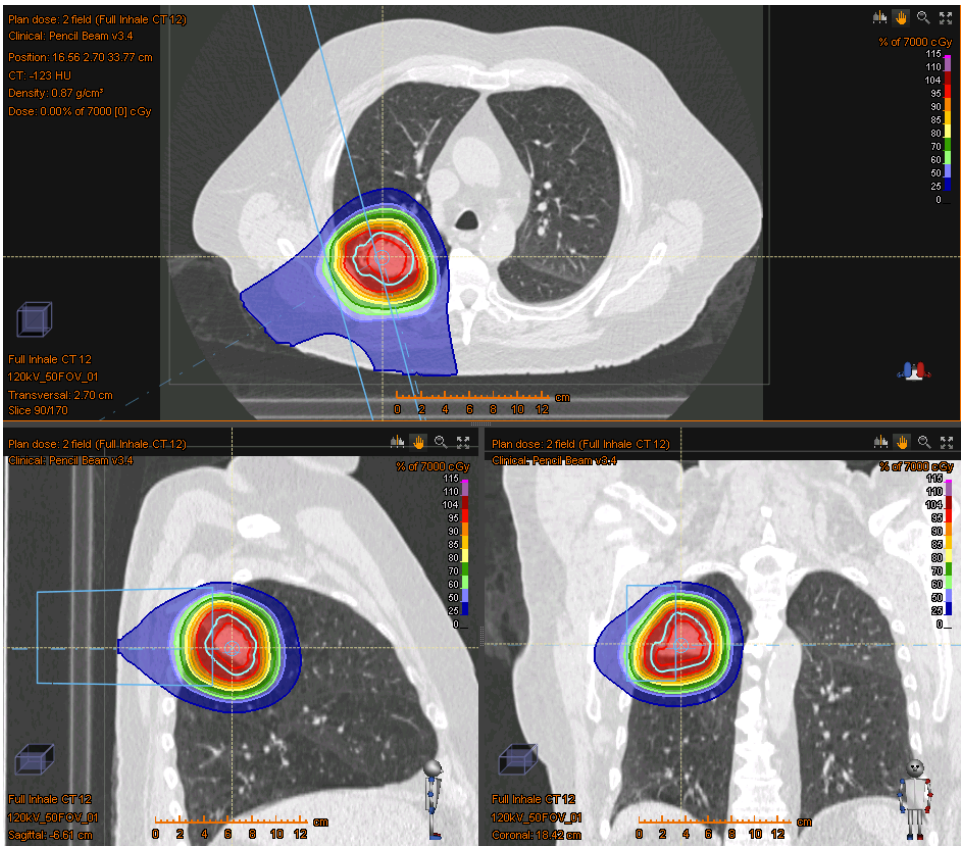

Figure 4.1. Two field lung proton plan used for model testing

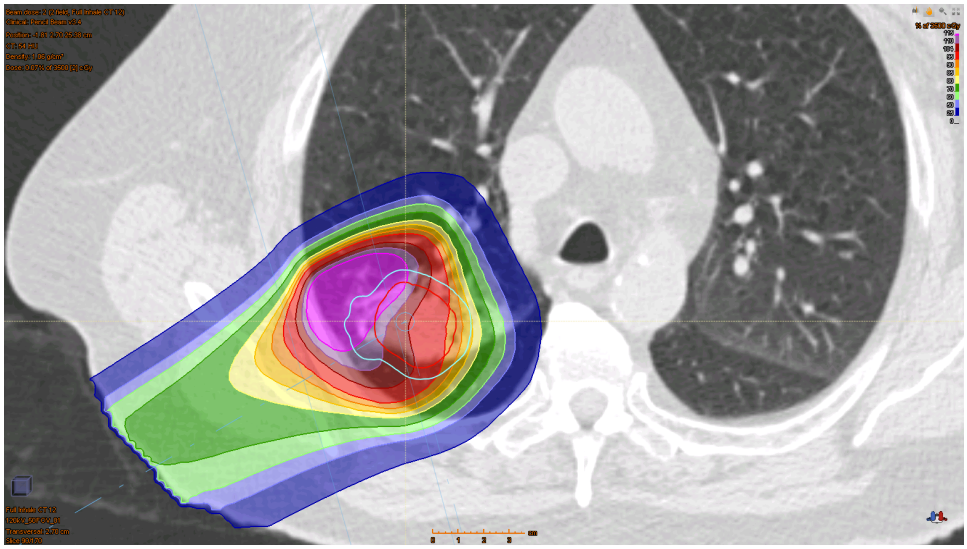

Figure 4.2. Field 1 - Contribution to target coverage using multi field optimization

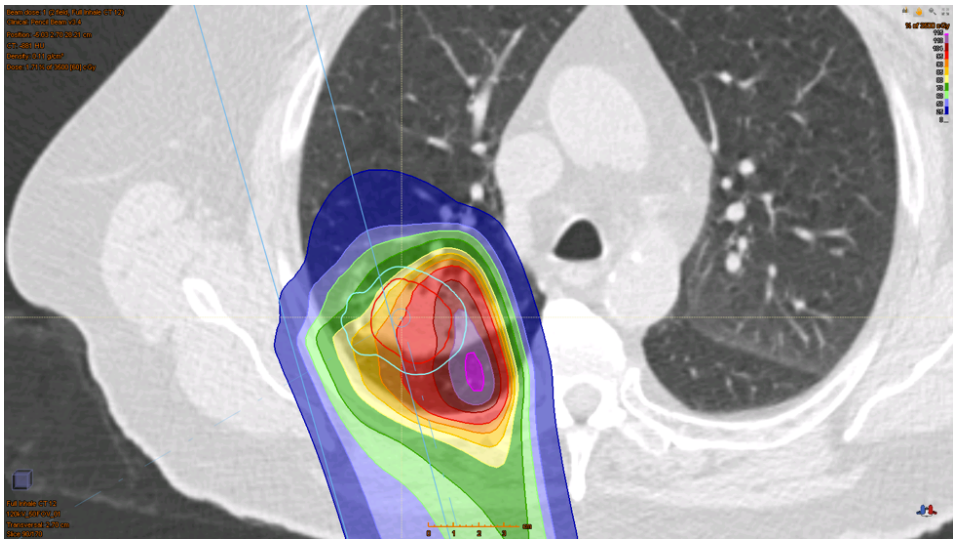

Figure 4.3. Field 2 - Contribution to target coverage using multi field optimization

The treatment plan shown in Figure 4.1 uses multi field optimization (MFO). MFO is a technique in which each field does not provide uniform coverage of the target volume. Alternatively, a field optimization strategy where each individual beam uniformly covers the target volume is known as single field optimization (SFO). An MFO approach was selected to evaluate the potential impact of the PMTM in treatment cases with respiratory motion. The MFO type of optimization used in this example evaluation is not typically applied to targets with respiratory motion because it is more susceptible to dose perturbation from respiratory motion.

Although MFO treatment plans can be more susceptible to dose to respiratory motion they are attractive in scenarios requiring more aggressive tissue sparing. The PMTM developed in this section may provide additional insight into the expansion of MFO to cases with respiratory target motion.

Each energy layer of the treatment plan shown in Figure 4.1 will be calculated on its corresponding 4D CT phase and deformed back to this phase of the 4D CT. The combined dose will provide a representation of the dose delivery as if the patient were to breath at 15 breaths per minute. After the composite dose is evaluated on a single phase of the 4D CT, the respiratory rate to achieve FM will be calculated to represent the delivery of each energy layer on the same phase of the 4D CT.

Figure 4.4 and Figure 4.6 display the respiratory amplitude of each energy layer delivery calculated by the PMTM for treatment field 1 and field 2. The respiratory rate used in the model was 15 breaths per minute. Figure 4.5 and Figure 4.7 display the corresponding respiratory amplitude associated with each energy layer delivery within the treatment field. Table 4.1 and Table 4.2 display the respiratory amplitude during each energy layer. An indication as to the inhale, 1, or exhale, -1, component of the respiratory cycle is displayed in the third column of the table corresponding to each treatment field. The results of the PMTM shown in Table 4.1 and Table 4.2 were used to calculate the dose from each energy layer onto the corresponding phase of the 4D CT.

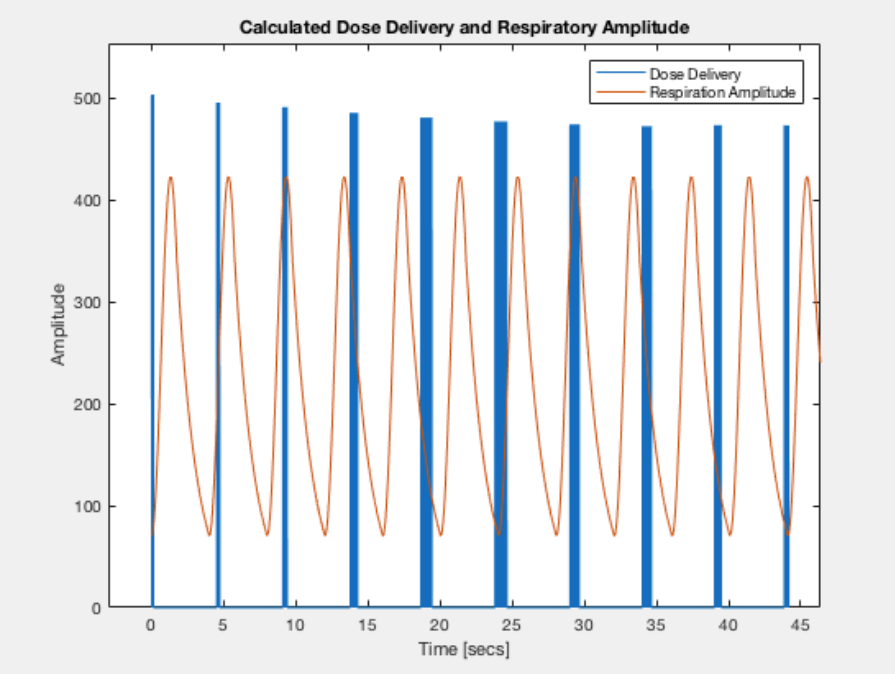

Figure 4.4. Field 1 – Modeled respiration and dose delivery overlay

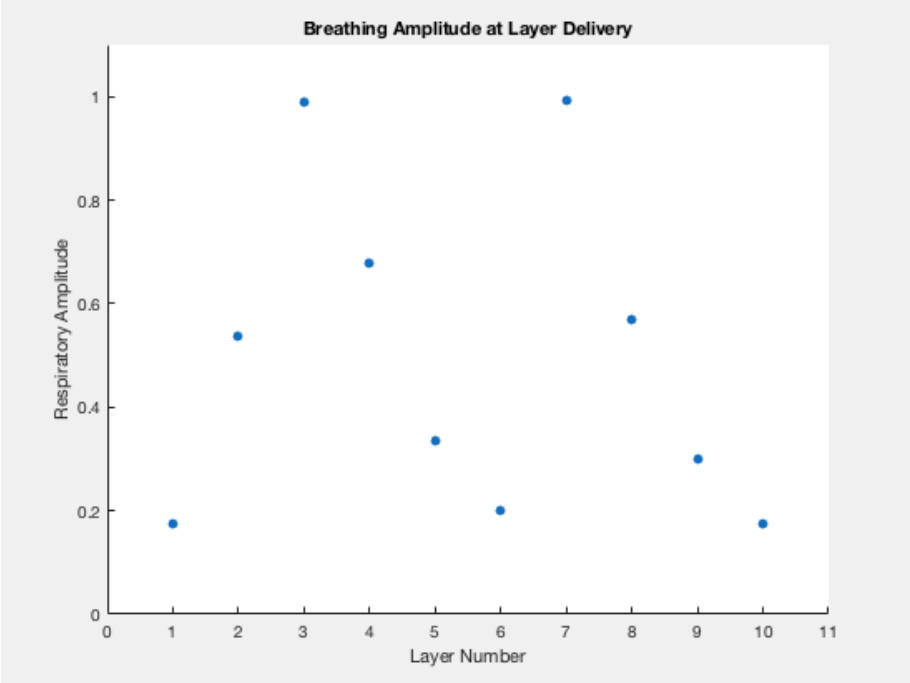

Figure 4.5. Field 1 – Modeled respiration and dose delivery intersection

Table 4.1. Field 1 - Layer and respiration intersection

Layer	Amplitude	In [1] or Ex [-1]
1	0.17	1
2	0.54	1
3	0.99	1
4	0.68	-1
5	0.34	-1
6	0.20	1
7	0.99	1
8	0.57	-1
9	0.30	-1
10	0.18	-1

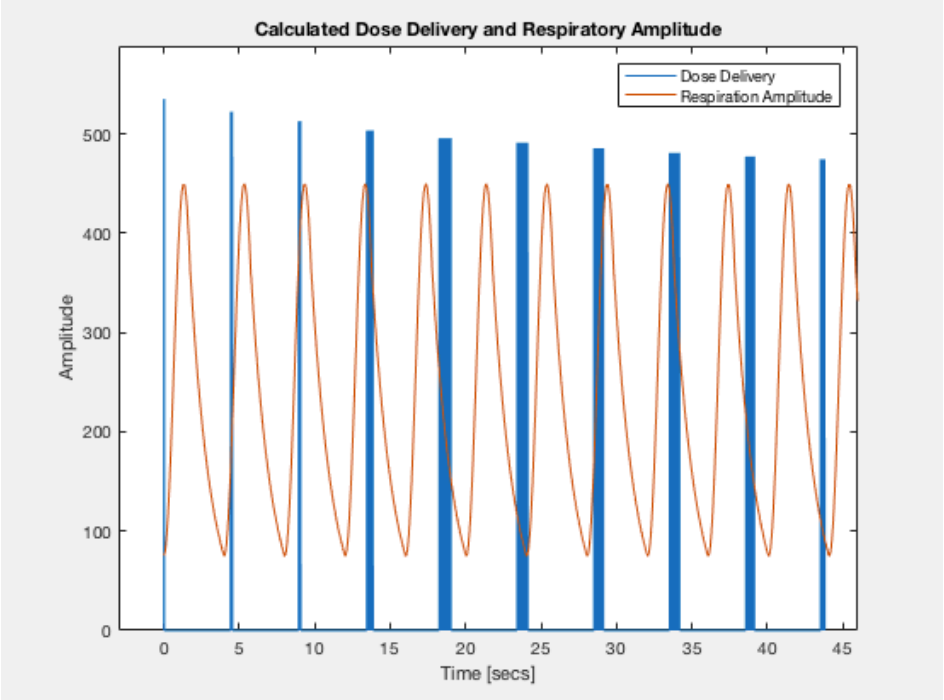

Figure 4.6. Field 2 – Modeled respiration and dose delivery overlay

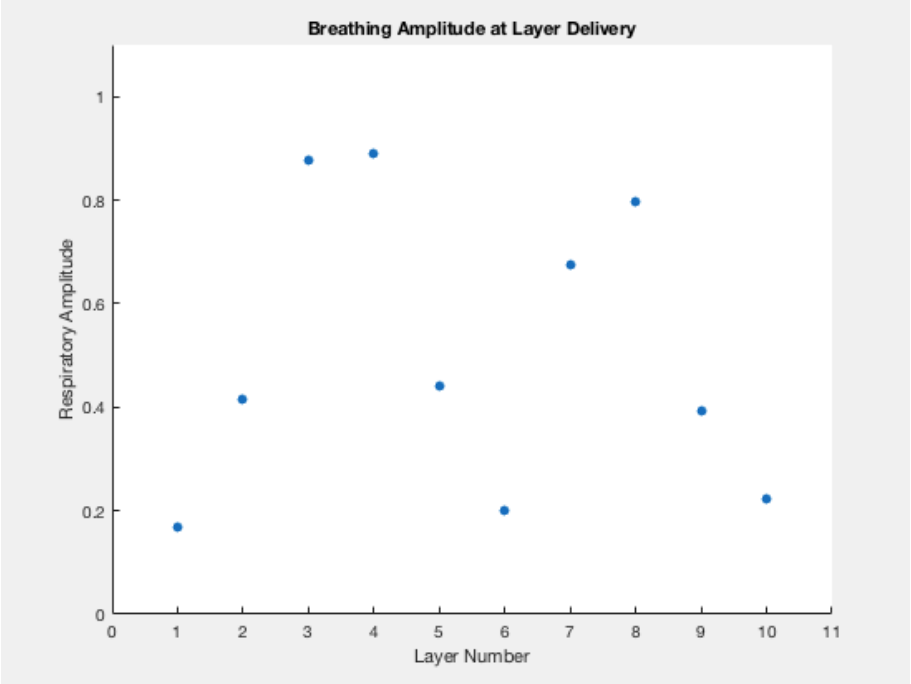

Figure 4.7. Field 2 – Modeled respiration and dose delivery intersection

Table 4.2. Field 2 - Layer and respiration intersection

Layer	Amplitude	In [1] or Ex [-1]
1	0.17	1
2	0.41	1
3	0.88	1
4	0.89	-1
5	0.44	-1
6	0.20	-1
7	0.67	1
8	0.80	-1
9	0.39	-1
10	0.22	-1

Multi Field Optimization Dose Perturbation Examination

This section will discuss the resulting dose perturbation of the patient machine time model (PMTM) on this two field multi field optimization (MFO) lung treatment plan. Using the PMTM and frequency matching (FM) the amount of potential dose perturbation cause by the energy layers of a radiation therapy treatment field being delivered on numerous different respiratory amplitude can be significantly reduced. This section will compare the dose distribution from the composite plan using FM and without FM.

Figure 4.8 displays the dose, without FM, from field 1 and field 2 that was delivered onto the full inhale phase of the 4D CT. Figure 4.12 shows the dose from both treatment fields as it was delivered onto the Full Inhale phase of the 4D CT. This dose distribution displays the result of the energy layers delivered from the amplitude and exhale or inhale that corresponds to each 4D CT phase. The dose from the energy layers delivered to the remaining phases of the 4D CT are shown in the Appendix. The 4D CT phases include: full inhale, 80% inhale, 60% inhale, 40% inhale, 20% inhale, Full exhale, 20% exhale, 40% exhale, 60% exhale, and 80% exhale.

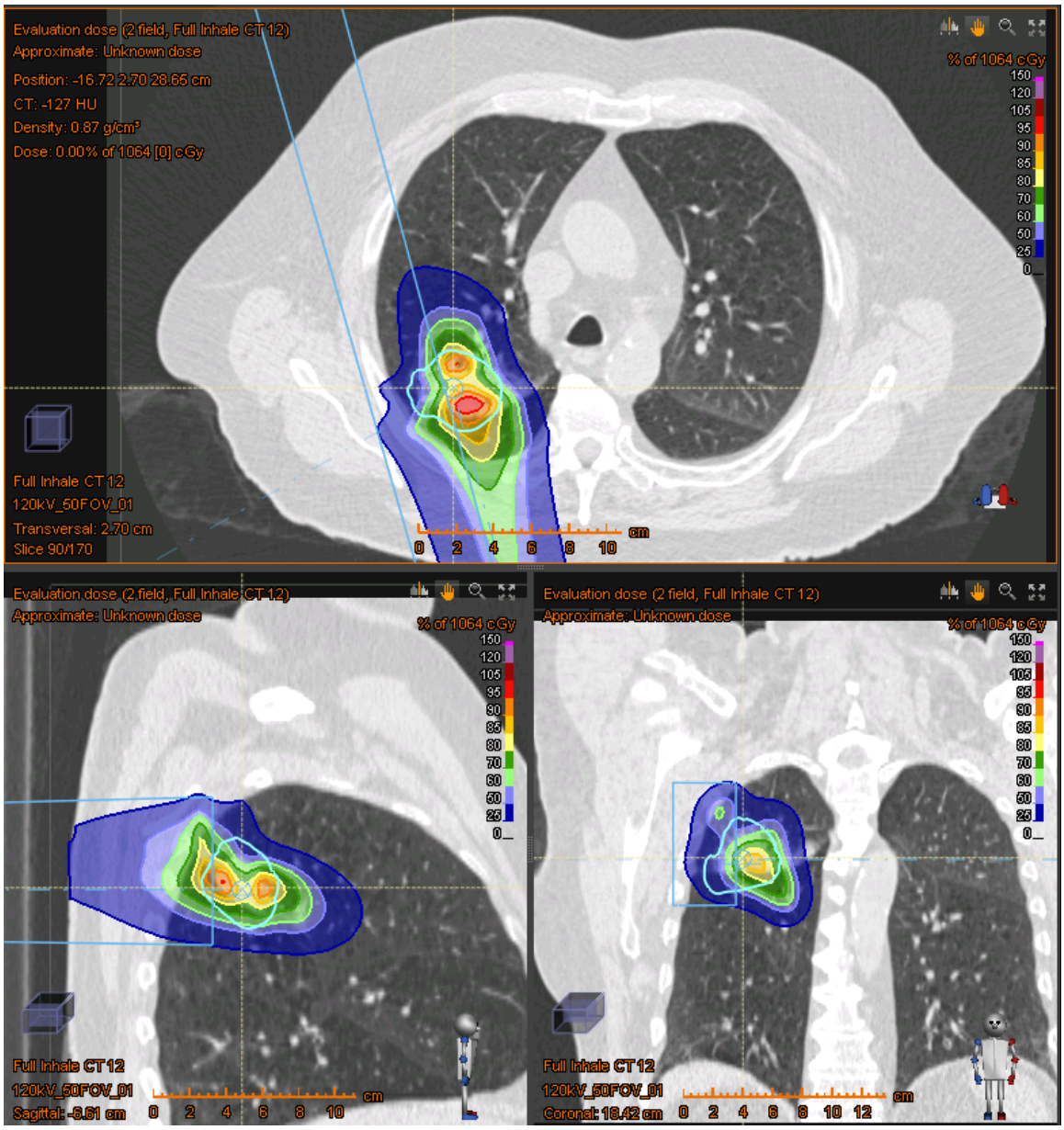

Figure 4.8. Field 1&2 – Dose delivered to Full Inhale CT phase

Figure 4.9 displays the composite dose from the treatment plan when FM is utilized to deliver all of the energy layers on the same respiratory amplitude phase of the 4D CT. As long as FM is used, is it possible to for all of the energy layers to be delivered on the same phase of the 4D CT during an individual fraction within a course of treatment.

Figure 4.10 displays the dose distribution when FM is not used. Notice that the tumor dose distribution is perturbed and no longer uniformly convers the target volume. This represents the worst case dose perturbation, when the individual fields do not full cover the target volume.

Figure 4.11 displays an axial comparison of the of the dose distribution on the phase matched CT in the top section and the dose from each energy layer delivered onto the corresponding phase of the 4D CT and then deformed back onto the 4D CT phase on which the unperturbed treatment plan was computed.

Figure 4.12 displays the dose difference between the nominal dose and the modeled delivery. The dose distribution shown is the result of the PMTM dose subtracted from the unperturbed dose to show the dose difference. This difference can be visualized in the plot in Figure 4.13. The dotted line displays the dose on the PMTM perturbed delivery and the solid line displays the dose distribution of the unperturbed single respiration phase delivery.

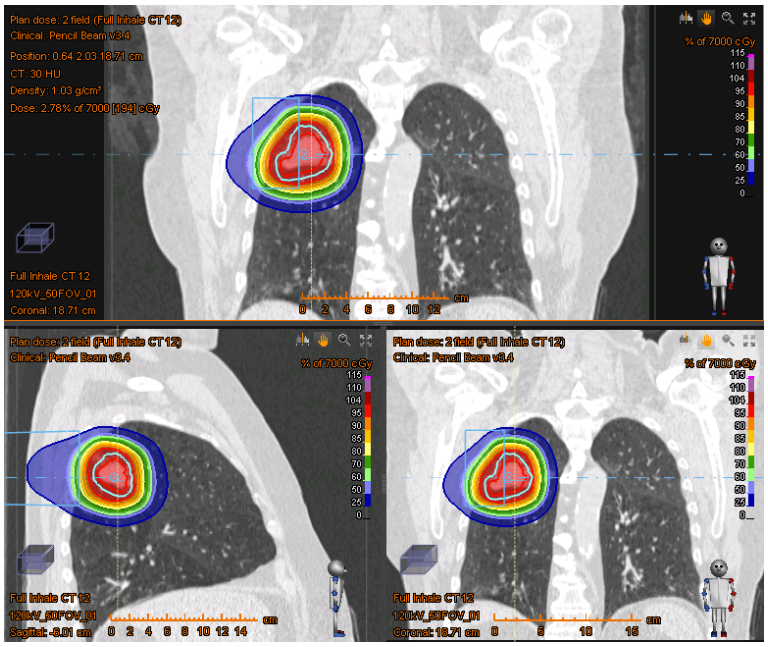

Figure 4.9. Composite treatment plan dose on Single Phase of 4D CT

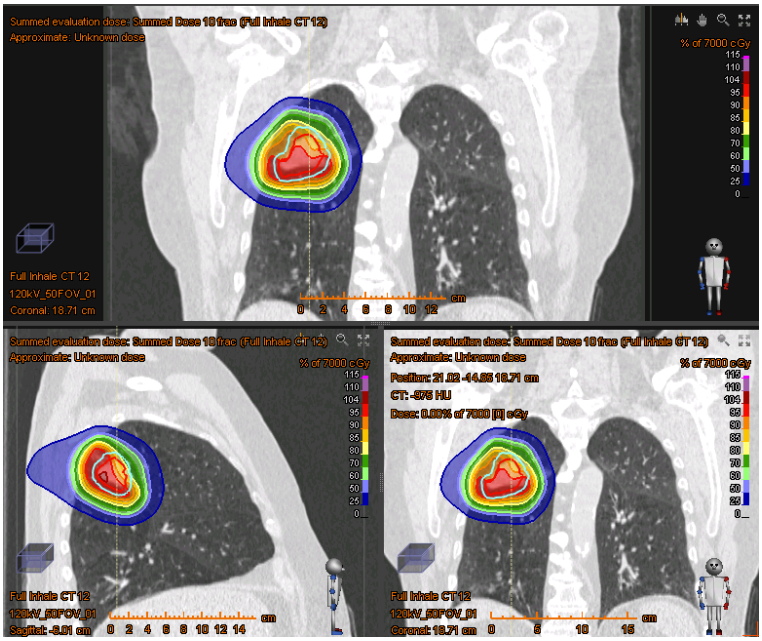

Figure 4.10. Reconstructed composite treatment plan dose using each energy layer's corresponding 4D CT phase as predicted by the PMTM

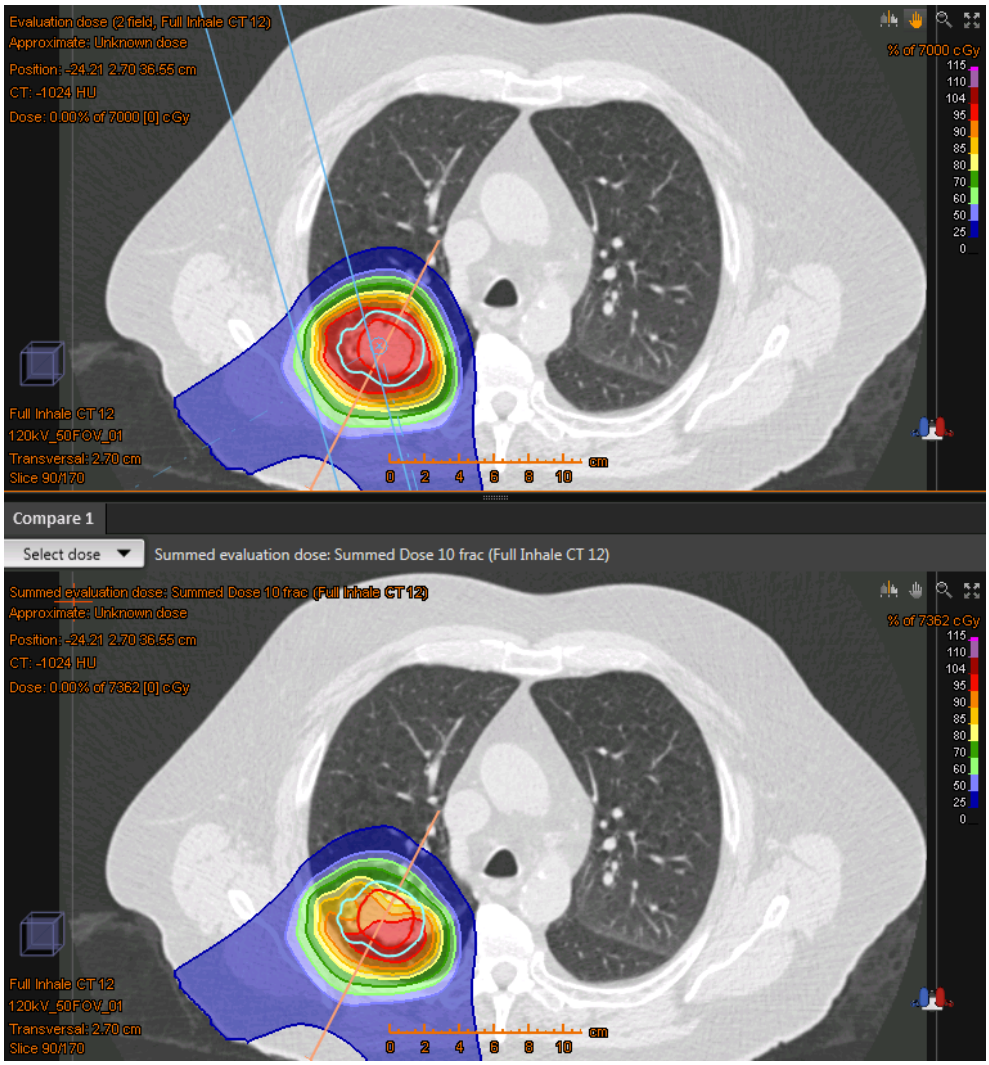

Figure 4.11. Dose line for comparison of unperturbed dose and patient machine time model delivery

Figure 4.12. Difference between unperturbed dose and patient machine time model delivery

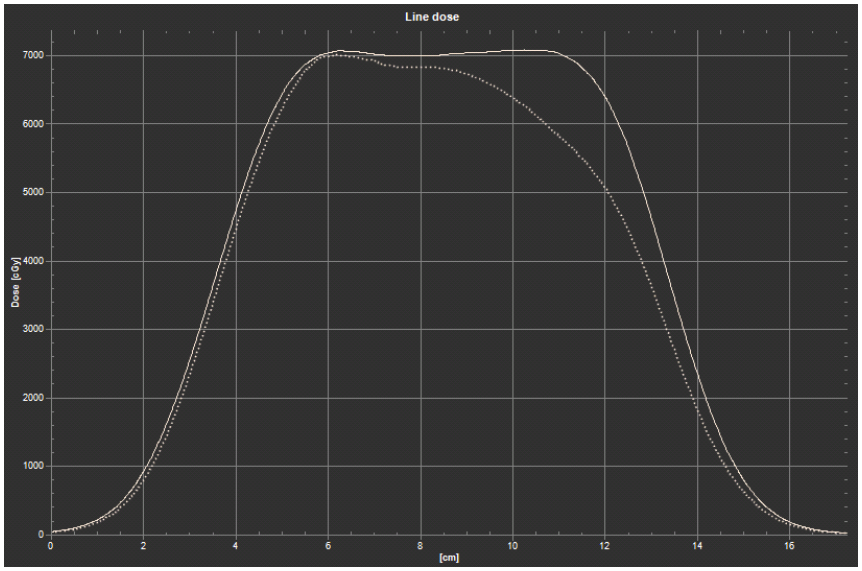

Figure 4.13. Difference between nominal dose and modeled perturbed delivery

Multi Field Optimization Frequency Matching

This section displays the use of the patient machine time model (PMTM) on the parameters of the two field lung treatment plan shown in Figure 4.1. Figure 4.14 displays the energy layers and respiratory cycle of field 1 at 12.3 breathes per minute, producing frequency matching (FM). FM in field 2 is achieved at 12.4 breaths per minute, shown in Figure 4.16. As shown previously in Figure 4.13, dose perturbation from respiratory motion in multi field optimization (MFO) pencil beam scanning (PBS) proton therapy can be significant. Figure 4.15 and 4.17 display the amplitude of each energy layers' delivery achieved by FM. Table 4.3 and 4.4 display the narrow range of respiratory amplitude intersections of each energy layer.

FM allows the composite dose distribution to remain unperturbed with little impact on the patient or treatment delivery time. The dose distribution achieved by frequency matching will match the dose distribution of a full treatment delivery on a single 4D CT phase. This unperturbed treatment delivery resulting from frequency matching is shown in Figure 4.9.

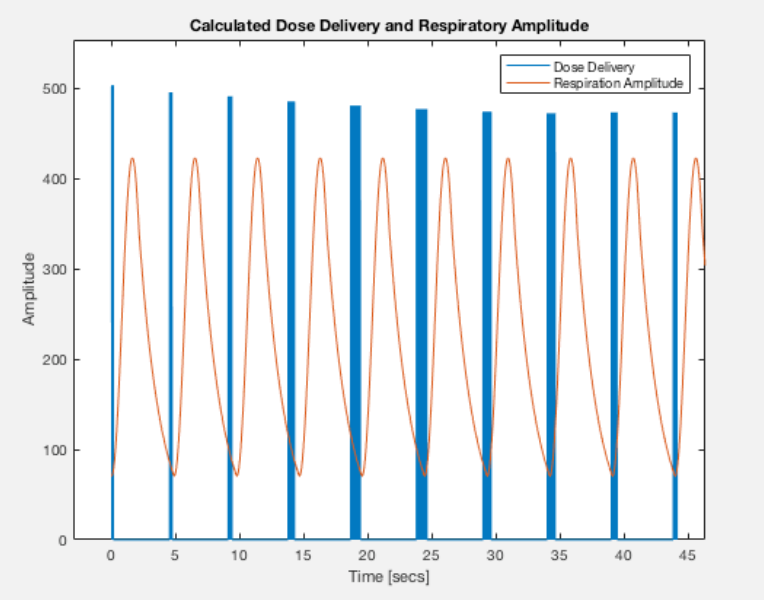

Figure 4.14. Field 1 – Predicted frequency matching using the patient machine time model

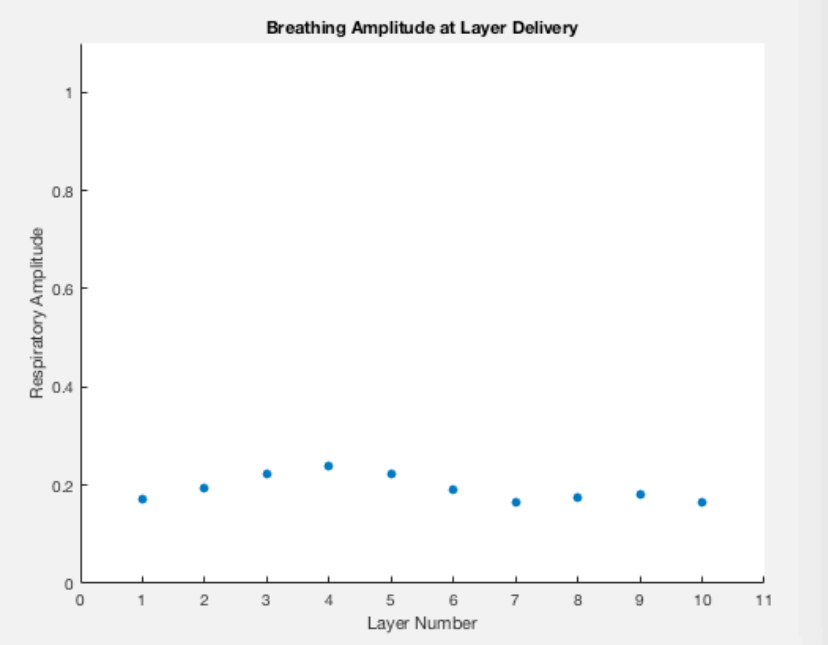

Figure 4.15. Field 1 – Respiratory amplitude at each energy layer

Table 4.3. Field 1 - Layer and respiration intersection

Layer	Amplitude	In [1] or Ex [-1]
1	0.17	1
2	0.19	-1
3	0.22	-1
4	0.24	-1
5	0.22	-1
6	0.19	-1
7	0.17	-1
8	0.17	1
9	0.18	1
10	0.17	1

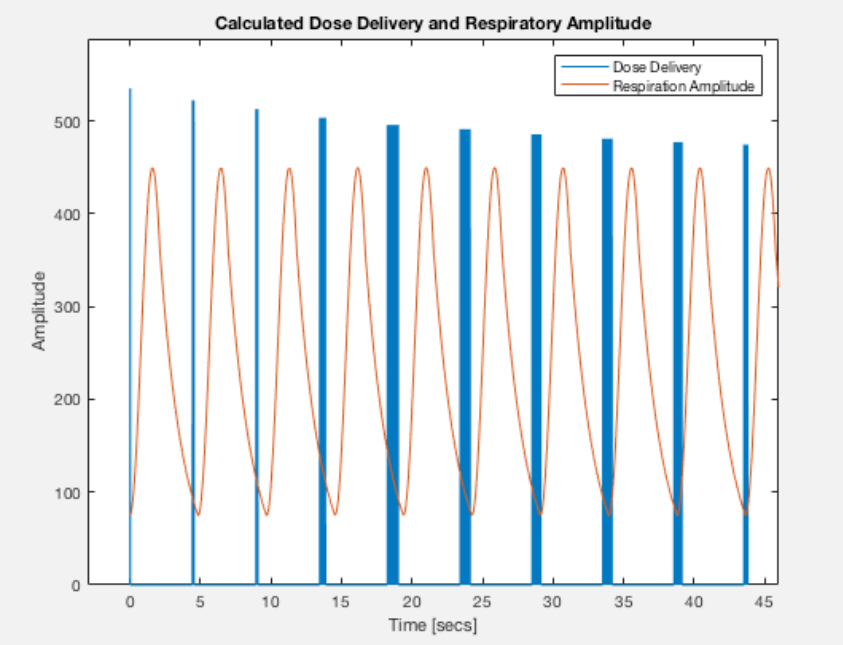

Figure 4.16. Field 2 – Predicted frequency matching using the patient machine time model

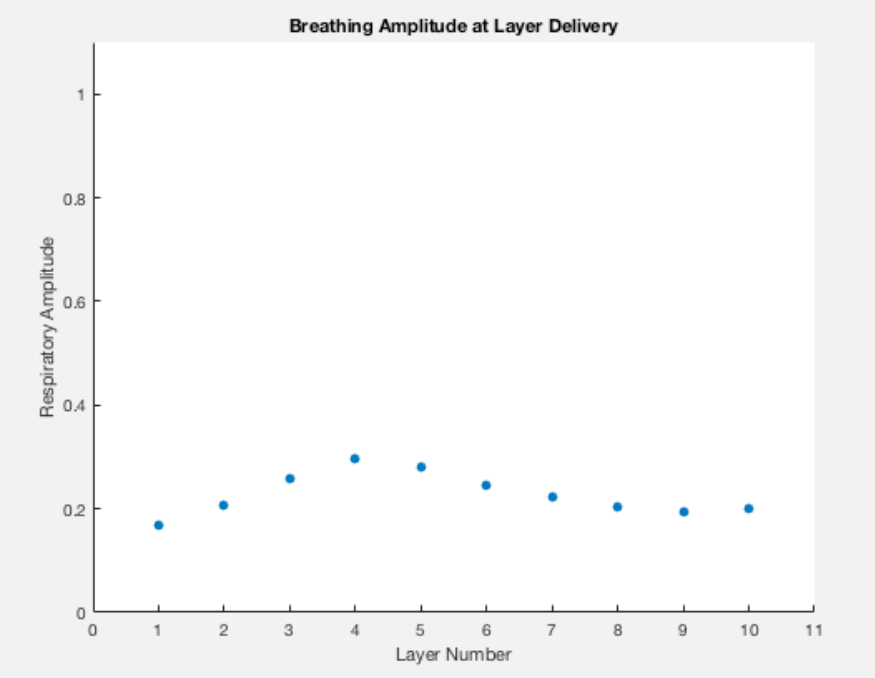

Figure 4.17. Field 2 – Respiratory amplitude at each energy layer

Table 4.4. Field 2 - Layer and respiration intersection

Layer	Amplitude	In [1] or Ex [-1]
1	0.17	1
2	0.20	-1
3	0.25	-1
4	0.28	-1
5	0.26	-1
6	0.22	-1
7	0.19	-1
8	0.17	-1
9	0.17	1
10	0.17	1

CHAPTER FIVE
CONCLUSIONS AND FUTURE WORK

Conclusions

The use of the patient machine time model (PMTM) in pencil beam scanning proton therapy could be useful to produce frequency matching (FM) between the respiratory frequency of the patient and the dose delivery frequency provided by the treatment machine. FM of the respiratory frequency and the machine delivery frequency has the potential to mitigate dose perturbation from respiratory target motion.

To achieve FM, it will be important to measure the respiratory rate of the patient and match it to the dose delivery rate of the treatment machine. In a frequency matched PBS proton therapy delivery, the patient may breathe at 14 breaths per minute and the machine may deliver the treatment field at a rate of 14 energy layers per minute.

Future Work

The work in this dissertation has demonstrated the potential for the patient machine time model in pencil beam scanning proton radiation therapy. There are three key areas for future work to bring frequency matching into clinical practice.

1) Measure the patient's respiration rate at the time of the treatment planning simulation
2) Frequency match the patient's respiration to the treatment machine's delivery
3) Frequency match the treatment machine's delivery to the patient's respiration

A camera based stereoscopic camera system known as No Dose Setup (NDS) has also been developed to aid in the reproducibility of patient setup for radiation therapy both in CT treatment simulation and in the treatment room. The system is currently being used to assist in patient setup as an additional tool, supplementing the orthogonal x-rays conventionally used to setup the patient. The system allows initial positioning of the patient to be conducted without radiation exposure. The NDS system provides real time image fusion between the patient's current position and reference target position.

A 10 patient 10 fraction study was conducted to compare traditional orthogonal X-ray patient setup with and without the camera based system. The NDS system was used to supplement setup prior to X-ray imaging. The use of the system allowed a 23% reduction in the total time the patient stayed in the treatment room and eliminated 50% of the X-rays used in the iterative process of setting up the patient.

The NDS system features will be expanded to include respiration rate monitoring of the patient from the video stream shown in Figure 5.1. The respiration amplitude

of the patient plotted over time is shown in the lower right corner of the NDS user interface in Figure 5.1. Significant improvements in respiration motion management are expected from the additional surface tracking technology of the NDS system. Surface tracking for patient setup and respiratory motion motioning should provide improvements in lung cancer treatments both in reduced X-ray setup imaging exposure and reduced dose perturbation allowed by frequency matching (FM). Continuous respiration rate monitoring of the patient combined with dynamic energy layer switching times between 3 and 5 seconds would enable FM to become the primary dose perturbation mitigation in pencil beam scanning proton therapy.

Through a collaboration with Oak Ridge National Laboratory (ORNL), Provision Center for Proton Therapy (PCPT), and George Washington University (GU), a seed grant was awarded to make progress towards adapting proton therapy treatment fields to compensate for respiratory motion.

In order to make strides towards real time motion adaptation one must first acquire an accurate representation of the patient's respiration rate. The first phase of the collaboration between ORNL, PCPT, and GU is to develop respiratory rate monitoring to supplement the stereoscopic camera based patient setup system. Figure 5.1 displays the image fusion produced by the stereoscopic camera system, overlaying the patient's current position and the patient's previous position. In the lower right corner of Figure 5.1 shows the envisioned location of the patient's respiration rate.

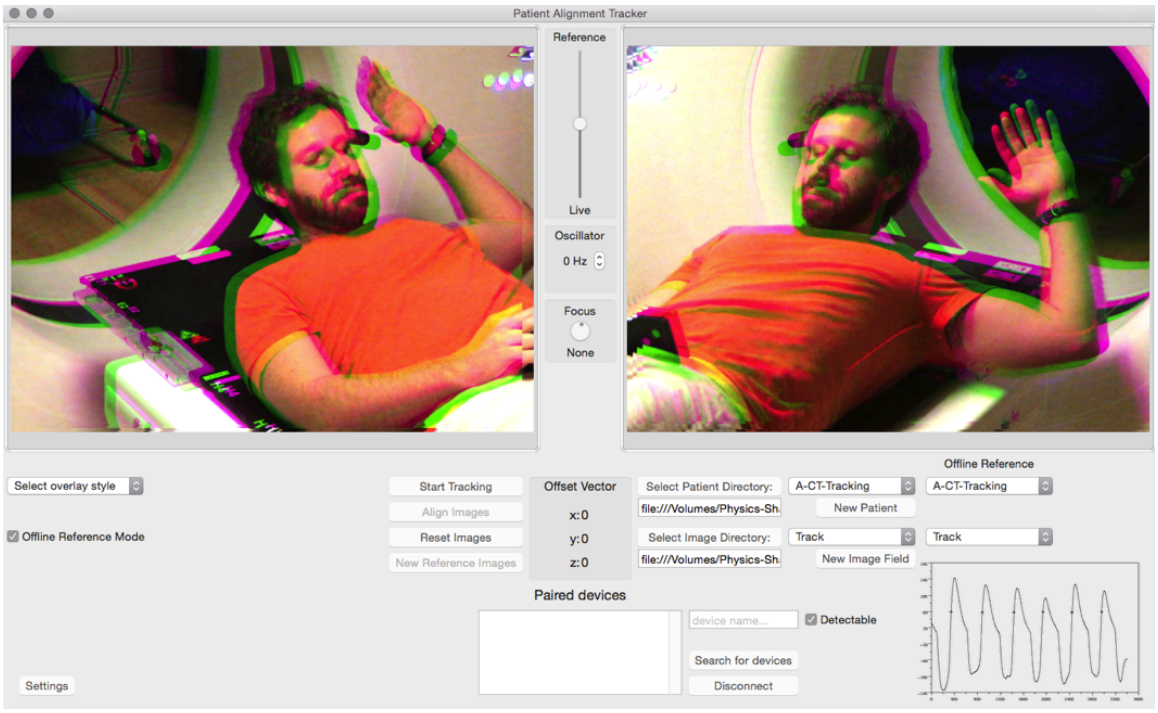

Figure 5.1. Respiration rate measurement at CT treatment simulation

Once the patient's respiration rate has been measured, the patient could be coached to modify their respiration rate slightly. A slight modification of the patient's respiration rate at the time of the CT simulation combined with the PMTM could result in FM of the respiration cycle and dose delivery.

The final phase would be to utilize modifiable machine delivery parameters to produce FM. This would allow the incorporation of the PMTM into the treatment planning optimization. This would also allow optimization of the treatment fields to be deliverable on any of the respiratory amplitudes represented in the ten 4D CT phases. Along with this optimization, FM would be sufficient to mitigate dose perturbation from respiratory motion.

LIST OF REFERENCES

1. A. N. Schreuder, S.G.H., J. R. Renegar, T. J. Netherton, H. Chen, M. D. Blakey, M. E. Artz, B. H. Robison, A. G. and M.F. Meek, *A REVIEW OF PROTON RADIATION THERAPY AND THE PATH TO WIDESPREAD CLINICAL ADOPTION.* MEDICAL PHYSICS INTERNATIONAL, 2016. **4**(1): p. 12.

2. Siegel, R., K. Miller, and A. Jemal, *Cancer Facts & Figures* American Cancer Society, 2016.

3. Inoue, T., et al., *Limited impact of setup and range uncertainties, breathing motion and interplay effects in robustly optimized intensity modulated proton therapy for stage III non-small cell lung cancer.* International Journal of Radiation Oncology*Biology*Physics, 2016.

4. Craft, D.L., et al., *Improved planning time and plan quality through multicriteria optimization for intensity-modulated radiotherapy.* Int J Radiat Oncol Biol Phys, 2012. **82**(1): p. e83-90.

5. Qin, B., et al., *Precise isochronous field shimming using correlation matrix for compact cyclotrons.* Nuclear Instruments and Methods in Physics Research Section A: Accelerators, Spectrometers, Detectors and Associated Equipment, 2012. **691**: p. 129-134.

6. W. Kleeven, M.A., E. Forton, S. Henrotin, Y. Jongen, V. Nuttens, Y. Paradis, E. Pearson, S. Quets, J. Van de Walle, P. Verbruggen, S. Zaremba, IBA, Louvain-La-Neuve, Belgium M. Conjat, J. Mandrillon, P. Mandrillon, AIMA Development, Nice, France, *THE IBA SUPERCONDUCTING SYNCHROCYCLOTRON PROJECT S2C2.* Cyclotrons, 2013. **MO4**(PB02): p. 4.

7. *Opera - Magnet Design Software.* 2016.

8. Grossman, P., F.H. Wilhelm, and M. Brutsche, *Accuracy of ventilatory measurement employing ambulatory inductive plethysmography during tasks of everyday life.* Biol Psychol, 2010. **84**(1): p. 121-8.

9. Carry, P.-Y., et al., *Evaluation of Respiratory Inductive Plethysmography.* Chest, 1997. **111**(4): p. 910-915.

10. Cole, A.J., et al., *Motion management for radical radiotherapy in non-small cell lung cancer.* Clin Oncol (R Coll Radiol), 2014. **26**(2): p. 67-80.

11. Mori, S., et al., *Four-dimensional measurement of lung tumor displacement using 256-multi-slice CT-scanner.* Lung Cancer, 2007. **56**(1): p. 59-67.

12. Dueck, J., et al., *Robustness of the Voluntary Breath-Hold Approach for the Treatment of Peripheral Lung Tumors Using Hypofractionated Pencil Beam Scanning Proton Therapy.* Int J Radiat Oncol Biol Phys, 2016. **95**(1): p. 534-41.

13. Mageras, G.S. and E. Yorke, *Deep inspiration breath hold and respiratory gating strategies for reducing organ motion in radiation treatment.* Semin Radiat Oncol, 2004. **14**(1): p. 65-75.

14. Li, H., X.R. Zhu, and X. Zhang, *Reducing Dose Uncertainty for Spot-Scanning Proton Beam Therapy of Moving Tumors by Optimizing the Spot Delivery Sequence.* Int J Radiat Oncol Biol Phys, 2015. **93**(3): p. 547-56.

15. Grassberger, C., et al., *Motion interplay as a function of patient parameters and spot size in spot scanning proton therapy for lung cancer.* Int J Radiat Oncol Biol Phys, 2013. **86**(2): p. 380-6.

16. Flanz, J.B., *OPERATION OF A CYCLOTRON BASED PROTON THERAPY FACILITY.* Cern Accelerator Conference, 2004.

17. Niek Schreuder, M., et al., *Gantry Rooms 1 and 2 & Fixed Beam Room Commissioning Report.* Provision Center for Proton Therapy, 2015.

18. M. J. Berger, J.S.C., and M. A. Zucker, *Stopping-power and range tables for electrons, protons, and helium ions.* NIST, 2000.

19. Akino, Y., et al., *Respiratory Motion Management of Liver Cancer in Uniform Scanning Proton Beam Therapy.* International Journal of Radiation Oncology*Biology*Physics, 2014. **90**(1): p. S915-S916.

20. Allen, A.M., et al., *Evaluation of the influence of breathing on the movement and modeling of lung tumors.* Int J Radiat Oncol Biol Phys, 2004. **58**(4): p. 1251-7.

21. Bernatowicz, K., et al., *Four-Dimensional Dose Reconstruction for Scanned Proton Therapy Using Liver 4DCT-MRI.* Int J Radiat Oncol Biol Phys, 2016. **95**(1): p. 216-23.

22. Caldwell, C.B., et al., *Can PET provide the 3D extent of tumor motion for individualized internal target volumes? A phantom study of the limitations of CT and the promise of PET.* International Journal of Radiation Oncology*Biology*Physics, 2003. **55**(5): p. 1381-1393.

23. Chang, J.Y., et al., *Consensus Statement on Proton Therapy in Early-Stage and Locally Advanced Non-Small Cell Lung Cancer.* Int J Radiat Oncol Biol Phys, 2016. **95**(1): p. 505-16.

24. Chen, T., et al., *Frequency filtering based analysis on the cardiac induced lung tumor motion and its impact on the radiotherapy management.* Radiother Oncol, 2014. **112**(3): p. 365-70.

25. Chera, B.S., et al., *Dosimetric comparison of three different involved nodal irradiation techniques for stage II Hodgkin's lymphoma patients: conventional radiotherapy, intensity-modulated radiotherapy, and three-dimensional proton radiotherapy.* Int J Radiat Oncol Biol Phys, 2009. **75**(4): p. 1173-80.

26. CRAIG W. STEVENS, M.D., PH.D.,* , et al., *RESPIRATORY-DRIVEN LUNG TUMOR MOTION IS INDEPENDENT OF TUMOR SIZE, TUMOR LOCATION, AND PULMONARY FUNCTION.* Int. J. Radiation Oncology Biol. Phys., 2001. **51**(1): p. 6.

27. De Ruysscher, D., et al., *Tumour Movement in Proton Therapy: Solutions and Remaining Questions: A Review.* Cancers (Basel), 2015. **7**(3): p. 1143-53.

28. Donnelly, E.D., et al., *Assessment of intrafraction mediastinal and hilar lymph node movement and comparison to lung tumor motion using four-dimensional CT.* Int J Radiat Oncol Biol Phys, 2007. **69**(2): p. 580-8.

29. Doyen, J., et al., *Proton beams in cancer treatments: Clinical outcomes and dosimetric comparisons with photon therapy.* Cancer Treat Rev, 2016. **43**: p. 104-12.

30. Gierga, D.P., et al., *The correlation between internal and external markers for abdominal tumors: implications for respiratory gating.* Int J Radiat Oncol Biol Phys, 2005. **61**(5): p. 1551-8.

31. Hackett, S., et al., *Respiratory gating reduces heart doses for proton radiotherapy of the breast and internal mammary chain.* Radiotherapy and Oncology, 2015. **115**: p. S537.

32. Harsolia, A., et al., *Dosimetric advantages of four-dimensional adaptive image-guided radiotherapy for lung tumors using online cone-beam computed tomography.* Int J Radiat Oncol Biol Phys, 2008. **70**(2): p. 582-9.

33. Hoisak, J.D., et al., *Correlation of lung tumor motion with external surrogate indicators of respiration.* Int J Radiat Oncol Biol Phys, 2004. **60**(4): p. 1298-306.

34. Hojin Jeong, S.B.L., 1 Seung Hoon Yoo,3 Young Kyung Lim,1 Tae Hyun Kim,1 Seyjoon Park,1 Gyu Young Chai,2 Ki Mun Kang,2a and D. Shin1a,

Compensation method for respiratory motion in proton treatment planning for mobile liver cancer. Journal of Applied Clinical Medical Physics, 2013. **Volume 14**(2).

35. Iwata, H., et al., *Long-term outcome of proton therapy and carbon-ion therapy for large (T2a-T2bN0M0) non-small-cell lung cancer.* J Thorac Oncol, 2013. **8**(6): p. 726-35.

36. Jan, N., et al., *Interfraction displacement of primary tumor and involved lymph nodes relative to anatomic landmarks in image guided radiation therapy of locally advanced lung cancer.* Int J Radiat Oncol Biol Phys, 2014. **88**(1): p. 210-5.

37. Jongen, Y., *REVIEW ON CYCLOTRONS FOR CANCER THERAPY.* Cyclotron Applications, 2010. **FRM1CIO01**: p. 5.

38. Koch, N., et al., *Evaluation of internal lung motion for respiratory-gated radiotherapy using MRI: Part I--correlating internal lung motion with skin fiducial motion.* Int J Radiat Oncol Biol Phys, 2004. **60**(5): p. 1459-72.

39. Kupelian, P.A., et al., *Implantation and stability of metallic fiducials within pulmonary lesions.* Int J Radiat Oncol Biol Phys, 2007. **69**(3): p. 777-85.

40. Laura I. Cerviño, A.K.Y.C., Ajay Sandhu, and Steve B. Jiang, *Diaphragm as an anatomic surrogate for lung tumor motion.* Department of Radiation Oncology, University of California San Diego, 2008.

41. Lemjabbar-Alaoui, H., et al., *Lung cancer: Biology and treatment options.* Biochim Biophys Acta, 2015. **1856**(2): p. 189-210.

42. Li, H., et al., *Robust optimization in intensity-modulated proton therapy to account for anatomy changes in lung cancer patients.* Radiother Oncol, 2015. **114**(3): p. 367-72.

43. Liu, W., et al., *Exploratory Study of 4D versus 3D Robust Optimization in Intensity Modulated Proton Therapy for Lung Cancer.* Int J Radiat Oncol Biol Phys, 2016. **95**(1): p. 523-33.

44. Macdonald, O.K., et al., *Proton beam radiotherapy versus three-dimensional conformal stereotactic body radiotherapy in primary peripheral, early-stage non-small-cell lung carcinoma: a comparative dosimetric analysis.* Int J Radiat Oncol Biol Phys, 2009. **75**(3): p. 950-8.

45. Matney, J., et al., *Effects of respiratory motion on passively scattered proton therapy versus intensity modulated photon therapy for stage III lung*

cancer: are proton plans more sensitive to breathing motion? Int J Radiat Oncol Biol Phys, 2013. **87**(3): p. 576-82.

46. McAvoy, S.A., et al., *Feasibility of proton beam therapy for reirradiation of locoregionally recurrent non-small cell lung cancer.* Radiother Oncol, 2013. **109**(1): p. 38-44.

47. Michalski, D., et al., *Four-dimensional computed tomography-based interfractional reproducibility study of lung tumor intrafractional motion.* Int J Radiat Oncol Biol Phys, 2008. **71**(3): p. 714-24.

48. MIT, *MIT Principles of Radiation Interactions.* MIT 22.55 Course, 2010.

49. Mori, S., G.T. Chen, and M. Endo, *Effects of intrafractional motion on water equivalent pathlength in respiratory-gated heavy charged particle beam radiotherapy.* Int J Radiat Oncol Biol Phys, 2007. **69**(1): p. 308-17.

50. Nelson, C., et al., *Assessment of lung tumor motion and setup uncertainties using implanted fiducials.* Int J Radiat Oncol Biol Phys, 2007. **67**(3): p. 915-23.

51. Noworolski, S.M., et al., *Respiratory motion-corrected proton magnetic resonance spectroscopy of the liver.* Magn Reson Imaging, 2009. **27**(4): p. 570-6.

52. Ohri, N., et al., *Radiation Therapy Noncompliance and Clinical Outcomes in an Urban Academic Cancer Center.* Int J Radiat Oncol Biol Phys, 2016. **95**(2): p. 563-70.

53. Olsen, J.R., et al., *Effect of novel amplitude/phase binning algorithm on commercial four-dimensional computed tomography quality.* Int J Radiat Oncol Biol Phys, 2008. **70**(1): p. 243-52.

54. Pedroni, E., et al., *Experimental characterization and physical modelling of the dose distribution of scanned proton pencil beams.* Physics in Medicine and Biology, 2005. **50**(3): p. 541-561.

55. Redmond, K.J., et al., *Respiratory motion changes of lung tumors over the course of radiation therapy based on respiration-correlated four-dimensional computed tomography scans.* Int J Radiat Oncol Biol Phys, 2009. **75**(5): p. 1605-12.

56. Seco, J., et al., *Treatment of non-small cell lung cancer patients with proton beam-based stereotactic body radiotherapy: dosimetric comparison with photon plans highlights importance of range uncertainty.* Int J Radiat Oncol Biol Phys, 2012. **83**(1): p. 354-61.

57. Shimizu, S., et al., *Development of a Real-Time Image Gated Proton Beam Therapy (RGPT) System and Its Initial Clinical Application to Respiratory Moving Liver Tumors.* International Journal of Radiation Oncology*Biology*Physics, 2015. **93**(3): p. S42.

58. Sio, T.T., et al., *Spot-scanned pancreatic stereotactic body proton therapy: A dosimetric feasibility and robustness study.* Phys Med, 2016. **32**(2): p. 331-42.

59. Soukup, M., M. Fippel, and M. Alber, *A pencil beam algorithm for intensity modulated proton therapy derived from Monte Carlo simulations.* Phys Med Biol, 2005. **50**(21): p. 5089-104.

60. T. S. Hong1, T.F.D., H. J. Mamon2, A. Niemierko1, J. Adams1, B. Yeap1, L. S. Blaszkowsky1, D. P. Ryan1, C. G. Willett3, and A.X. Zhu1, *Pilot of Respiratory Gated Proton Beam Therapy for Liver Tumors.* I. J. Radiation Oncology, 2009. **75**(3).

61. Tsunashima, Y., et al., *Correlation between the respiratory waveform measured using a respiratory sensor and 3D tumor motion in gated radiotherapy.* Int J Radiat Oncol Biol Phys, 2004. **60**(3): p. 951-8.

62. Widesott, L., M. Amichetti, and M. Schwarz, *Proton therapy in lung cancer: clinical outcomes and technical issues. A systematic review.* Radiother Oncol, 2008. **86**(2): p. 154-64.

63. Willoughby, T.R., et al., *Evaluation of an infrared camera and X-ray system using implanted fiducials in patients with lung tumors for gated radiation therapy.* Int J Radiat Oncol Biol Phys, 2006. **66**(2): p. 568-75.

64. Yan, P., et al., *Elimination of Phase Delay of External Surrogate-based Respiratory Gating System to Reduce PTV Margins using a Novel Ultrasound-based Apparatus.* International Journal of Radiation Oncology*Biology*Physics, 2011. **81**(2): p. S122.

65. Zhang, X., et al., *Intensity-modulated proton therapy reduces the dose to normal tissue compared with intensity-modulated radiation therapy or passive scattering proton therapy and enables individualized radical radiotherapy for extensive stage IIIB non-small-cell lung cancer: a virtual clinical study.* Int J Radiat Oncol Biol Phys, 2010. **77**(2): p. 357-66.

APPENDIX

In Chapter 4, the model of the multi field optimization dose perturbation makes reference to the dose that is predicted to be delivered from the treatment plan on each phase of the 4D CT. This Appendix supplements the Figure 4.8 to provide the complete set of dose to the corresponding 4D CT phases as predicted by the PMTM: full inhale, 80% inhale, 60% inhale, 40% inhale, 20% inhale, Full exhale, 20% exhale, 40% exhale, 60% exhale, and 80% exhale. Figure 4.10 displays the resulting composite treatment plan dose using each of the 4D CT phase shown below.

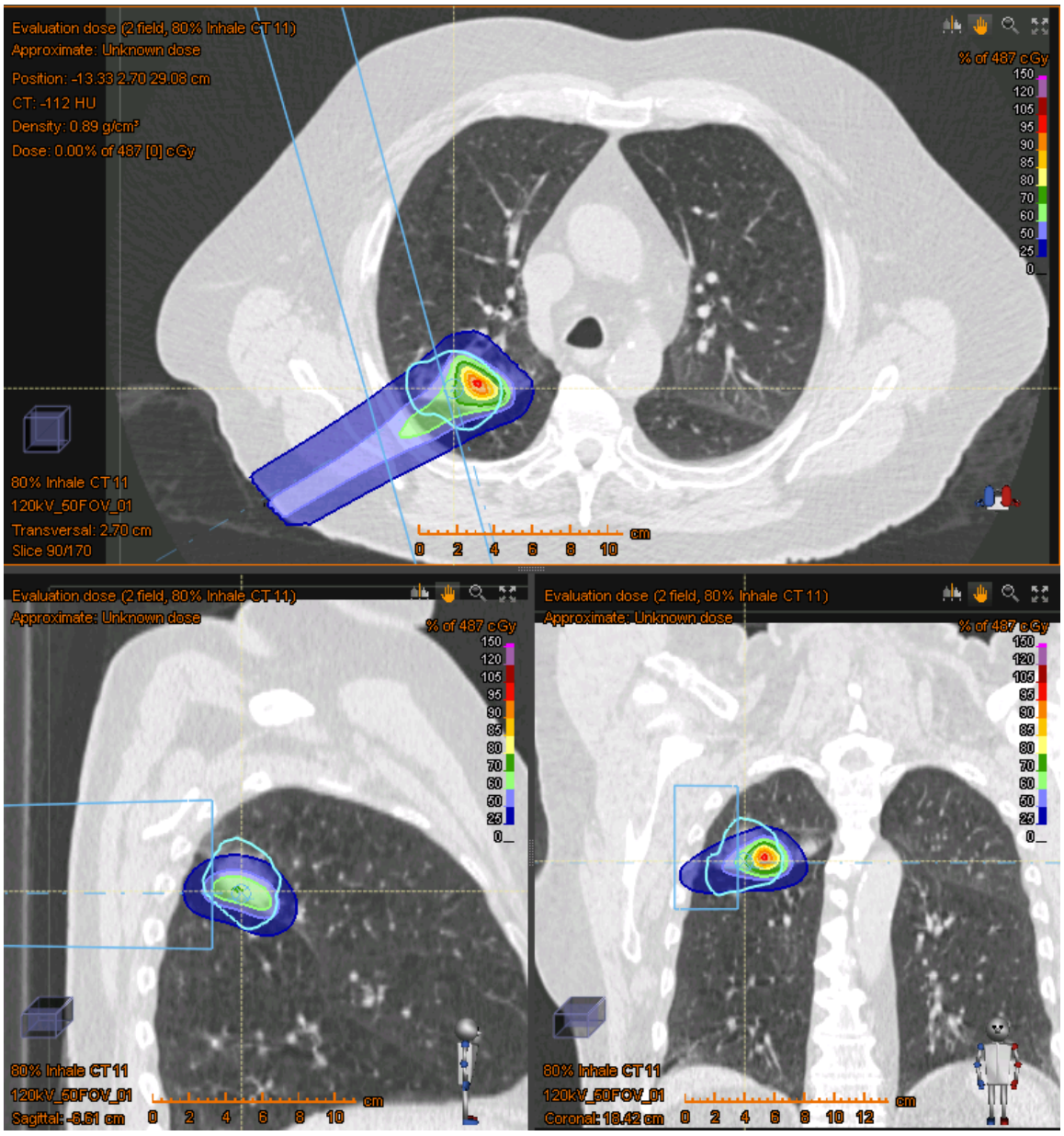

Figure A.1. Field 1&2 – Dose delivered to 80% inhale CT phase

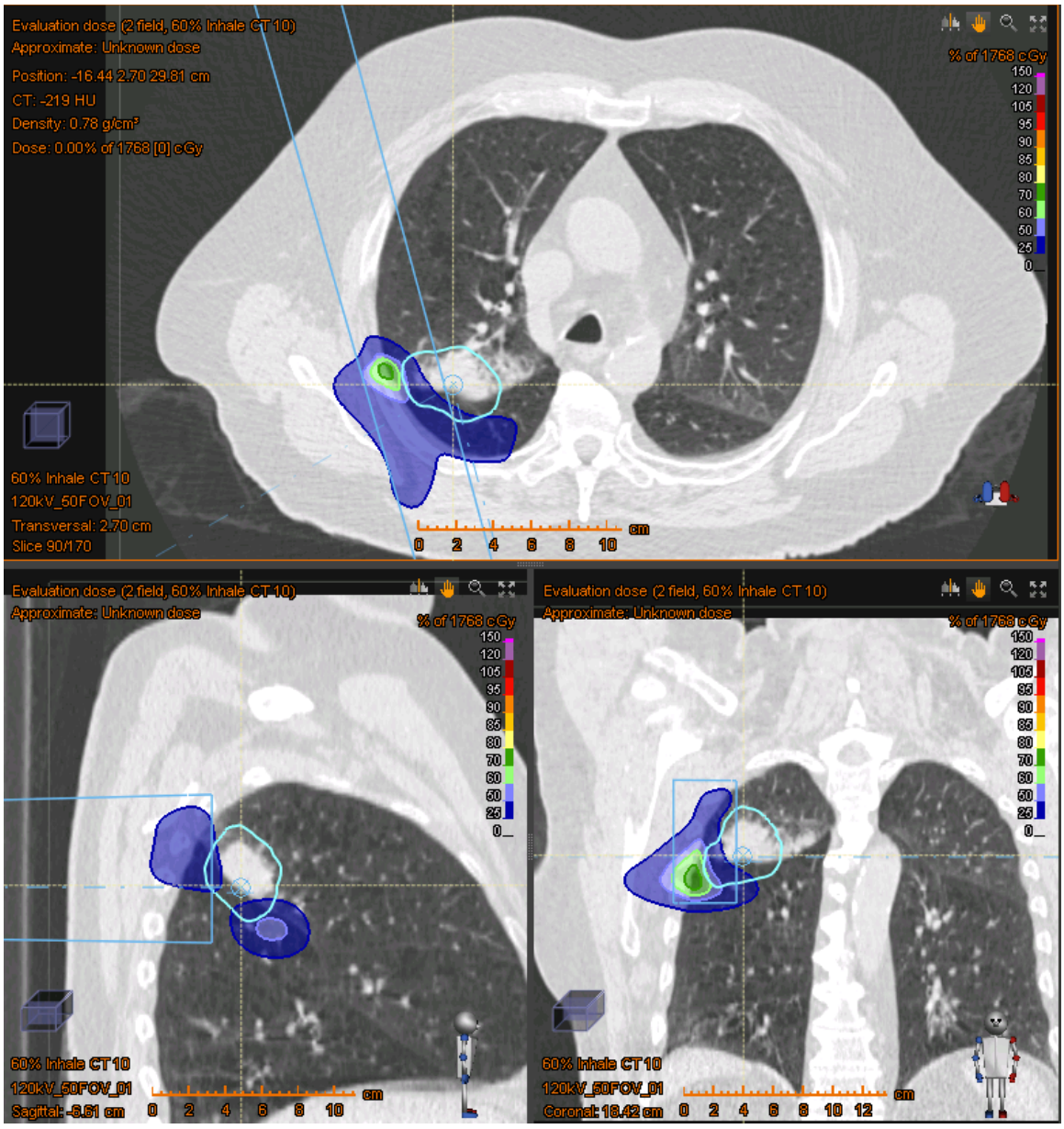

Figure A.2. Field 1&2 – Dose delivered to 60% inhale CT phase

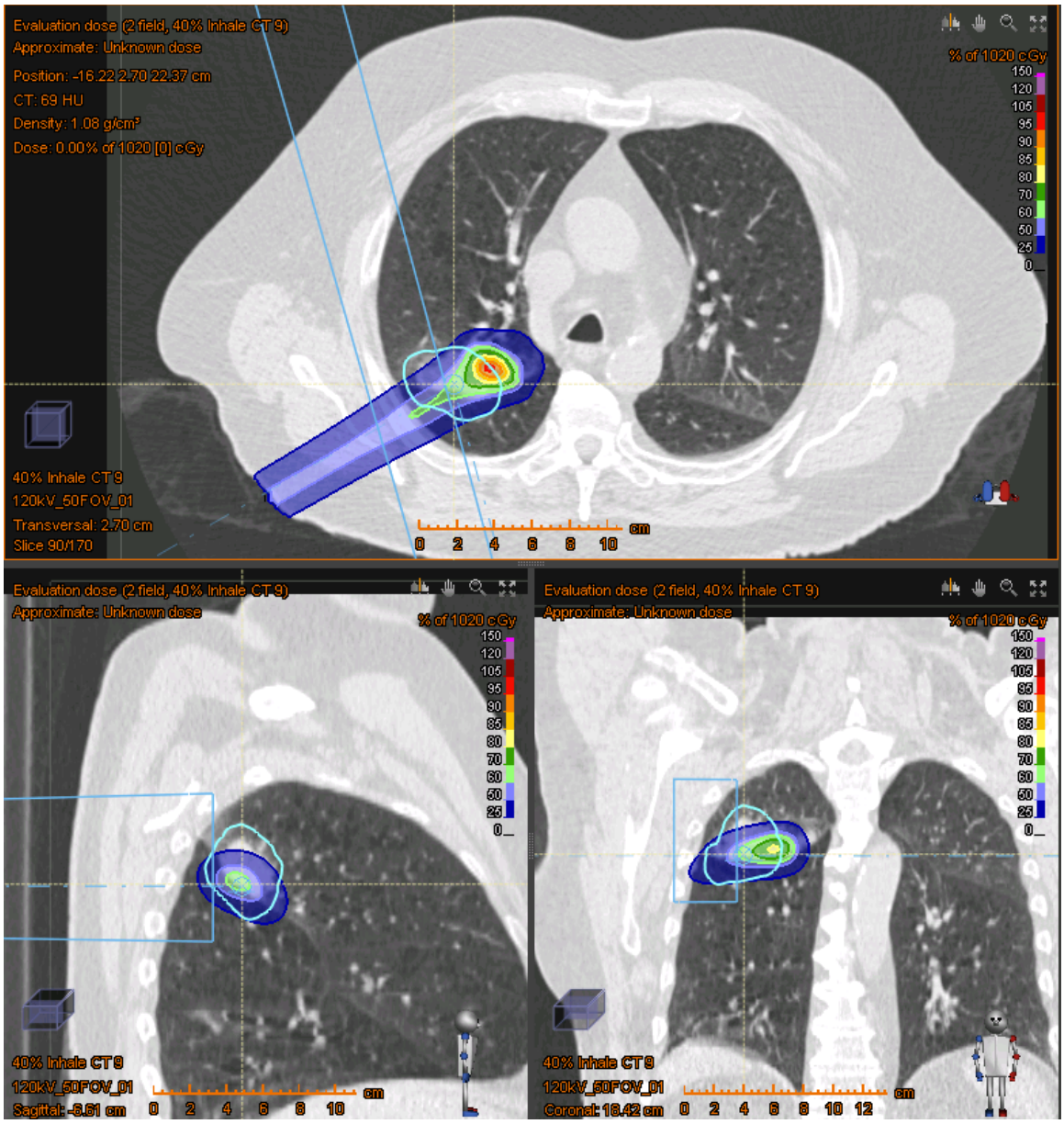

Figure A.3. Field 1&2 – Dose delivered to 40% inhale CT phase

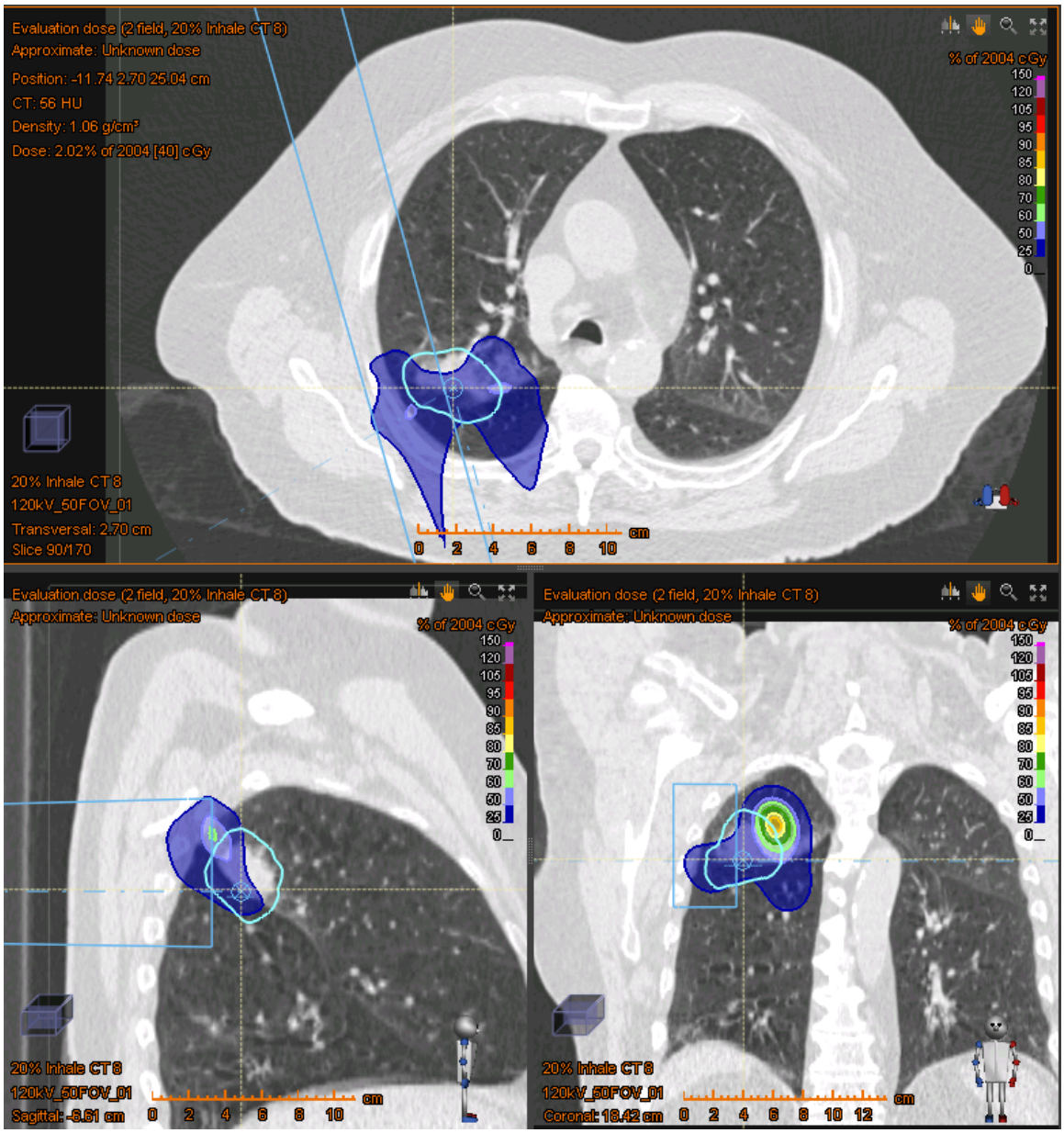

Figure A.4. Field 1&2 – Dose delivered to 20% inhale CT phase

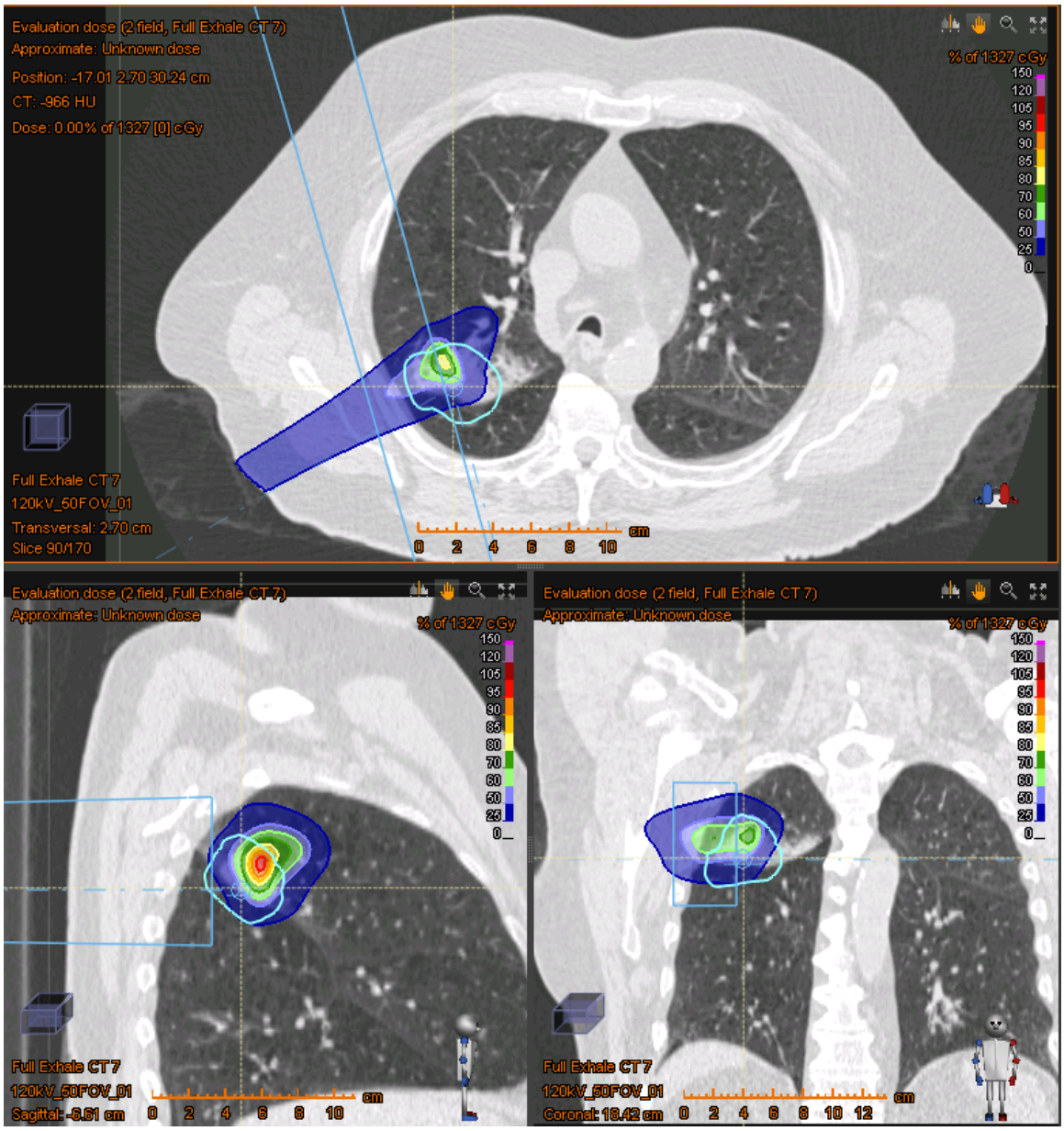

Figure A.5. Field 1&2 – Dose delivered to full exhale CT phase

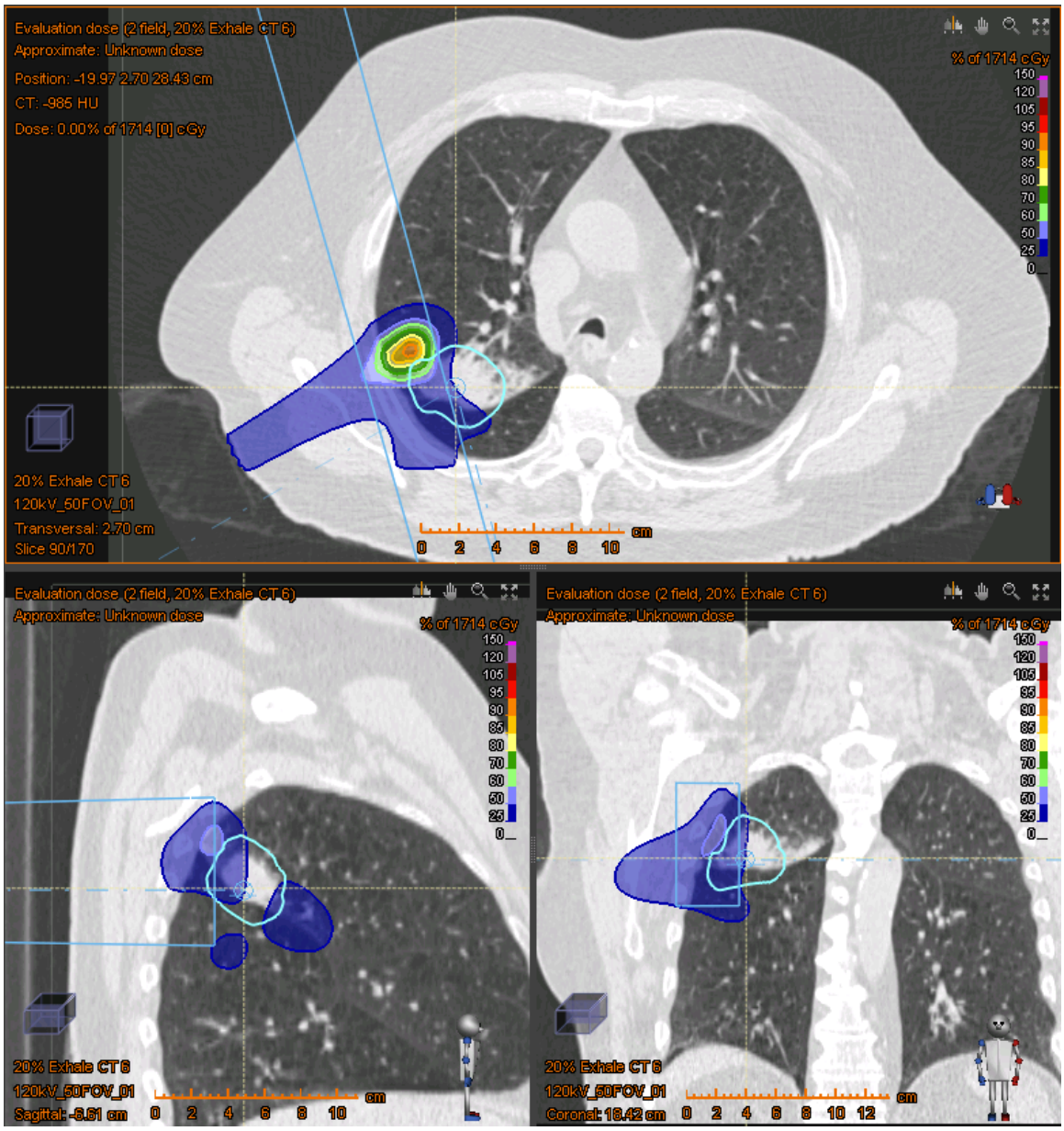

Figure A.6. Field 1&2 – Dose delivered to 20% exhale CT phase

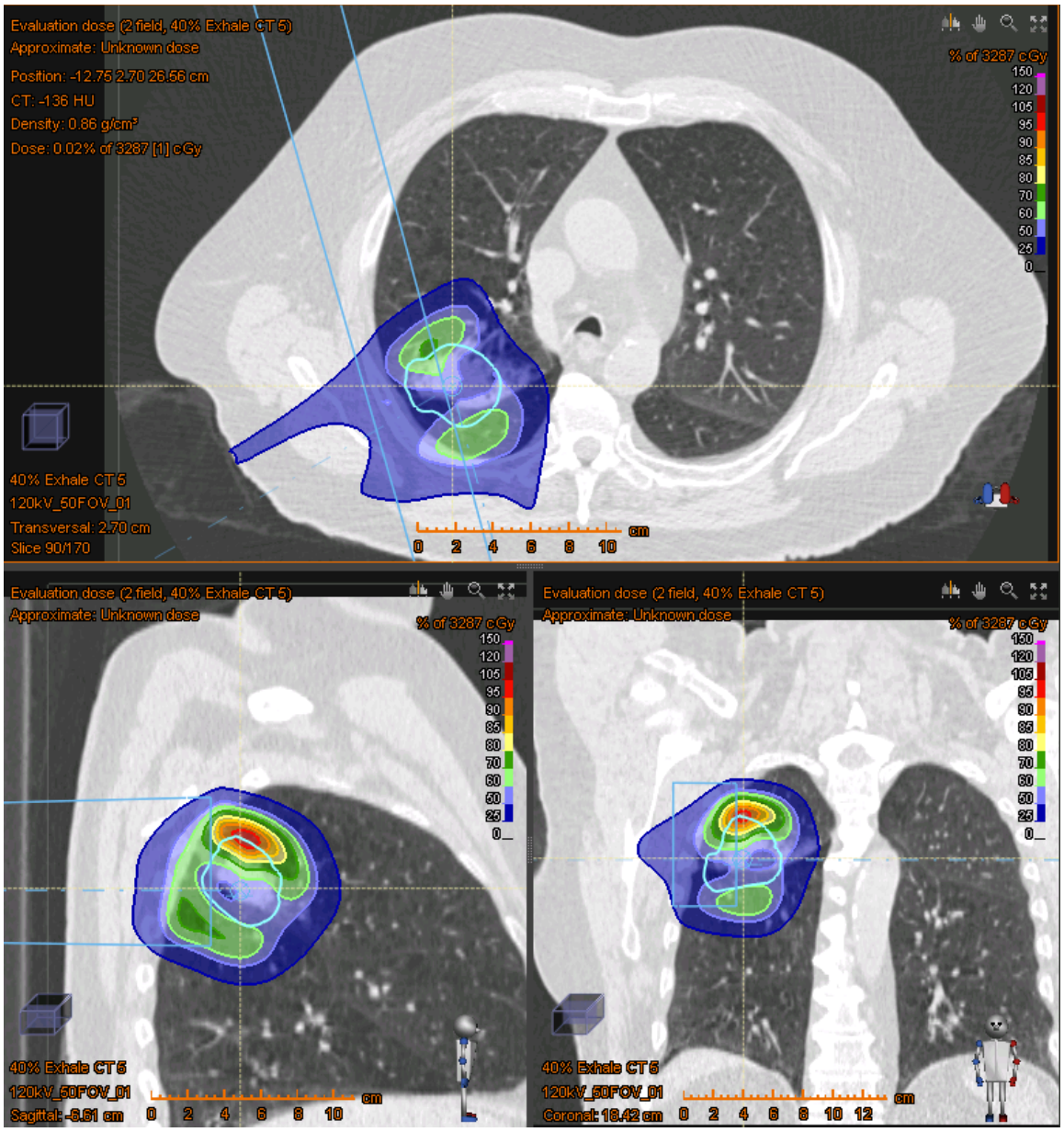

Figure A.7. Field 1&2 – Dose delivered to 40% exhale CT phase

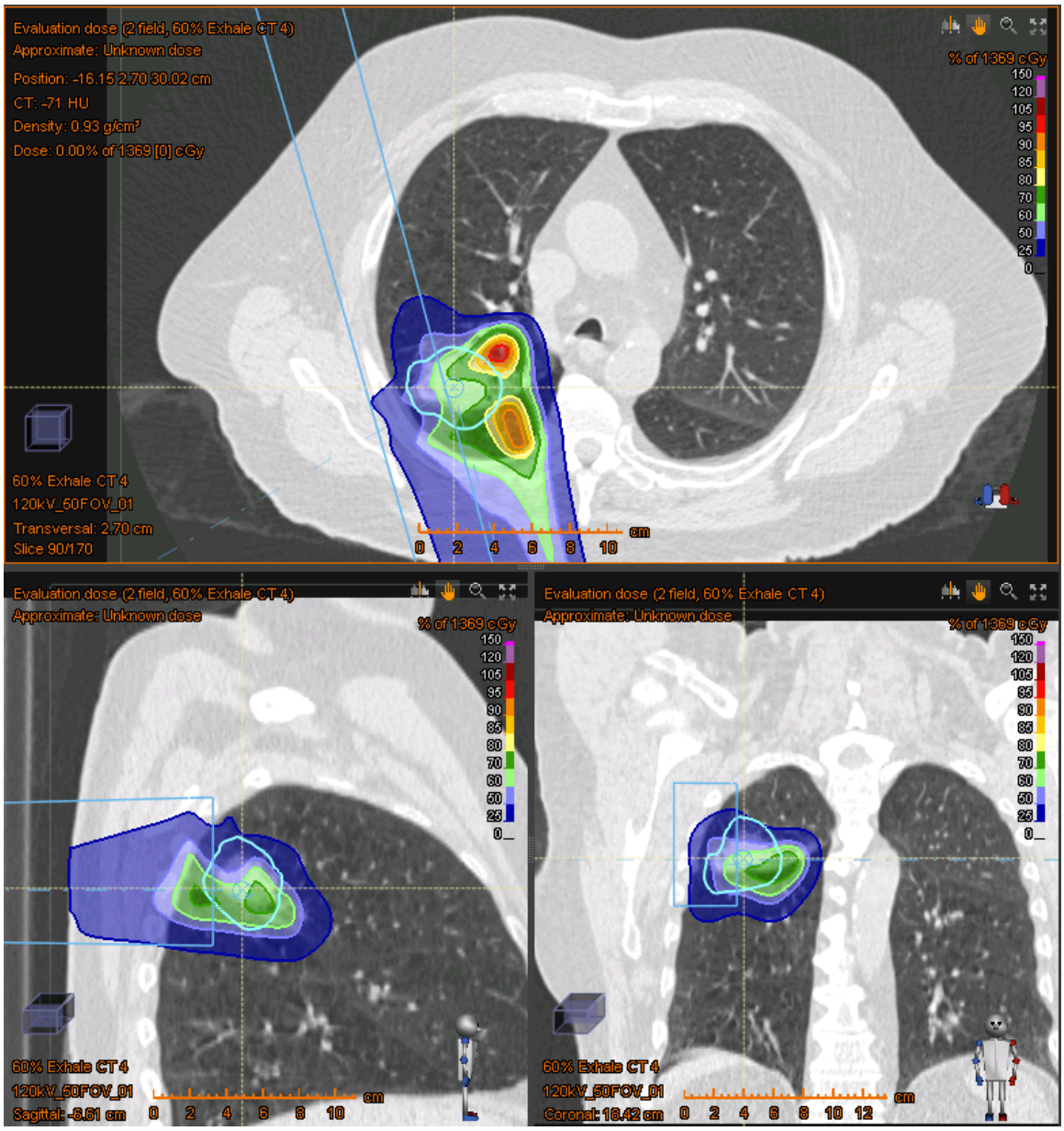

Figure A.8. Field 1&2 – Dose delivered to 60% exhale CT phase

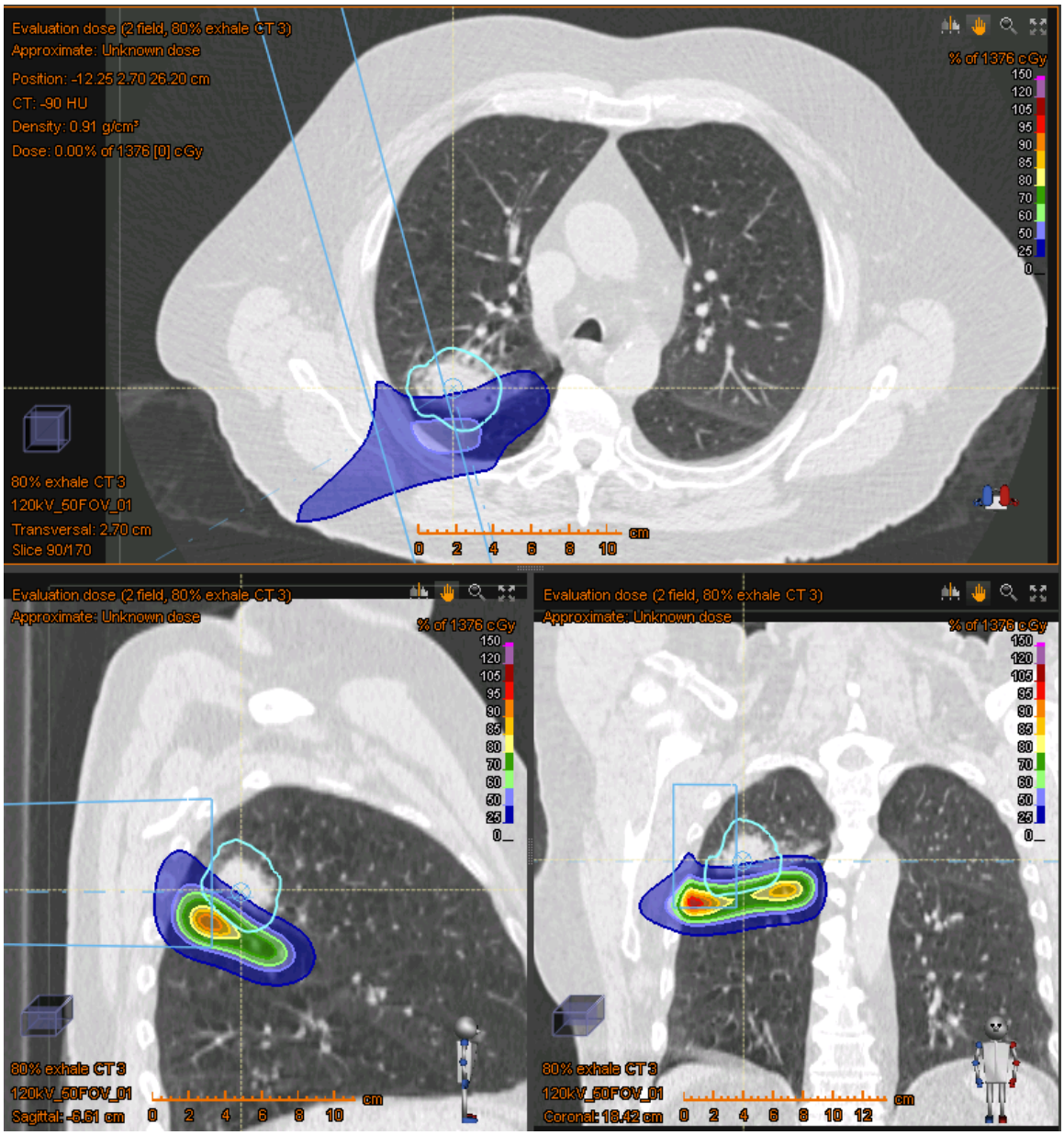

Figure A.9. Field 1&2 – Dose delivered to 80% exhale CT phase

VITA

Mark Artz completed his undergraduate and master's degree at the Massachusetts Institute of Technology and is finishing his PhD at the University of Tennessee. His current PhD research focused on treatment plan dose perturbation from respiratory motion.

As a graduate student at MIT, Mark developed various technologies for pencil beam scanning proton therapy. These projects included an electron cyclotron resonance proton ion source as well as superconducting proton therapy gantry.

While working in the clinic at Provision Center for Proton Therapy, Mark has focused on clinical machine commissioning, pencil beam scanning treatment plan optimization, and improving patient setup.

Mark grew up in Pompano Beach, Florida, and enjoys swimming, water skiing and scuba diving.